TITLE

The Effects of the Use of Full Potentials in the Calculation of X-Ray Absorption Near-Edge Structure by the Multiple-Scattered-Wave X-alpha Method

AUTHOR

David Laurence Foulis,

The Effects of the Use of Full Potentials in the Calculation of X-Ray Absorption Near-Edge Structure by the Multiple-Scattered-Wave X-alpha Method

by

David Laurence Foulis, B.Sc. (Hons.)

A thesis submitted
to the University of Warwick,
for the degree of Doctor of Philosophy;

describing research conducted
as an external student of the Department of Physics
at the Hamburg Outstation of the
European Molecular Biology Laboratory
and at the Frascati National Laboratories
of the Istituto Nazionale di Fisica Nucleare.

November, 1988.

I. CONTENTS.

II. ACKNOWLEDGEMENTS.

The work reported in this thesis was done under the supervision of Dr. Robert F. Pettifer, at the Hamburg Outstation of the European Molecular Biology Laboratory (EMBL-HH) and at the Laboratori Nazionali di Frascati dell'Istituto Nazionale di Fisica Nucleare (INFN-LNF). It is a pleasure to acknowledge the wider friendship that has grown out of our shared fascination with the subject of Physics, and to thank Robert for his continued support and encouragement and for the hospitality and kindness shown to me by himself and his family.

The work was also done in collaboration with Dr. C.R. "Rino" Natoli of the INFN-LNF and I should like to express my gratitude for his interest and support especially during my time as his guest worker in Frascati.

I should like to thank the EMBL for the provision of a three-and-a-half year pre-doctoral fellowship at the Hamburg Outstation and the INFN-LNF for their hospitality and financial support during my sixteen month stay. I also thank the European Molecular Biology Organization (EMBO) for the provision of a short-term fellowship to visit EMBL-HH for two weeks in October 1987.

Of the many people in Hamburg whose friendliness and assistance made my stay such an enjoyable and fruitful one, I should like to make particular mention of, and thank, the following:
Dr. J. Röhler and his group who provided the experimental spectrum of chromium hexacarbonyl used in this thesis, and Dr. D. Fong who helped with the associated computer problems; P. Bendall, S. McLaughlin, D. Dainton and F. Golding who helped with many of the programming problems that arose in the course of my work; the lab secretaries E. Peters and D. Millard whose help, both official

and unofficial, made life much easier for a Briton living in a foreign country; Dr. K. Wilson for his assistance as Head of Outstation at EMBL-HH; and my colleague Dr. C. Hermes whose discussions of the experimental side of X-ray absorption spectroscopy helped broaden my understanding of the subject. Of the people in Frascati I should like to acknowledge the many interesting discussions of the work with Dr. M. Benfatto, Dr. C. Brouder, T. Tyson and P. Sainctavit. In the Physics Department at Warwick University I wish to thank Dr. B. Holland for his critical appraisal of my work on several occasions; Prof. H. Mykura for his administrative assistance; and Dr. P.V. Smith for his careful reading of the draft of this thesis.

I should like to acknowledge the patience and assistance of my family during the last, difficult phase of thesis-writing, particularly that of my mother Mrs. M. Foulis and my aunt Mrs. S. Kilpatrick. Finally, I should like to express a special thanks to Mlle. Nathalie Pipon, whose personal support during the last three years has been a significant factor leading to the completion of the work.

III. DECLARATION.

This thesis represents work done as part of a continuing and wider collaboration between Dr. R.F. Pettifer (RFP), Dr. C.R. Natoli (CRN), Dr. M. Benfatto (MB) and myself. The aim of my part was to apply the non-muffin-tin theory set out in the Natoli et al. (1986) paper, to calculate X-ray absorption near-edge structure for some model systems. This was to be done by modifying the muffin-tin-based programs (deriving ultimately from those of Smith and Johnson (1969) and Natoli et al. (1980)) according to the new theory. To this end in March 1984 CRN sent me copies of the old programs so that I could familiarize myself with them. This was followed in May 1984 by a month-long visit to INFN-LNF to consult with CRN and MB in which I was provided with early drafts of their 1986 paper and much advice. I developed the non-muffin-tin programs at EMBL-HH with advice from RFP until March 1987, and then at INFN-LNF with advice from CRN and MB until July 1988.

The direction of the work has not turned out entirely as planned. Firstly I had to develop and clarify some points of the theory. In particular, this involved the theory for bound states (Sec. 3.2) which, although really only a minor adaptation of the continuum case given in Natoli et al. (1986), is not quite straightforward; the atomic t-matrix symmetry theorem (3.68) which we believe to be new; and some work (not included herein) on the treatment of molecular point symmetry in the non-muffin-tin case. The development of the computational approach and the writing and testing of the new programs is my own work and the results are entirely original. The only qualifications to this statement are the following: RFP contributed much in the way of advice about

numerical methods for the program MLPSHX in particular; CRN helped to debug the main programs ENESHX and CNTSHX; the decision about the best way to implement the numerical scheme for the interstitial T-matrix integration was greatly clarified by discussions with CRN and MB; the interpretation of the new non-muffin-tin results in Chapter 5 owes much to RFP and CRN; and the actual new programs contain a certain amount of code taken over directly from the old ones (see App. B), although unfortunately a lot less than was originally hoped.

Of the material presented here some has been published or displayed elsewhere. Calculations with the old muffin-tin programs for zinc selenide, supporting the conclusions of Sec. 2.4, were presented as a poster to the conference "Progress in X-ray Studies by Synchrotron Radiation" (April 1985 Strasbourg, France). Some of the chromium hexacarbonyl results from Secs. 2.4 and 4.2 were presented to the conference "EXAFS and Near-Edge Structure IV" (July 1986 Fontevraud, France) and published in the conference proceedings (Foulis et al. (1986)). In the near future we intend to submit the results in Chapter 5 for publication.

This thesis was prepared according to the guidelines given in the document PHYS/PG/2 (University of Warwick (1985)).

IV. LIST OF TABLES.

V. LIST OF ILLUSTRATIONS.

VI. NOTATION, UNITS AND ABBREVIATIONS.

In this work we do not introduce any new notation. We have not tried particularly to follow the conventions in the literature, although our notation for the derivation of the full-potential scattered-wave (FP-SW) secular equations owes much to Johnson (1973) and Natoli et al. (1986). Bearing in mind the large number of equations presented here, and the means at our disposal, we have decided to write them by hand. The mathematical notation that we used is standard, although several particular conventions should be noted. An integration in which the region is not specified should be taken over the whole region of the variable involved. For a vector $\vec{r}$ we denote its magnitude by $r \equiv |\vec{r}|$ and the corresponding unit vector by $\hat{r} \equiv (1/r)\vec{r}$. A matrix (finite or infinite) is denoted by $\underset{\sim}{M}$. The use of set theory notation, i.e. set inclusion $\subset$, membership $\in$, union $\cup$, intersection $\cap$, boundary ∂, complementation $^-$, and the empty set $\emptyset$; is intended as no more than a convenience for the compact specification of the various regions of the molecular partition.

The physical units used herein are the theoretical "atomic units", in which the electron mass, the Bohr radius, the positron charge and Planck's (reduced) constant all have unit magnitude. Only two units in this system have special names; these being the Bohr of length and the Hartree of energy. Any other unit is denoted simply by "au"; although occasionally, to avoid ambiguity, we also indicate its composition in terms of the fundamental quantities of mass (M), length (L), time (T) and electric charge (C). In conformity with the literature of this branch of physics however, we use also several non-standard units. Instead of the Hartree, our fundamental unit of energy is the Rydberg (or half a

Hartree). In addition, but mainly in connection with experimental spectra or molecular structures, we use the electron-volt (eV), the megabarn (Mb) and the Ångström (Å). We list below the values (taken from Cohen and Taylor (1987)) of some fundamental constants and conversion factors, in SI and atomic units. As usual, the numbers in brackets within a value refer to the estimated (one standard deviation) uncertainty in the last digits of the mantissa. If no uncertainty is quoted, then the value is to be interpreted as being exact by definition.

Electron mass, $m_e = 9.1093897(54)\times10^{-31}$ kg = 1 au(M).

Bohr radius, $a_0 = \hbar/m_e c\alpha = 0.529177249(24)\times10^{-10}$ m

= 1 Bohr (au(L)).

Atomic time unit, $a_0^2 m_e/\hbar = a_0/c\alpha = 2.41888433(22)\times10^{-17}$ s

= 1 au(T).

Positron charge, $e = 1.60217733(49)\times10^{-19}$ C = 1 au(C).

Planck's (reduced) constant, $\hbar = 1.05457266(63)\times10^{-34}$ J s

= 1 au(ML^2T^{-1}).

Speed of light in vacuum, $c = 2.99792458\times10^{8}$ m s^{-1}

= 137.0359895(61) au(LT^{-1}).

Permeability of vacuum, $\mu_0 = 4\pi\times10^{-7}$ H m^{-1}

= $6.69176350(60)\times10^{-4}$ au(MLC^{-2}).

Permittivity of vacuum, $\varepsilon_0 = 1/\mu_0 c^2 = 8.854187817...\times10^{-12}$ F m^{-1}

= $e^2/4\pi\hbar c\alpha = 1/4\pi$ au($M^{-1}L^{-3}T^2C^2$).

Fine-structure constant, $\alpha = 1/137.0359895(61)$.

Newton's gravitational constant, $G = 6.67259(85)\times10^{-11}$ m^3 kg^{-1} s^{-2}

= $2.40000(32)\times10^{-43}$ au($M^{-1}L^3T^{-2}$).

Rydberg energy, $m_e c^2\alpha^2/2 = 2.1798741(13)\times10^{-18}$ J

= 1/2 Hartree (au(ML^2T^{-2})) = 13.6056981(41) eV.

Megabarn, 1 Mb = 10^{-22} m^2 = $3.5710643(33)\times10^{-2}$ $Bohr^2$.

Several standard and non-standard abbreviations are used in

this work and we give a glossary of them below.

ASR	Atomic sphere region (of molecular partition).
EMR	Extra-molecular region (of molecular partition).
(E)XAFS	(Extended) X-ray absorption fine structure.
FP	Full potential.
FWHM	Full width at half maximum.
IR	Interstitial region (of molecular partition).
Irrep	Irreducible representation (of a group).
LHS	Left-hand side (of an equation).
LRO	Long-range order (theory of XAFS).
(M)SW	(Multiple) scattered-wave (method/theory).
MT	Muffin-tin (potential approximation).
OS	Outer sphere (enclosing a molecule).
RHF	Restricted Hartree-Fock (hamiltonian/method).
RHS	Right-hand side (of an equation).
SCF	Self-consistent field.
SHX	Spherical harmonic expansion.
SRO	Short-range order (theory of XAFS).
SSR	Spherically symmetric region (= an ASR or the EMR).
XANES	X-ray absorption near-edge structure.
XAS	X-ray absorption spectrum/spectroscopy.

VII. SUMMARY.

In this work we describe the effects of the relaxation of the muffin-tin (MT) potential approximation (and the consequent use of full potentials (FPs)) in the ab initio calculation of X-ray absorption near-edge structure (XANES) by the multiple-scattered-wave (MSW) $X\alpha$ method. In doing so we demonstrate the validity and computational feasibility of the extended FP-MSW theory due to Natoli et al. (1986). We describe certain refinements to this theory and the development of a practicable computational approach for its realization. With the results of the newly-developed computer programs for certain model systems we show that the FP-MSW method leads to much higher accuracies in both bound-state energy eigenvalues and in photoionization cross-sections near the threshold. Our FP-MSW XANES calculations for the chromium hexacarbonyl ($Cr(CO)_6$) system therefore demonstrate, because the results are still significantly different from the experimental spectrum (although closer than the MT case), that there remain other deficiencies in the physical model. Although beyond the scope of this work, we strongly suspect that the bulk of the remaining error would be accounted for by a better treatment of inelastic loss and (to a lesser extent) exchange-correlation. Our final conclusion is that the use of FPs is necessary (and now feasible) for the accurate calculation of XANES.

We begin with an introduction to X-ray absorption spectroscopy (XAS) and then concentrate on XANES giving the motivation in terms of its structural significance and describing the necessity and difficulty of accurate ab initio calculations. The central part of XANES calculations is the solution of Schrödinger's equation for the initial and final molecular states in the absorption process, and we summarize the approximations to the full many-body equation that make it tractable. This leads to a discussion of the MT approximation and an illustration of its deficiences. We review various remedies that have been proposed and concentrate on the FP-MSW theory of Natoli et al. (1986). We then give a detailed presentation of the theory and develop the necessary representation of the potential in terms of spherical harmonic expansions (SHXs). It is shown that, for symmetric molecules with up to two coordinating shells of atoms, five to ten partial waves per prototype atom serve to make the SHX representation from one to three orders of magnitude more accurate than the MT case.

The development of the FP-SW bound-state eigenvalue program ENESHX is described and the program tested with the hydrogen molecular ion (H_2^+). By comparison with the MT results we find that the error is reduced to less than 12% in the worst case (the ground state) and less than 0.2% for the highest levels. Calculations for the $Cr(CO)_6$ system do show changes of as much as -0.4 Ryd. for the valence levels (stemming mostly from the better treatment of the interstitial region). The successfully-tested ENESHX is then adapted to produce the FP-SW continuum photoionization cross-section program CNTSHX which is then tested with a Li^{2+} ion pseudo-cluster whose exact analytic cross-sections are known. Above about 1 Ryd. from threshold, the CNTSHX cross-sections are within 1% of the exact values, compared to 7% for the MT case. Below 1 Ryd. the CNTSHX error remains less than 5%. CNTSHX is then run for $Cr(CO)_6$ with the results described above.

Chapter 1. INTRODUCTION.

Section 1.1: X-Ray Absorption Spectroscopy and XANES.

This thesis is concerned with the relaxation of the "muffin-tin" (MT) approximation in the ab initio calculation of X-ray absorption near-edge structure (XANES). While treating the theoretical foundations in detail, and including some further elaborations, our main emphasis is on the development of the computational approach and the results obtained for model systems.

Consider X-ray absorption spectroscopy (XAS) in its simplest form as follows. Fig. 1.1 gives a schematic representation of the experimental situation. A monochromatic beam of X-rays of initial intensity I_o traverses a material sample of thickness t, emerging with an intensity I given by Beer's law:

$$I = I_o e^{-\mu t} \qquad (1.1),$$

in which the attenuation coefficient μ consists of contributions from absorption and scatter. In practice, the detectors of the transmitted beam usually have a wide enough angle of acceptance that the small-angle scatter (which dominates the scattering process) is captured. The scatter not detected is then negligible and μ is identified with photoelectric absorption. This absorption coefficient is a function of the photon energy E, and may be expressed as

$$\mu(E) = \sum_i n_i \, \sigma_i(E) \qquad (1.2);$$

where σ_i is the total cross-section for a given type of absorber i, and n_i is the number density of that absorbing species within the sample.

The main business of experimental XAS is to measure μ as a function of energy. The particular energy range we consider is in the X-ray region with photon wavelengths from about 10 Å to 0.1 Å

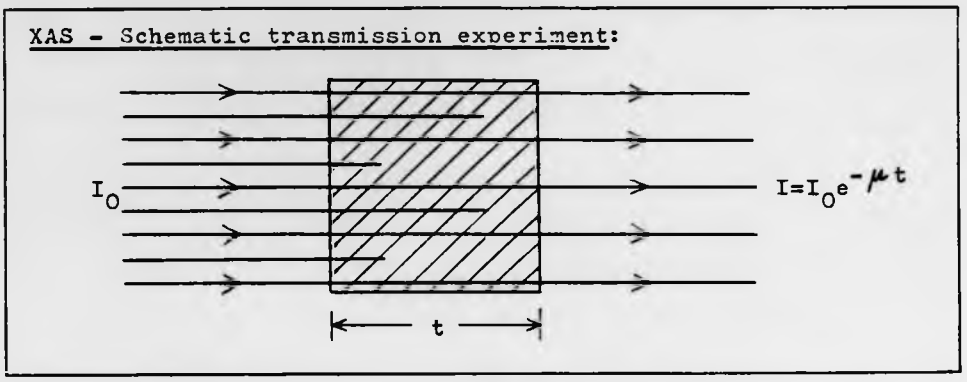

Figure 1.1: A schematic XAS transmission experiment. A collimated monochromatic beam of X-rays, entering from the left, traverses a homogeneous slab of material at right angles to its uniform, parallel, plane surfaces. The beam enters with intensity I_0 and emerges with diminished intensity I, the losses being due to absorption within the material.

(corresponding to photon energies roughly from 1.2 to 120 keV). In this range the cross-sections in (1.2) are dominated by the photoelectric effect for excitation of inner-shell electrons. The most marked feature of μ as it varies with energy is the appearance of absorption edges - step-like jumps in μ as the photon energy becomes sufficient to eject an electron from an inner shell (K, L, M etc.) of an atom in the sample.

On the high-energy side of an absorption edge the absorption coefficient resumes a slow decline with increasing energy. It quite often happens, in the region of an edge, that there are extra oscillations in the absorption coefficient. These are known as the X-ray absorption fine structure (XAFS) and may occur from about 10 eV below the edge up to several hundred eV above the edge. Their amplitude is typically 10 to 20 percent of the edge jump within 100 eV of the edge, diminishing to indetectability by the time we reach about 1500 eV above the edge. (This limit depe-

nds on the atoms surrounding the absorbing atom and the temperature of the specimen.) Within a few eV of the edge the absorption coefficient may oscillate by more than 100% of the edge jump, giving rise for example to so-called "white lines".

A schematic representation of a typical absorption edge is shown in Fig. 1.2. Note the arbitrary division of the edge spect-

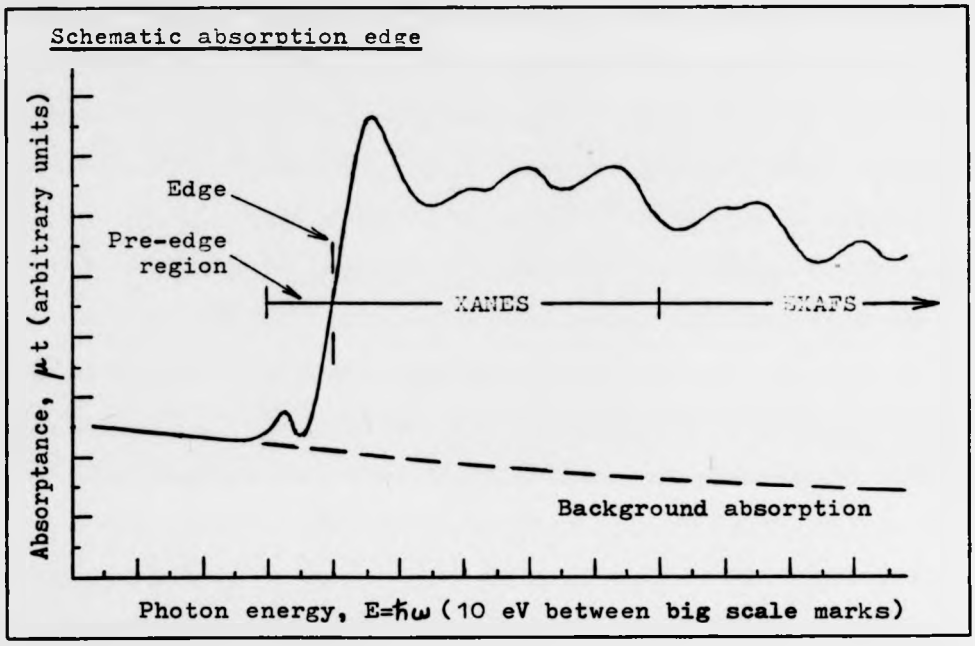

Figure 1.2: Typical features of an absorption edge. At an energy characteristic of one particular type of absorber in the sample, the cross-section (see (1.2)) makes a step-like jump when the photon has sufficient energy to excite a core electron into the continuum. In the pre-edge region one sometimes sees peaks corresponding to transitions to bound final states. Above the edge the structure, arising from modifications of the final state due to the presence of neighbouring atoms, is divided into the XANES which extends to about 50 eV and the EXAFS which continues from there. To extract a particular edge one must remove the continuous background, due to other atoms or

other edges on the same atom, by extrapolating upwards in energy some asymptotic form fitted to a smooth region below the edge.

---

rum into various regions; the pre-edge region, the XANES and the extended X-ray absorption fine structure (EXAFS). Although there is no exact boundary between the XANES and the EXAFS, the two are commonly divided at about 50 eV above the edge, for reasons we now discuss.

The first publication of a measured X-ray absorption spectrum was that of M. de Broglie (1913) and the first published observations of fine structure above an edge were those of H. Fricke (1920). Following the advent of modern wave mechanics it was fairly quickly realized that the fine structure resulted from the modification of the electron's final state by the presence of neighbouring atoms; and soon after Kronig (1931,1932a,1932b) laid the foundations of the present theoretical understanding of XAFS. In the ensuing 40 years the development of the theory was pursued along two separate lines; the long-range order (LRO) theory based on the attribution of the fine structure to variations in the electron's density of states due to allowed and forbidden bands in a crystal; and the short-range order (SRO) theory based on scattering of electron waves by neighbouring atoms. In this time many necessary further elements were included in the theoretical treatment and by the mid-1970s the SRO theory was found to be the more appropriate, since the fine structure is determined by near neighbours of the photoionized atom rather than all atoms in the solid. It is on the basis of the SRO theory that most modern treatments of XAFS are based. One should see Azároff's (1963) review for an account of the earlier history of the field, together with the more recent reviews (for example that of Hayes and Boyce

(1982)). The detailed theory is given by Lee and Pendry (1975) and Ashley and Doniach (1975), and most later treatments are based on their work. (Note however, that Müller and co-workers have developed a successful LRO theory for periodic systems (see e.g. Müller and Wilkins (1984)).)

It is from a consideration of the theory that the division between XANES and EXAFS arises. This theory is formulated in terms of scattering of the photoelectron wave by various neighbours before returning to its source at the excited atom to cause interference leading to the observed variations in cross-section. In the EXAFS region, in which the photoelectron energy is above 50 eV, the scattering from individual atoms tends to be concentrated in the forward and backward directions. Furthermore, the mean free path of the excited electron is reduced because of inelastic losses such as coupling to plasmons or electron-hole pairs. Both of these effects mean that EXAFS is dominated by events in which the photoelectron is scattered only once and then returns to the source (or, in some cases, by a limited number of multiple-scattering paths). Because of this, the theoretical description of EXAFS has been much more successful than that of XANES.

In the XANES region the scattering of electrons away from the forward and backward directions is much stronger, and this is coupled with the fact that the mean free path is much greater since the inelastic losses are weaker. This all means that the XANES is dominated by multiple scattering and its theoretical description is correspondingly more difficult. Also the energy of the excited electron becomes comparable to the fluctuations of the crystal or molecular potential (arising from covalent bonds for example) in the XANES region; thus complicating the description in terms of individual scattering events.

Because of its dependence on the coordination geometry of the excited atom and the atomic selectivity inherent in an X-ray absorption edge, XAFS is potentially a highly flexible, structural probe for all kinds of materials. This potential has in fact been partially realized, primarily for the EXAFS region (see Hayes and Boyce (1982) for further references) by virtue of its treatment in terms of single scattering events. A concomitant limitation however, is that the analysis of EXAFS (by empirical means or the fitting of first-principles calculations) has mainly provided only radial distances of neighbouring atoms and sometimes their identities. (Although note for example recent results of Pettifer et al. (1986) giving orientational information from a multiple-scattering analysis of EXAFS.)

XANES, on the other hand, should provide information about the detailed local geometry around the absorbing site; particularly relative orientations and bond angles. Analysis of XANES is attractive also for practical reasons. Primarily this is because the amplitude of the XANES is usually greater than for EXAFS and thus easier to measure. This is partly because the existence of disorder (either thermal or static) tends to wash out EXAFS at higher photoelectron momenta, but also because the backscattering from atoms diminishes as well.

The main drawback involved in the analysis of XANES is its considerable complication. The only approach possible in this region is the use of first-principles (ab initio) calculations of the cross-sections and subsequent comparison with experiment. It is in the general area of accurate ab initio calculations of XANES that this thesis is intended as a contribution. In particular, we consider calculations within the framework of the so-called multiple-scattered-wave (MSW) method and show what happens

when the MT approximation to the one-electron potential is dropped. Although we only treat the MSW theory, the MT approximation is widely used in other theoretical approaches to XANES and consequently our results have much wider implications.

Section 1.2: Scope and Plan of Thesis.

The main scope of the thesis is the implementation of a non-MT extension to the scattered-wave (SW) method for the calculation of XANES, with the purpose of answering questions about the size and importance of non-MT corrections and the feasibility of the computations. Even this seemingly direct task turned out to be much larger and more complicated than it appeared at first sight. We found, at each stage of the work, that there were many more ramifications and important new questions than could be treated within the framework of a thesis. Therefore we have presented the work as a direct logical progression that we summarize in this section. The detailed developments given are only those sufficient to support the final conclusions, while other important points are just outlined or mentioned in passing.

In Chapter 2, we summarize the main approximations to the full many-body Schrödinger equation that bring it into a more tractable form. The muffin-tin approximation is then introduced and we briefly review the present state of XANES calculations that make use of it. We then restrict ourselves to considering the SW method as the one most amenable to the incorporation of non-MT potentials (and the only one for which such an extension was available in the literature). At this point we introduce our model compound chromium hexacarbonyl ($Cr(CO)_6$) and present some MT-based SW calculations of its XANES at the chromium K-edge. This is done to illustrate the problems arising from the deficiencies of the MT

approximation and the inadequacy of the usual ad hoc schemes that are used to try to ameliorate them. While we have sufficient extra material to present a full-scale survey of all aspects of MT deficiencies in the SW method, the volume of this material is prohibitive. We nevertheless discuss these deficiencies and review the literature of serious means that have been proposed for going beyond the MT approximation. This leads up to the introduction of the Natoli et al. (1986) paper as our theoretical foundation.

In Chapter 3 we develop the full-potential scattered-wave (FP-SW) theory. The derivation of the (unpublished) bound-state equations is given in detail, while the continuum case from Natoli et al. (1986) is merely sketched. The programs that we have developed to apply the theory, rely heavily on the use of molecular point symmetry and group theory to reduce the size of the secular matrices and consequently the computational effort involved. We have only outlined the associated theory and there is a considerable amount of further detail that would be needed to make it a rigorous treatment. In fact, the full details are not yet completely worked out for the FP case. Even for the MT case (as described by Diamond (1973)) there are some deficiencies, and we intend to present a full treatment, in the framework of the FP-SW method, at a later date.

The greater part of the work reported in this thesis was the development of the computer programs that realize the theory of Chapter 3, but this has not been reflected in our presentation of it. We describe only the main computational means whereby the particularly new features of the FP-SW method are incorporated. The first of the programs, MLPSHX, is described in Chapter 4. Here we are concerned with the central problem of modelling the

potential accurately, in a form that is usable by the main FP-SW programs. Ultimately we should test in detail the sensitivity of the results from the later programs to the accuracy with which the potential is modelled. For the purposes of this thesis we content ourselves with the demonstration that the resulting potential model is a much closer representation of the real case than the MT approximation. Presumably therefore, the greater part of any benefits that may come from the use of a FP at all will result from our model without further adjustment of parameters.

In Chapter 5 we describe the development of the main FP-SW programs and the results that they give for some model systems. Although our interest is in XANES calculations, we wrote first the program ENESHX that applies the FP-SW theory for bound states. This was because the theory is simpler for bound states and, with the hydrogen molecular ion results, we have an absolute test of both the program and the theory. The XANES program CNTSHX, that applies the continuum wavefunction theory, is sufficiently similar that the well tested parts of ENESHX may be taken over almost directly. The main thing lacking from our treatment of the program results is an analysis of their sensitivity to various parameters used in the potential model and the wavefunction expansions. There are also many different numerical integration, interpolation and special function routines used in the programs, and a detailed mathematical error analysis of them all is beyond the scope of this thesis. Our approach to such questions is to create a sufficient margin of accuracy, by taking various expansion parameters and integration meshes well beyond the usual values, so that any remaining inaccuracies are dominated by those stemming from the physical model itself.

In Chapter 6 we conclude that the results in the previous cha-

pter are sufficient for us to be able to answer the limited main questions posed; namely those about the extent of the changes in going from MT to FP, the correctness of our theoretical approach and the feasibility of the calculations themselves at least for a limited class of systems with modest computational resources. With the most serious approximation disposed of we then comment on the future steps that need to be taken towards accurate XANES calculations.

Chapter 2. MUFFIN-TIN BASED CALCULATIONS OF XANES.

Section 2.1: General Approximations to the Schrödinger Equation.

The main part of all XANES calculations is the solution of the appropriate dynamical equations for the interacting assembly of nuclei and electrons that comprises a molecule. At the energies that we consider in XAS the inner structure of the nuclei is quite irrelevant and all particles may be considered as point-like masses with a given intrinsic spin. Also the possibility of annihilation and creation of even the electrons does not arise. Therefore, since our most ambitious requirements for accuracy would be, say, one percent in the cross-sections, the whole apparatus of quantum field theory (in particular QED) may be safely ignored.

The first non-trivial question to arise is whether a relativistic treatment is necessary. Certainly, the electrons can have speeds which are a significant fraction of the speed of light, especially for the core electrons in heavy atoms. The nuclei, being several thousand times more massive than the electrons, tend to move much more slowly and a non-relativistic treatment of them would be adequate. In fact it is usual to make the so-called Born-Oppenheimer approximation in which the nuclei are taken to be stationary (see e.g. Schiff (1968) p.447). The dynamical problem for the electrons is then solved separately in what is thus the fixed, external field of the nuclei. If desired the behaviour of the nuclei, under the influence of the cloud of electrons, may be treated as a perturbation. Under certain circumstances the Born-Oppenheimer approximation does break down with the excitation of rotational and vibrational modes, at high momenta. This is not expected to be a problem for us since XANES is known to be

temperature independent provided no phase transition occurs.

We are still left with the problem of whether to treat the electron motion relativistically or not. There is in fact a large body of evidence to show that the neglect of relativistic effects can lead to significant errors. For example, Loucks (1967) shows that the inclusion of relativistic effects is necessary in the calculation of band-structures for solids containing heavy atoms. A review of this general question is given by Desclaux (1980). For our purposes, considering the degree of accuracy in XANES calculations, we can reasonably neglect relativistic effects as long as we restrict our attention to low-Z atoms (i.e. the 3d transition elements or lower). Since relativistic effects will be serious only for the deep-lying core levels and not so much for the slowly propagating states near the ionization threshold, their main result in X-ray absorption will be to change the ionization threshold position rather than the details of the XAFS. (See also Kutzler et al. (1980))

(We note here in passing that there has been developed a relativistic version of the scattered-wave (SW) method for molecules. This is given in Yang and Rabii (1975) and Yang (1978), and a calculation for uranium hexafluoride (UF_6) presented by Case and Yang (1980) (ground state only). More interesting from our point of view are the calculations of Arratia-Perez and Yang (1985) for the ground states of certain metal hexacarbonyls, including our model compound $Cr(CO)_6$. They indicate that, even in $W(CO)_6$, relativistic effects are qualitatively unimportant for the valence levels. While a full treatment of the electron dynamics requires the inclusion of relativistic effects, their importance in our systems is expected to be small and we do not consider them further.)

We must now use the many-body Schrödinger equation for M electrons in the Coulomb fields of the N nuclei. The wavefunction Ψ then satisfies the time-independant equation at energy E:

$$-\left\{\sum_{i=1}^{M}\nabla_i^2+\sum_{i=1}^{M}\sum_{j=1}^{N}\frac{2Z_j}{|\vec{r}_i-\vec{R}_j|}-\sum_{i=2}^{M}\sum_{j=1}^{i-1}\frac{2}{|\vec{r}_i-\vec{r}_j|}\right\}\Psi=E\Psi \quad (2.1);$$

where the electron positions are $\vec{r}_i$ and the fixed nuclear positions and charges are $\vec{R}_i$ and Z_i respectively. Note that the wavefunction is a function also of the spins s_i of the electrons; i.e. $\Psi(\vec{r}_1, s_1, \vec{r}_2, s_2, \ldots, \vec{r}_M, s_M)$, and must be anti-symmetric under the exchange of any two electron indices. The hamiltonian in (2.1) has no terms involving spin and in fact we ignore all spin effects except those arising from the Pauli exclusion principle.

Since there can be several hundred electrons even for quite small molecules, the solution of (2.1) is quite intractable with any known analytic or numerical method presently available. The crucial approximation that we make now is the so-called one-electron approximation in which each electron is treated as moving in an average field due to the nuclei and the probability density of the other electrons. The usual way this approximation is implemented is the self-consistent-field Hartree-Fock method (see for example McWeeny and Sutcliffe (1984) and references therein). It may be developed by assuming that the wavefunction is an anti-symmetrized product (a Slater determinant) of one-electron orbitals and then using the variational principle to optimize them. In other words we assume that

$$\Psi(\vec{r}_i, s_i) = (M!)\sum_{\pi} sgn(\pi)\prod_{i=1}^{M} u_i(\pi(i)) \quad (2.2);$$

where the individual spin-orbitals

$$u_i(j) \equiv \phi_i(\vec{r}_j)\,\chi_i(s_j) \quad (2.3)$$

are mutually orthogonal and normalized. We further restrict the form of the wavefunction (2.2) by assigning the electrons two at a time to a given space part of a spin-orbital, but giving them

orthogonal spin parts.

The use of the hamiltonian of (2.1) with the variational constraints (2.2,3) leads to the restricted Hartree-Fock (RHF) equations for the orbitals

$$\left[-\nabla^2 + V_N(\vec{r}) + V_C(\vec{r})\right]\phi_m(\vec{r}) + \int V_E(\vec{r},\vec{s})\,\phi_m(\vec{s})\,d^3s = E_m\phi_m(\vec{r}) \quad (2.4);$$

which has the form of a one-electron equation for each orbital with a potential made up of the nuclear Coulomb field

$$V_N(\vec{r}) \equiv \sum_{i=1}^{N} \frac{2Z_i}{|\vec{r} - \vec{R}_i|} \quad (2.5),$$

the electrons' Coulomb term

$$V_C(\vec{r}) \equiv 2\sum_{m=1}^{M/2} \int \phi_m^*(\vec{s})\,\phi_m(\vec{s}) \frac{2}{|\vec{r} - \vec{s}|}\,d^3s \quad (2.6)$$

and the non-local exchange term

$$V_E(\vec{r},\vec{s}) \equiv -\sum_{m=1}^{M/2} \phi_m(\vec{r}) \frac{2}{|\vec{r} - \vec{s}|} \phi_m^*(\vec{s}) \quad (2.7).$$

While (2.4) has in fact been used successfully (see McWeeny and Sutcliffe (1984) again), the non-local term makes it very unwieldy for anything other than atoms. A further approximation is then made to replace (2.7) by a simpler, local potential. The most common one is that derived from the theory of the free-electron gas, and introduced by J.C. Slater (see especially his review - Slater (1972)) under the name "Xα". For the local electron density

$$\rho(\vec{r}) \equiv 2\sum_{m=1}^{M/2} \phi_m^*(\vec{r})\,\phi_m(\vec{r}) \quad (2.8),$$

this potential is

$$V_{X\alpha}(\vec{r}) \equiv -6\alpha\left[(3/8\pi)\rho(\vec{r})\right]^{1/3} \quad (2.9)$$

where α is a parameter chosen (for free atoms at least) so that the total energy matches that of the full RHF method (Schwarz (1972)). The Xα method has been fairly successful in several calculational schemes for the ground states of various solid-state and molecular systems, Its validity for excited or ionized states is rather questionable (see for example Pettifer and Cox (1983)) however, as indeed is that of the whole variational scheme and

the RHF method itself. A general review of the Xα method in various calculational schemes is given by Gadiyak et al. (1982).

In making the one-electron approximation we do in fact ignore several non-trivial many-body aspects of the photoionization process. The existence of many other excitation channels than the promotion of a core electron to a continuum final state, often modifies substantially the photoabsorption cross-section. The dynamical effects of the core hole, the possibility of "shake up" or "shake off" effects (in which additional electrons are excited to bound or continuum states respectively), and inelastic effects which shorten the outgoing electron's lifetime (such as the excitation of plasmons or electron-hole pairs), should all be included in a proper treatment. (See discussions in Hayes and Boyce (1982) and Pendry (1983) for example.) Much effort has been made to incorporate a description of these effects into the one-electron scheme in an approximate way by, for example, the use of complex potentials. Questions then arise about which are the correct one-electron states to use (Stern and Rehr (1983)). It is clear that much work remains to be done in this area before a satisfactory general approach is developed. (The recent work of Bardyszewski and Hedin (1987) seems to be an important step in the right direction.)

So far nothing has been said about how the interaction with the radiation field is to be treated. There has been no indications that the usual time-dependant perturbation theory approach is inadequate for XANES calculations. The use of the dipole approximation (see e.g. Schiff (1968) p.404) is usually sufficient, although Hahn et al. (1982) have reported the detection of non-trivial features in the pre-edge region arising from quadrupole transitions.

It will be clear from the foregoing that there are various possible sources of inaccuracy in the approximations that we have already made. In this work we do not consider them in any detail, but take them as something to be held constant while we dispose of the most serious approximation that we introduce in the next section. Nevertheless they should be eventually considered and we make some comments about this in Chap. 6.

Section 2.2: The "Muffin-Tin" Approximation.

We are now left with solving an effective one-electron Schrodinger equation for the orbitals, with a potential which is the sum of (2.5,6 and 9). (The last two involve the orbitals themselves so that the equation is really a set of non-linear, coupled equations. However, it is usual to take an iterative approach so that the potentials are derived from a previous set of approximate orbitals and the solution of the equations gives a more accurate set of orbitals. It is then hoped that this process will converge quickly to a self-consistent-field (SCF) solution to the original equations. The original approximate potentials are usually derived from an electron density of a superposition of free-atom densities.)

Wherever it comes from the one-electron potential is complicated function of position and the solution of the associated Schrödinger equation is still very difficult. In general however, the potential tends to have certain characteristics. Near an atomic nucleus it is dominated by the Coulomb singularity and, within a distance of the order of one Bohr, it does not depart very much from spherical symmetry about the nucleus. Furthermore, in the region between the atoms, the potential is not very deep and varies quite slowly. With these characteristics in mind, and for the

sake of mathematical tractability, it is common to make the so-called "muffin-tin" (MT) approximation for the functional form of the potential. In this approximation the atomic nuclei are enclosed by non-overlapping MT spheres and the potential is taken to be spherically symmetric inside them. The mathematical separation of the Schrödinger equation in a central field can then be made and the remaining difficult part is the solution of the radial equation. In the interstitial region between the spheres the potential is taken to be flat so that the electron motion is governed by the free-particle equation whose solutions are well known. The main problem is now the matching of the solutions in the various regions according to the relevant boundary conditions.

Since its introduction by Slater (1937) (in the context of the augmented plane-wave method) the MT approximation has been used with varying degrees of success in a wide range of calculations of things such as band structures, molecular electronic structures and photoabsorption cross-sections. It tends to be more accurate for close-packed systems such as metals and less so for open, covalently bonded systems where the concentration of electron density along the bonds is badly modelled by spherically symmetric atoms and a flat interstitial region.

A typical prescription for the construction of an initial MT potential is that of Mattheiss (1964) in which we use free-atom electron densities (from Clementi and Roetti (1974) or Herman and Skillman (1963)) superimposed at the appropriate positions. For each atom we first solve Poisson's equation for the Coulomb part of the potential. This is quite easy since each atomic density is spherically symmetric. Using the formalism of Löwdin (1956), the overlapping part of the neighbouring atom potentials is spherically symmetrized and added to the atom's own potential. In the

interstitial region the sum of all the atomic Coulomb potentials is volume averaged to give a constant potential. A similar procedure is then followed with the electron density and (2.9) used to give the $X\alpha$ part of the MT potential.

Section 2.3: Survey of Ab Initio XANES Calculations.

The use of the MT approximation underlies virtually all of the current types of calculations of XANES. We briefly review the most successful, general methods that are now in use. These methods fall into two categories i.e. band-structure based methods and multiple-scattering methods.

The band-structure methods are exemplified by the results of Müller and co-workers (see Müller and Wilkins (1984) and further references therein). Their approach is based on the use of the linear augmented plane-wave method of Andersen (1975) and has given very impressive results for 3d and 4d transition metals. Because of its restriction to periodic systems and the calculation of the final states in the ground-state potential with no core hole, the applicability of this method seems rather limited. Also its successes are associated only with metals for which the MT approximation is not so bad. There appears to be no immediate prospect that the formalism can be easily generalized to accomodate non-MT potentials.

A more general approach is provided by the multiple-scattering methods of which there are two main types. These are not restricted to periodic systems and, indeed, are most frequently applied to molecules or clusters of atoms taken from crystalline or amorphous solids (wherein lies their great utility).

The first of these methods is due to Durham and co-workers (see the recent review by Durham (1988) for further references).

This method is an extension of the usual single-scattering EXAFS theory (e.g. that of Lee and Pendry (1975)) to the near-edge region. It takes into account explicitly the details of the scattering of the excited electron by the atoms of the cluster and has been reasonably successful at reproducing qualitatively features of the XANES of a variety of systems. Nevertheless it is tied to the MT approximation for the potential and is still less than satisfactory for open, covalently bonded clusters.

The other multiple-scattering method is an adaptation of the band-structure formalism of Korringa (1947), Kohn and Rostoker (1954), to clusters. Under the name "multiple-scattered-wave $X\alpha$ method" it was developed by Johnson and co-workers (see Johnson (1966), Smith and Johnson (1969), Slater and Johnson (1972), Johnson and Smith (1972), Johnson (1973) (a review of the theory and main applications) and Johnson (1975) (a complete review of applications) for bound states, and by Dill and Dehmer (1974) for continuum states and photoionization. Applications to XANES were made by Natoli et al. (1980) and by Kutzler et al. (1980), with similar results to those of Durham and co-workers. It is somewhat more cumbersome than their method and uses likewise the MT approximation. However, as we describe later, its greater generality allows it to be adapted for more realistic, non-MT potentials; and it is for this reason that we restrict our attention from now on to this method.

It may turn out to be possible to incorporate non-MT potentials into the other XANES methods, but this has not been demonstrated and we do not consider them further. A general overview of the problems of XANES may be seen in Pendry (1983) and Doniach et al. (1984).

Section 2.4: Calculations for Chromium Hexacarbonyl.

To get an idea of the kind of results that the MT-based scattered-wave (SW) method gives, we performed some calculations for a model compound chromium hexacarbonyl $Cr(CO)_6$. This molecule was chosen because (a) it has high symmetry reducing the computational effort; (b) many of its electrons are involved in bonds, particularly in the CO ligands; and (c) it has been extensively studied (see Arratia-Perez and Yang (1985) and references therein) by different methods as a prototype for CO bonding to metals. It consists of a central chromium atom coordinated by six carbonyl ligands in an octahedral configuration such that the carbon atoms are adjacent to the chromium atom. The point group is thus O_h for which there are ten irreducible representations (irreps) denoted A_{1g}, A_{1u}, A_{2g}, A_{2u}, E_g, E_u, T_{1g}, T_{1u}, T_{2g} and T_{2u} according to the Mulliken (1955) scheme. Chromium hexacarbonyl is a white, crystalline solid at room temperature of density 1.77 g cm^{-3}. It crystallizes according to the Pnma space group with four molecules per unit cell and cell dimensions: a = 11.769(12) Å, b = 11.092(11) Å and c = 6.332(6) Å (Whitaker and Jeffery (1967)). The mean bonding distances (uncorrected for thermal vibration) are 1.909(3) Å (3.6075(57) Bohr) for chromium-carbon and 1.137(4) Å (2.1486(75) Bohr) for carbon-oxygen.

There have been many electronic structure calculations performed for this molecule, particularly the SW-Xα ones of Johnson and Klemperer (1977) and the relativistic SW ones of Arratia-Perez and Yang (1985). These are of course only bound-state calculations and there seems to have been no previous application of the SW method to the XANES of chromium hexacarbonyl.

Our SW calculations for $Cr(CO)_6$ follow the general scheme given in Natoli et al. (1980) and Kutzler et al. (1980), and we use

the same programs, given to us by CRM, as were mentioned above. In brief, the program suite operates as follows. Given the structure of some molecule the program MOLPOT uses superimposed free-atom charge densities to generate an initial approximation to the one-electron molecular potential. For molecules with point symmetry, the program MOLSYM generates the linear combinations of spherical harmonics at the atomic sites which transform according to the irreps of the point group. (The use of these linear combinations reduces the size of the secular matrices arising in the SW formalism. Although point symmetry is not a necessity, this particular group of programs is optimized to use them.) The initial potential is passed to the program ENERGY which searches for the bound-state eigen-energies. Having found these energies the program SCF iterates on the successive densities arising from the one-electron bound-states in the successive potentials until it reaches self-consistency. The self-consistent final potential may be the ground state, a bound excited state or an ionized state, depending upon the previously specified occupation numbers of the one-electron states found by ENERGY. The program CONTNM then calculates the photoionization cross-sections from a core level in the SCF ground state to either discrete, bound final states or to the continuum of the ionized state.

The form of the potential used by these programs is of course restricted to the MT form, and one must decide upon the various parameters of the approximation beforehand. Firstly, we choose the α values in the Xα potential for each atom in the molecule from Schwarz's (1972) paper. This means $\alpha(Cr) = 0.71352$, $\alpha(C) = 0.75928$ and $\alpha(O) = 0.74447$. For the volume outside the atoms we take a weighted average of these as 0.74892. The more important decision is how to choose the radii of the atomic spheres and the

outer sphere enclosing the molecule. There is a certain degree of arbitrariness in this choice, but often it is chosen to minimize the potential discontinuities at the sphere boundaries. For $Cr(CO)_6$ we chose the C and O spheres so that they touched and so that the potential was matched at the contact point. The Cr sphere was then increased to touch the C spheres and the outer sphere (OS) brought in to be tangent to the O spheres. This meant that the sphere radii were: b(OS) = 6.815 Bohr, b(Cr) = 2.5177 Bohr, b(C) = 1.0897 Bohr and b(O) = 1.0588 Bohr. For each sphere we had also to decide on the maximum l for the partial waves in the wavefunction expansion. For the bound-state part of the calculations (ENERGY and SCF) these were l(max) = 6(OS), 6(Cr), 3(C) and 3(O); somewhat more than would usually be taken. For the XANES calculations we took l(max) = 9(OS), 9(Cr), 5(C) and 5(O). These choices stem from earlier experience with the programs, for a wide variety of systems, of the appropriate l-truncations at which the expansions tend to be well converged.

The usual way of calculating XANES with CONTNM is to take the dipole matrix element between the core wavefunction in the self-consistent ground state and the continuum wavefunction in the self-consistent ionized state. However, we shall consider two further cases. The first uses the initial overlapped free-atom potential from MOLPOT for the initial and final states. The second uses this potential for the initial state, but a variety of "Z+1" potential (see e.g. Pendry (1981)), constructed by MOLPOT, for the final state. In our version of the Z+1 potential, we use the wavefunctions of manganese for the excited chromium, with a 1s electron removed to model the core hole.

A plot of the three different final-state potentials may be seen in Fig. 2.1. Note particularly the large discontinuities, in

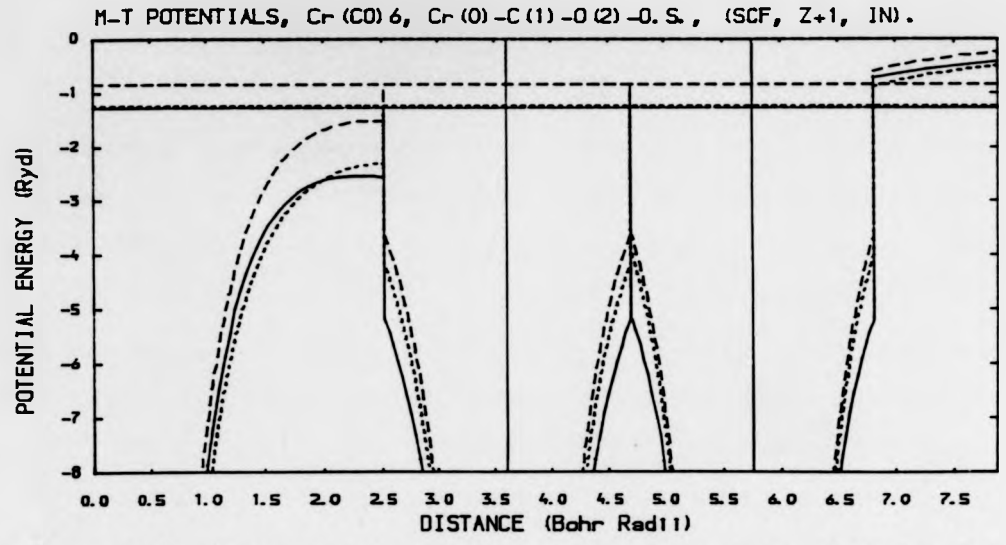

Figure 2.1: MT potentials of 3 final states used for CONTNM - SCF (solid line), Z+1 (fine broken l.), IN (coarse br. l.) Values along traverse (L to R) from Cr nucleus, through C and O nuclei (vertical lines), to just outside outer sphere.

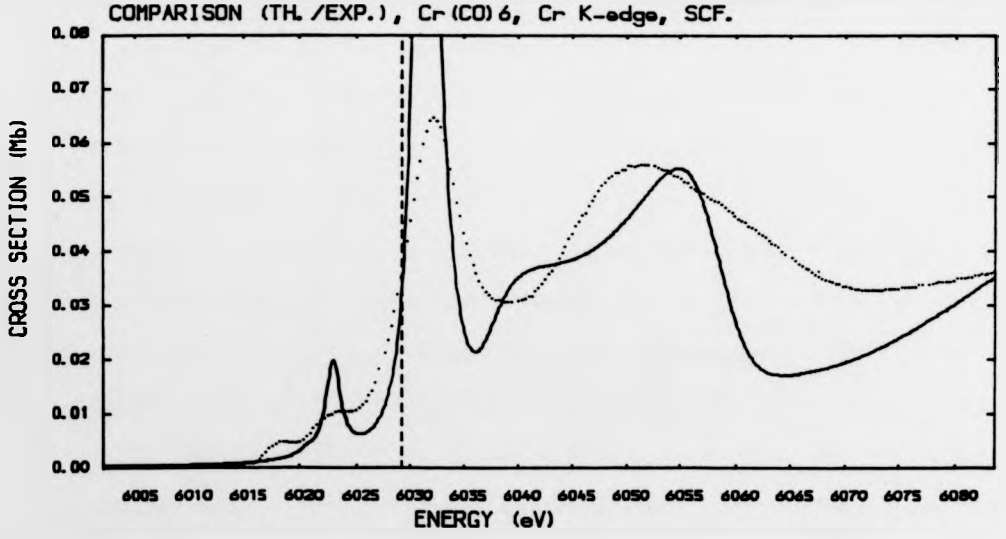

Figure 2.2: Comparison of experimental XANES (dotted line) of chromium hexacarbonyl with the theoretical values (solid line) from CONTNM. The broken vertical line shows the continuum threshold. The peak at 6031 eV goes up to 0.208 Mb.

all three cases, at the C and O sphere boundaries. Here the potential jumps suddenly by 3 to 4 Ryd., comparable with the range of photoelectron energies in XANES. These extreme values stem from the short length of the C-O triple bond, combined with the large volume of the interstitial region making the average potential high relative to the potentials at the edges of the atomic spheres.

In Fig. 2.2 we see the comparison between theory and experiment for the Cr K-edge XANES of chromium hexacarbonyl. The theoretical curve results from the use of CONTNM with self-consistent ground-state and ionized potentials. It has been convoluted with a Lorentzian of 1.5 eV full width at half maximum (FWHM) to model the effects of core-hole lifetime and instrumental resolution (as in Natoli et al. (1980)). The position of the ionization threshold should, in principle, be obtained from the difference between the total energies of the ground and ionized states given by SCF. The resulting value in this case is about 439 Ryd. (= 5973 eV), but this is not a good enough estimate because the fundamental approximation to the hamiltonian is not sufficiently accurate. Therefore we shift the theoretical curve so that the first continuum peak is aligned with the corresponding experimental one.

The experimental curve was from a crystalline powder sample at room temperature (prepared by RFP) and was measured by J. Röhler and his group (Köln University) on the Kiel EXAFS beam-line in HASYLAB (DESY, Hamburg) in April 1985. The energy resolution of the experiment was about 1 eV. Since absolute cross-sections are not normally available for experimental curves, we have (following a suggestion of RFP) normalized it to the edge jump of 42.03 kb for chromium from the tables of McMaster et al. (1969), to get an approximate idea of how good the theoretical values were.

In fact the average magnitude of the theoretical curve is about right. The size of the oscillations is too large, particularly the main continuum peak just above the threshold. The shape of the broader, second peak is also quite distorted. Below the edge we do indeed find the two bound-state peaks that appear in the experimental curve, but they are of the wrong strength and separation.

In Fig. 2.3 we see a comparison that includes the other two choices for the initial and final states. These curves are of the same poor quality as the SCF case. (If anything the "INIT" case appears to be closest to experiment and, surprisingly, the SCF case the worst.) Clearly the poor approximation that the MT gives for the potential of chromium hexacarbonyl is having a very deleterious effect on the quality of the theoretical XANES calculations.

Several ad hoc schemes to ameliorate the bad effects of the MT approximation for open, covalently bonded systems, have been proposed in the literature. We tried the two most promising of these schemes for chromium hexacarbonyl and we show the results below. The first of these allows the MT spheres to overlap each other, partly so that the volume of the interstitial region is reduced (and also the potential discontinuities at the sphere boundaries) and partly to model in a crude way the build up of charge between atoms that is associated with a covalent bond. This scheme is discussed in Rösch et al. (1973) and, with an example, in Herman et al. (1974). The second scheme, suggested by Keller (1971), tries to partition as much of the interstitial volume as possible into empty interstitial spheres which are then treated in a scattering sense as pseudo-atoms. In Fig. 2.4 the MT potentials that we used to test these schemes are shown.

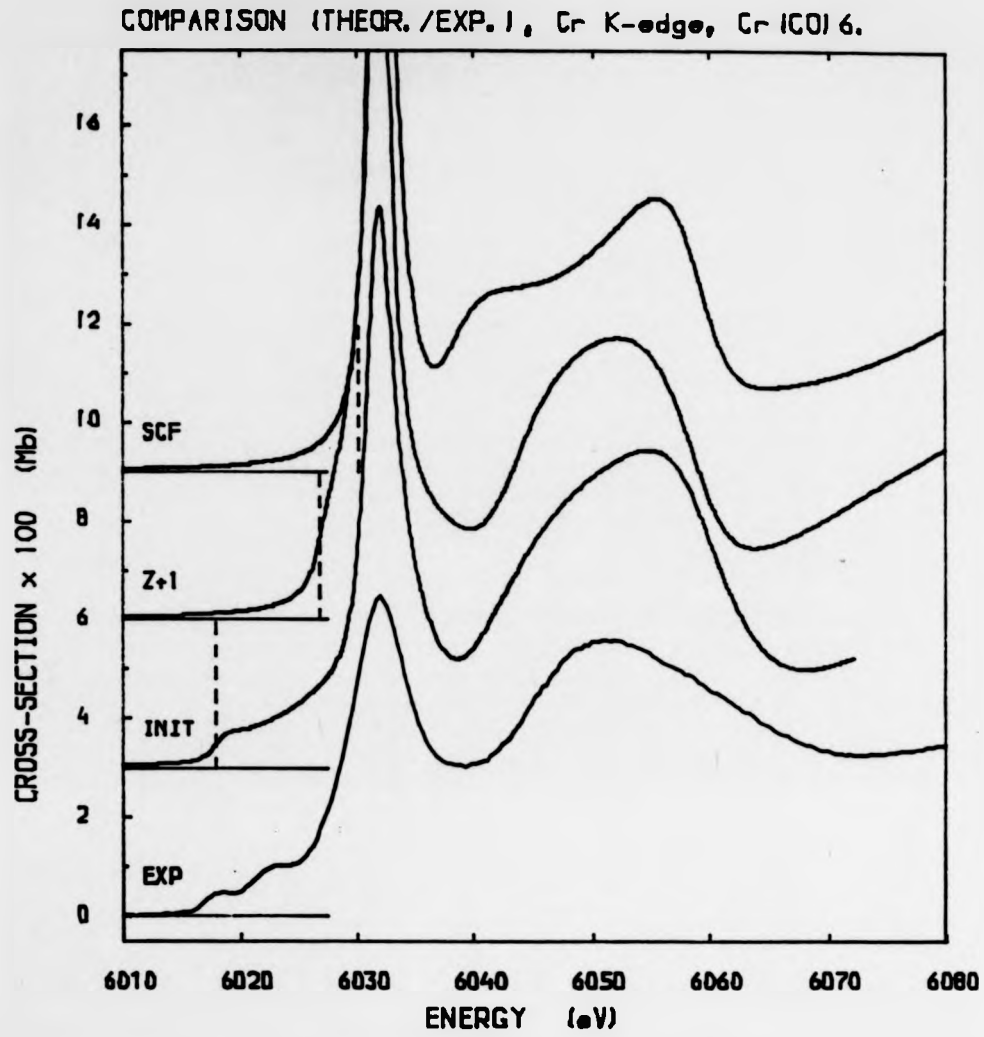

Figure 2.3: Chromium hexacarbonyl Cr K-edge XANES comparison between experiment and theory for 3 final states in the case of touching spheres. The peak heights at 6031 eV are 0.208 Mb for SCF and 0.164 Mb for Z+1. The broken lines for each theoretical curve mark the continuum threshold. No bound-state transitions have been included in the theoretical curves.

The choice of sphere radii for the MT potentials in these calculations follows the criteria of Norman (1976) in an attempt to reduce the inherent arbitrariness of the whole MT approximation.

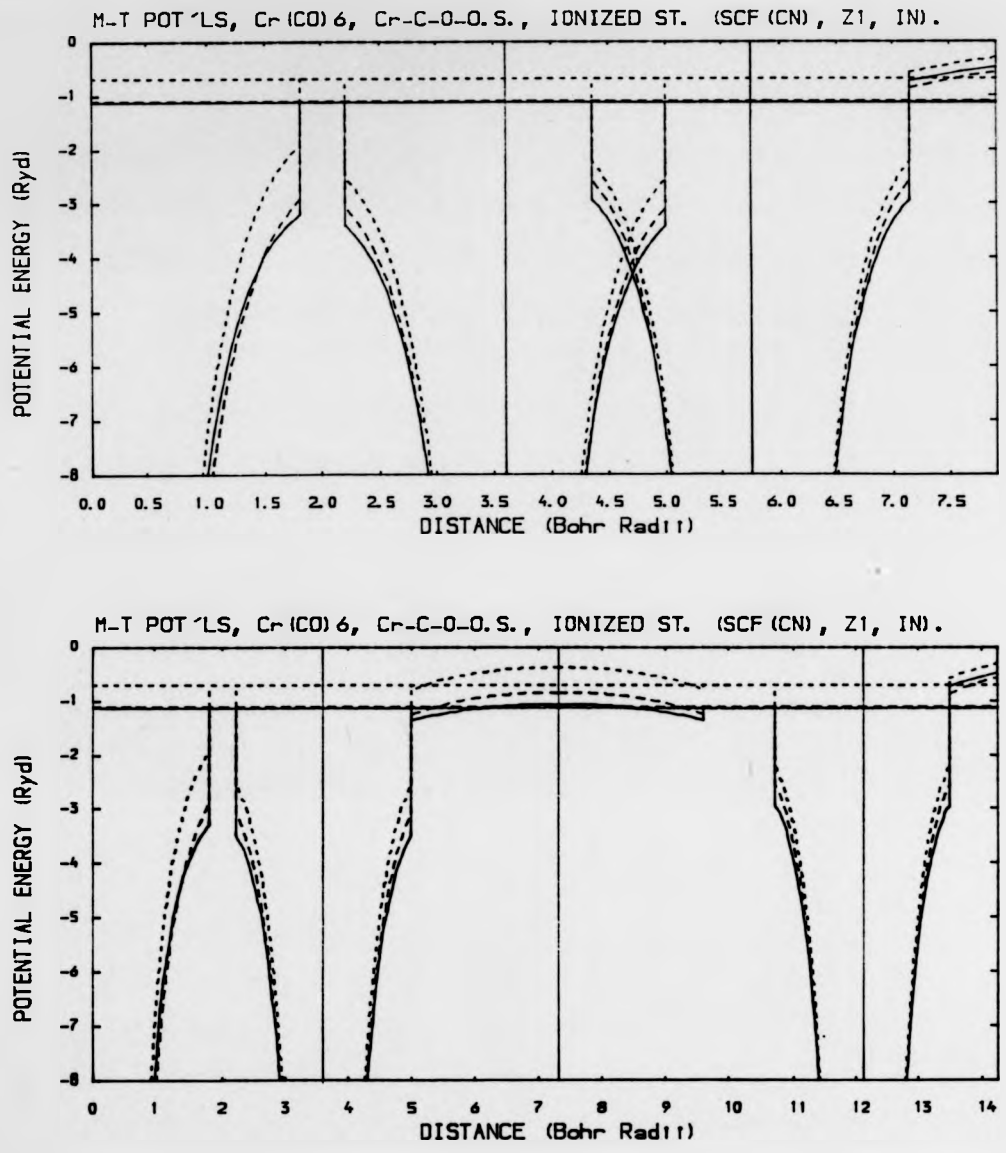

Figure 2.4: MT potentials of the three final states used, in the overlapping-sphere and empty-interstitial-sphere cases (top and bottom respectively), for CONTNM. The empty-spheres potential is that of the overlapping-spheres case with eight empty spheres included and the traverse shown being diverted between C and O to the centre of an empty sphere.

These new radii, 30% overlapped from touching C and O spheres, are: b(OS) = 1.8305 Bohr, b(Cr) = 1.3199 Bohr, b(C) = 1.3965 Bohr and b(O) = 1.3967 Bohr. Eight spheres, with b(ES) = 2.3053 Bohr, with centres on the corners of a cube (maintaining O_h symmetry), touching the Cr and outer spheres, are then introduced to give the empty-sphere potential. In Figs. 2.5 and 2.6 we see the resu-

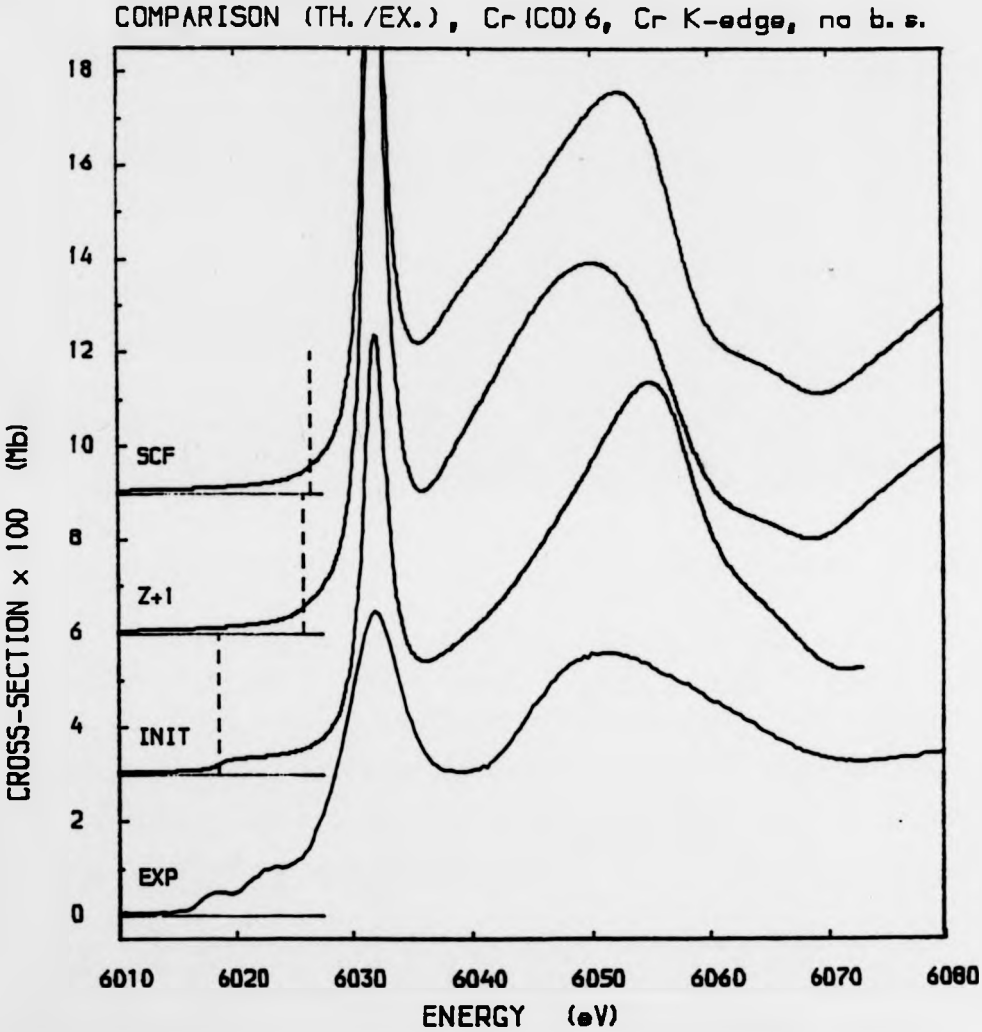

Figure 2.5: $Cr(CO)_6$ Cr K-edge XANES comparison between experiment and theory for 3 final states in the overlapping spheres case. The 6031 eV peak heights are 0.156 Mb (SCF) and 0.167 Mb(Z+1).

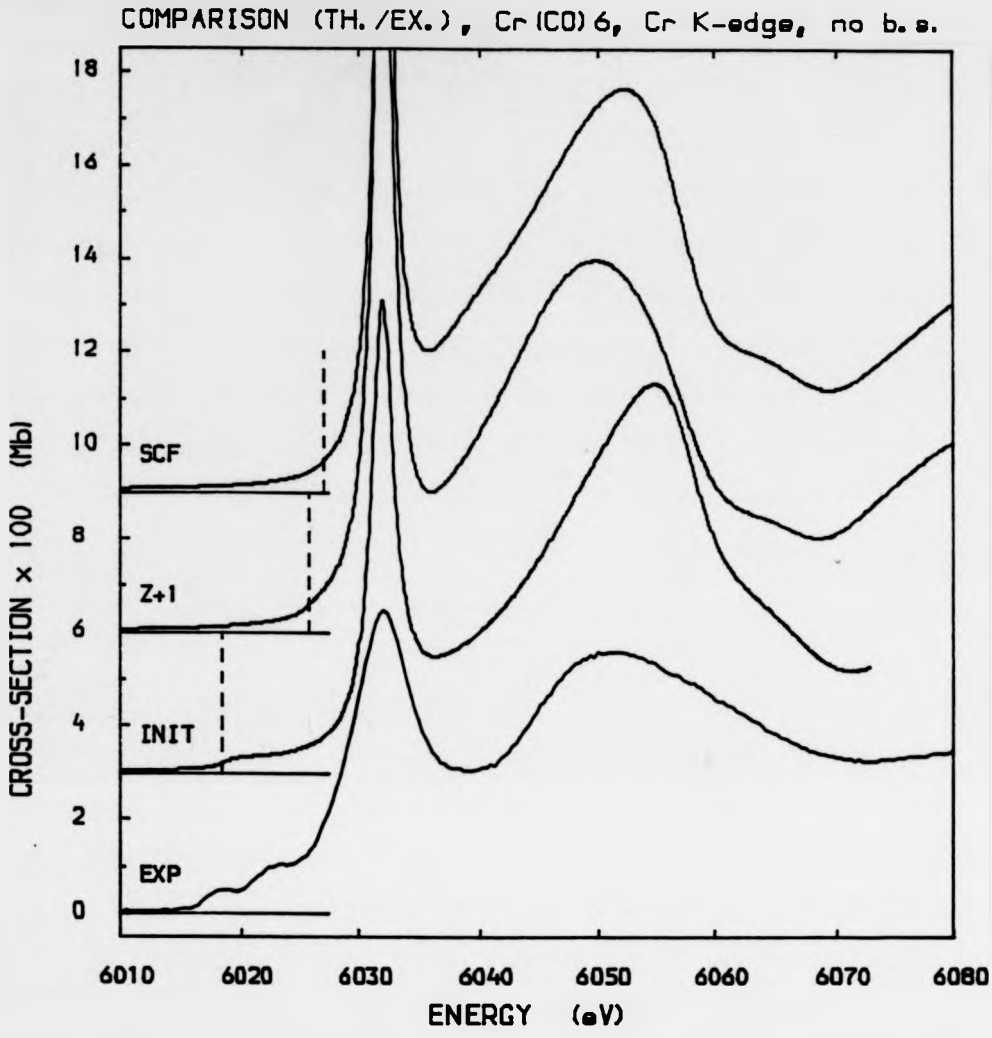

Figure 2.6: $Cr(CO)_6$ Cr K-edge XANES comparison between experiment and theory for 3 final states in the empty-interstitial-sphere case. The 6031 eV peak heights are 0.165 Mb (SCF) and 0.177 Mb (Z+1).

lts of CONTNM for the two new MT potentials. It is clear that they do not give any great improvement over Fig. 2.3, the use of empty interstitial spheres in particular hardly having any effect at all. We note in general that the form of the theoretical curves is quite sensitive to the choice of final state, which is its-

elf a non-trivial question of the physics of the photoionization process. On the other hand it is also sensitive to the unphysical parameters of the MT partition of space. What is surprising to us is that the use of self-consistency brings no improvement and it may be that the MT constraint, since it is reimposed at each iteration, may "sabotage" the whole SCF process.

Further ad hoc schemes may be devised to ameliorate the problems of the MT approximation while remaining within it. (For example one might simply remove any discontinuities by resetting the atomic potentials upwards.) Such schemes however, are devoid of any physical content since they are merely responding to the arbitrary parts of the MT approximation rather than making any contact with the original full potential.

Section 2.5: Discussion and Review.

It is instructive to try to relate deficiencies in theoretical XAFS with particular features of the MT approximation. Such a relationship may be seen even at the higher energies characteristic of EXAFS. In single-scattering expressions for the EXAFS (see e.g. Lee and Pendry (1975)) one finds that the amplitude of the EXAFS is proportional to the sum of terms for each scattering atom with, as coefficient, the back-scattering amplitude of that atom. Fig. 2.7 shows theoretical back-scattering amplitudes (actually their moduli) for an oxygen atom in which the MT radius is varied. One can see that there are spurious oscillations in the curves whose wavelength and phase depend on the (unphysical) MT radius. Since EXAFS is an oscillatory phenomenon, any spurious oscillations arising from the theory must be entirely unwelcome. Note that the size of these oscillations increases as we go down in energy to the XANES region.

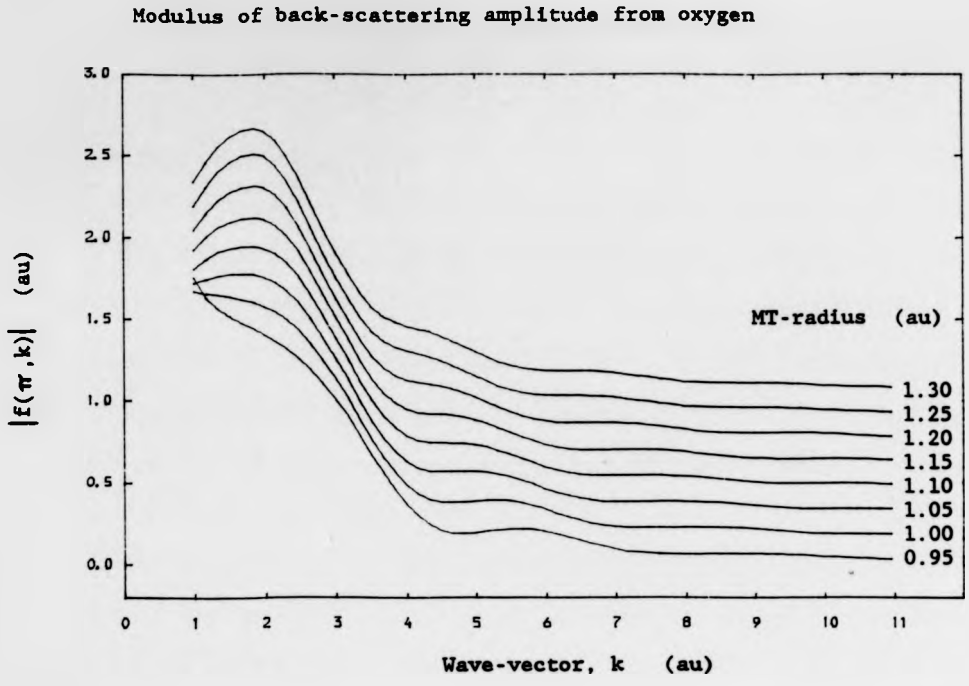

Figure 2.7: Effects of MT sphere potential discontinuities on back-scattering amplitudes. These amplitudes were calculated with the phase-shift program MTAHARA. Normally such amplitudes may be used in ab initio EXAFS fitting programs (like EXAFSFT described by Pettifer and Cox (1983)) to extract structural information from experimental spectra by, say, a least-squares procedure. One suspects that any spurious oscillations arising from the MT approximation would tend to distort the results.

It is clear that, at least for a certain class of systems for which the MT approximation is bad, the attainment of greater accuracy in ab initio XANES calculations requires a more serious attempt to go beyond that approximation. We now turn to a consideration of schemes that have appeared in the literature.

There have been several groups who, while not presenting any generally applicable method for incorporating non-MT corrections,

have performed detailed calculations to investigate their nature and extent. Danese and co-workers (see Danese (1974,1977) and Danese and Connolly (1974)) use a Monte Carlo integration method to estimate MT errors in ground-state total energy calculations by the SW method for some diatomic systems. In particular, they found that the non-MT corrections result in qualitative and quantitative improvements in the potential curves (as a function of nuclear separation) of these two systems. (MT calculations failed even to give binding, whereas the inclusion of non-MT corrections gave binding energies and equilibrium nuclear separations within 10% of their experimental values.)

Rumble and Truhlar (1980) have investigated the deficiencies of the MT approximation in the SW calculation of the total cross-section for electron-N_2 scattering at 5 to 30 eV. They found errors of up to 30% in the cross-sections when compared with those from reasonably well-converged close coupling calculations (that do not use the MT approximation).

More general approaches seem to begin with the work of Beleznay and Lawrence (1968) who relax the restriction of constancy on the interstitial region potential and derive the resulting modifications to the KKR secular determinants in band-structure calculations. Evans and Keller (1971) remove the restriction on spherical symmetry of the potential in the atomic spheres and show how to solve the resulting coupled radial equations. A large review by Lloyd and Smith (1972) brought together in one consistent treatment the available material on multiple-scattering theory that includes non-MT developments.

A major idea was the extension by Williams and Morgan (1974) of SW theory to band-structure calculations based on atom-centred space-filling polyhedral cells. There have been many re-workings

of this idea, most importantly those of Faulkner (1979,1985,1986) and Brown and Ciftan (1983,1985,1986). Other variants have been given by Keister (1983), Gonis (1986), Zeller (1987), Badralex (1987,1988) and Molenaar (1988). Numerical tests have been made with several systems, e.g. the empty lattice (Faulkner (1985)), Si (Williams and Morgan (1974)), Cu and graphite (Altmann et al. (1978). But the results, while generally indicating a great improvement over the MT case, are unclear and inconclusive, and a controversy has arisen in the literature over convergence problems in certain mathematical expansions, that stem from the non-sphericity of the atomic cells.

With special reference to molecular clusters Scherz (1972) adds a spherically symmetric part to the interstitial-region potential, while Ziesche (1974) introduces a scheme similar to that of Williams and Morgan (1974) above (describing similar problems of convergence). Siegel et al. (1976) relax the spherical symmetry restriction in the atomic spheres, but their formalism is unnecessarily cumbersome. A better version of the same thing was given by Volkov and Poluyanov (1980).

The clearest treatment of the non-MT SW formalism was that of Natoli et al. (1986), deriving in many respects from the work of Lloyd and Smith (1972). This treatment allows the generalization of the potential both in the atomic spheres and in the interstitial region and the remainder of this thesis is based upon it.

Chapter 3. EXTENDED SCATTERED-WAVE THEORY.

Section 3.1: The Partition of Molecular Space.

Having chosen an appropriate one-electron potential $V(\vec{r})$, the main task is to solve the Schroedinger equation for an electron in that potential. This is the case whether we are looking for bound states or calculating photoionization cross-sections. The essence of the scattered-wave (SW) method lies in the division of three-dimensional space ($\mathbb{R}^3$) and the subsequent separate treatment of the solution in each region.

In particular, we have a molecule (or finite cluster of atoms) whose atomic nuclei have position vectors $\vec{R}_i$ referred to the origin of coordinates O; where $i = 1,2,\ldots,N$ runs through all the atoms. These nuclear positions are thus the locations of the Coulomb singularities in $V(\vec{r})$. We now partition the molecular space as follows. Each atomic centre is enclosed in a spherical region τ_i of radius b_i ;

$$\tau_i \equiv \{\vec{r} \in \mathbb{R}^3 : |\vec{r} - \vec{R}_i| < b_i\} \qquad (3.1).$$

These "atomic spherical regions" (ASRs) are taken to be mutually disjoint (non-overlapping) so that

$$(i \neq j) \Rightarrow (\tau_i \cap \tau_j = \emptyset \ , \quad b_i + b_j \leqslant |\vec{R}_i - \vec{R}_j|) \qquad (3.2).$$

The whole molecule is then enclosed in an "outer sphere" (OS) (or molecular sphere) τ_o of radius b_o centred on $\vec{R}_o$, which contains all the ASRs. Thus

$$\tau_o \equiv \{\vec{r} \in \mathbb{R}^3 : |\vec{r} - \vec{R}_o| \leqslant b_o\} \qquad (3.3)$$

with $\tau_i \subset \tau_o$ and $|\vec{R}_i - \vec{R}_o| + b_i \leqslant b_o$ for $i = 1,2,\ldots,N$ (3.4).

We denote the surfaces of all these spheres by

$$\partial\tau_i \equiv \{\vec{r} \in \mathbb{R}^3 : |\vec{r} - \vec{R}_i| = b_i\} \qquad \text{for } i = 0,1,\ldots,N \quad (3.5).$$

The "extra-molecular region" (EMR) is that outside the OS, i.e. $\bar{\tau}_o$ (the complement of τ_o). The "interstitial region" (IR), den-

oted I, is that within the OS but outside the ASRs; so that

$$I \equiv \tau_o \cap \left(\bigcup_{i=1}^{N} \tau_i\right) \qquad (3.6).$$

The ASRs and the EMR together will be collectively called the "spherically symmetric regions" (SSRs). Here the radial Schrödinger equation is solved explicitly, whilst in the IR an indirect approach is used. Thus we have our complete partition of space,

$$\mathbb{R}^3 = I \cup \overline{\tau_o} \cup \left(\bigcup_{i=1}^{N} \tau_i\right) \qquad (3.7).$$

It will usually be the case that $\vec{R}_o = \vec{0}$ and that the photo-absorbing atom will be $i = 1$ with $\vec{R}_1 = \vec{R}_o$. We define the relative position vectors, between sphere centres, to be

$$\vec{R}_{ij} \equiv \vec{R}_i - \vec{R}_j \qquad (3.8).$$

For some general position vector $\vec{r}$ we denote the position vector relative to sphere centre $\vec{R}_i$ as

$$\vec{r}_i \equiv \vec{r} - \vec{R}_i \qquad (3.9).$$

Section 3.2: Secular Equation in the Bound-State Case.

We seek a bound-state solution $\Psi(\vec{r})$ to the Schrödinger equation with potential $V(\vec{r})$ such that $V(\vec{r}) \longrightarrow 0$ as $r \longrightarrow \infty$, and $V(\vec{r})$ has poles at $\vec{R}_i$ ($i = 1,2,\ldots,N$). To do this we use the integral version of the equation;

$$\Psi(\vec{r}) = \int G_o^+(\vec{r},\vec{s})\, V(\vec{s})\, \Psi(\vec{s})\, d^3s \qquad (3.10),$$

where G_o^+ is the appropriate free-particle Green function. The following development is an adaptation of the continuum case of Natoli et al. (1986) made by us to be similar to the MT bound-state algebra of Johnson (1973) in certain (particularly notational) respects.

To reduce the effect of the non-constant IR potential, we reset the zero of the potential to V_o and we choose this to be the average of the potential in the IR. Thus $V(\vec{r}) \rightarrow V(\vec{r}) - V_o$ and

$$V_o = \overline{V_I} \equiv \int_I V(\vec{s})\, d^3s \,/\, \int_I d^3s \qquad (3.11).$$

If the energy of the bound state is E, then we must therefore consider the two energy ranges $E < V_o$ and $V_o < E < 0$ differently.

Our first step is to split up the integration in (3.10) according to the partition of (3.7). Thus

$$\psi(\vec{r}) = \left(\int_I + \int_{\tau_o} + \sum_{i=1}^{N} \int_{\tau_i} \right) G_o^+(\vec{r},\vec{s})\, V(\vec{s})\, \psi(\vec{s})\, d^3s \qquad (3.12).$$

We then use Green's Theorem to convert the volume integrals over the SSRs into surface integrals over their spherical boundaries. The theorem is used in the form

$$\int_\tau [P(\nabla^2 + E)Q - Q(\nabla^2 + E)P]\, d^3s = \int_{\partial\tau} [P\nabla Q - Q\nabla P]\cdot \hat{n}\, d\sigma \qquad (3.13),$$

where $\hat{n}$ is the outward pointing normal to the surface $\partial\tau$. Making the correspondances $P(\vec{s}) \rightarrow G_o^+(\vec{r},\vec{s})$ and $Q(\vec{s}) \rightarrow \psi(\vec{s})$, and noting (A32) and that

$$(\nabla^2 + E)\,\psi(\vec{s}) = V(\vec{s})\,\psi(\vec{s}) \qquad (3.14),$$

we get, for any volume τ, that

$$\int_\tau G_o^+(\vec{r},\vec{s})\, V(\vec{s})\, \psi(\vec{s})\, d^3s = \int_\tau \psi(\vec{s})\, \delta^3(\vec{r}-\vec{s})\, d^3s$$

$$+ \int_{\partial\tau} [G_o^+(\vec{r},\vec{s})\nabla\psi(\vec{s}) - \psi(\vec{s})\nabla_s G_o^+(\vec{r},\vec{s})]\cdot\hat{n}\, d\sigma \qquad (3.15).$$

From (3.12,15) we then obtain

$$\psi(\vec{r})\,\delta_I(\vec{r}) = \int_I G_o^+ V\psi + \left(\int_{\partial\tau_o} + \sum_{i=1}^{N} \int_{\partial\tau_i} \right) [G_o^+\nabla\psi - \psi\nabla G_o^+]\cdot\hat{n}\, d\sigma \qquad (3.16),$$

where we have defined

$$\delta_\tau(\vec{r}) \equiv \int_\tau \delta^3(\vec{r}-\vec{s})\, d^3s \qquad (3.17)$$

and used the resulting properties

$$\delta_A(\vec{r}) + \delta_B(\vec{r}) = \delta_{A\cup B}(\vec{r}) + \delta_{A\cap B}(\vec{r}) \qquad \delta_{\mathbb{R}^3}(\vec{r}) = 1 \qquad (3.18).$$

The next step is to use explicit forms for G_o^+ and to take advantage of the spherical nature of the surface integrals in (3.16), to expand them out in a more convenient form. Before we do this we need expressions for $\psi(\vec{r})$ inside the SSRs from which we can obtain the values and gradients on their boundaries. In Natoli et al. (1986) it is shown that we must first expand the potential in a SSR in spherical harmonics about its centre;

$$V(\vec{r}) = \sum_L V_L^i(\vec{r}_i)\, Y_L(\hat{r}_i) \qquad (i = 0,1,2,\ldots,N\ ;\ L \equiv (\ell,m,\alpha)) \quad (3.19).$$

The wavefunction in the SSR is then written

$$\Psi(\vec{r}) = \sum_L \sum_{L'} C_L^i\, R_{LL'}^i(r_i)\, Y_L(\hat{r}_i) \qquad (3.20),$$

where the C_L^i are as yet undetermined coefficients and the $R_{LL'}^i$ satisfy the coupled radial Schrödinger equations

$$\left(\frac{1}{r^2}\frac{d}{dr}\left(r^2\frac{d}{dr}\right) + E - \frac{\ell(\ell+1)}{r^2}\right) R_{LL'}^i(r) = \sum_{L''} U_{LL''}^i(r)\, R_{L''L'}^i(r) \qquad (3.21)$$

with (using (A30) from App. A)

$$U_{LL'}^i(r) \equiv \sum_{L''} I(L,L',L'')\, V_{L''}^i(r) \qquad (3.22).$$

At this stage we must consider the two energy ranges separately and we take the case $E < V_0$ first, defining $\kappa \equiv \sqrt{V_0 - E}$. We now use the negative energy Green function of (A33) and the wavefunctions of (3.20) to expand (3.16). The precise way these may be used depends upon which regions of the partition the variable $\vec{r}$ and the dummy variable $\vec{s}$ lie in; the relation between the two determining how the re-expansion formulae (A40-44) are applied. The possible relations are shown in Fig. 3.1 and we refer to them individually as we proceed.

We consider three general cases with $\vec{r} \in \tau_i$, $\vec{r} \in \bar{\tau}_0$ and $\vec{r} \in I$. For each case we treat the individual terms on the RHS of (3.16) separately as sub-cases, bringing them all together at the end.

Case 1: $\vec{r} \in \tau_i$ for some $i = 1,2,\ldots,N$:-

Sub-case (i): $\vec{s} \in I$:- This term is left in the form

$$\text{Term}\ (i,I) \equiv \int_I G_0^+(\vec{r},\vec{s})\, V(\vec{s})\, \Psi(\vec{s})\, d^3s \qquad (3.23).$$

Sub-case (ii): $\vec{s} \in \partial\tau_i$:- From Fig. 3.1(a) it may be easily seen that $\vec{r} - \vec{s} = \vec{r}_i - \vec{s}_i$ and that $r_i < s_i$. The Green function (A33) may be therefore expressed as

$$G_0^+(\vec{r},\vec{s}) = -\kappa \sum_L (-1)^\ell i_\ell(\kappa r_i)\, k_\ell^{(1)}(\kappa s_i)\, Y_L(\hat{r}_i)\, Y_L(\hat{s}_i) \qquad (3.24).$$

Using (3.20,24) we have

$$\text{Term}\ (i,i) \equiv \int_{\partial\tau_i} \left[G_0^+(\vec{r},\vec{s})\nabla\Psi(\vec{s}) - \Psi(\vec{s})\nabla_s G_0^+(\vec{r},\vec{s})\right]\cdot \hat{s}_i\, b_i^2\, d\Omega_i$$

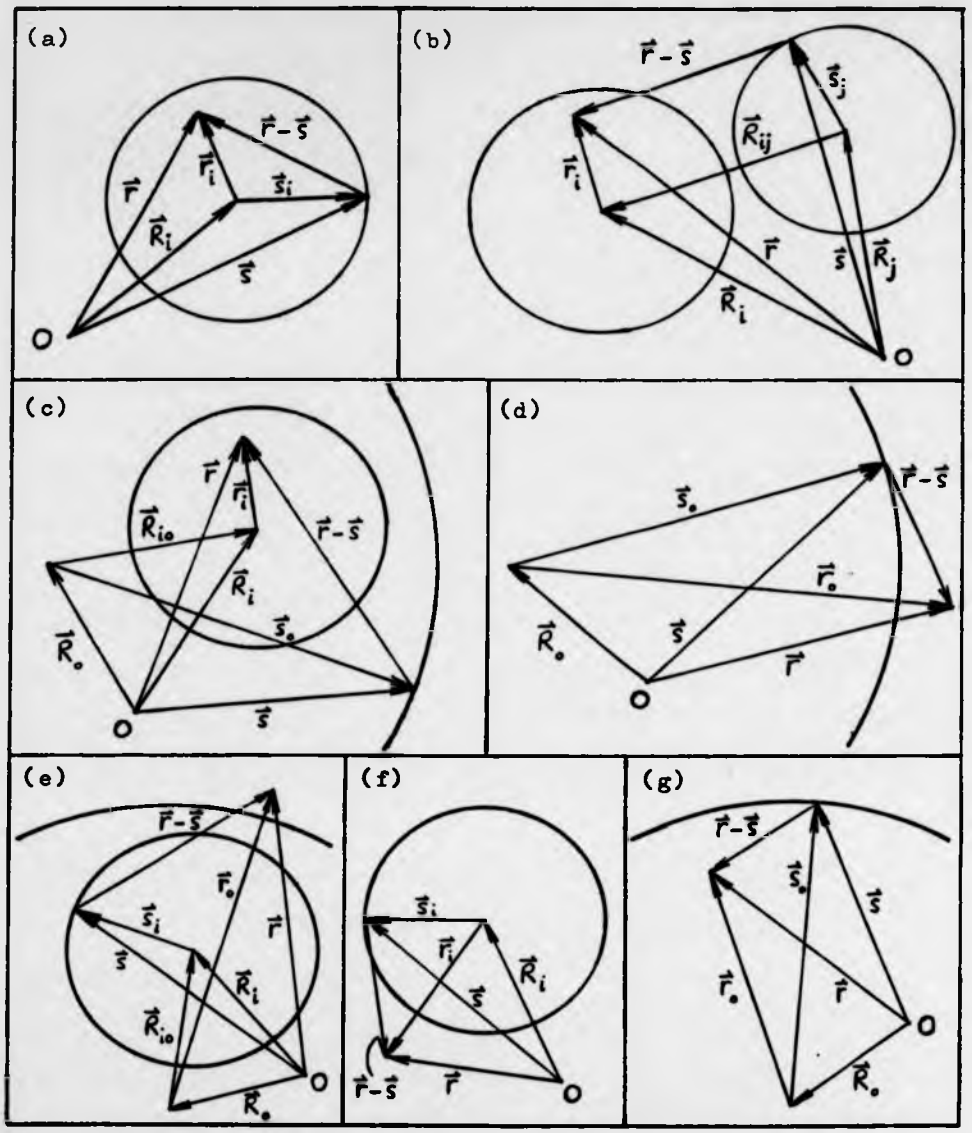

Figure 3.1: Various relevant relations between vectors involved in the evaluation of the surface integral terms arising in the solution of the Schrödinger equation.

$$= \int_{\partial\tau_i} \left[G_o^+ \frac{\partial\psi}{\partial s_i} - \psi \frac{\partial G_o^+}{\partial s_i} \right] b_i^2 \, d\Omega_i$$

$$= -\kappa b_i^2 \sum_L (-1)^l i_l(\kappa r_i) Y_L(\hat{r}_i) \left\{ \sum_{L'} \sum_{L''} C^i_{L'} \int_{\partial\tau_i} Y_L(\hat{s}_i) Y_{L''}(\hat{s}_i) \, d\Omega_i \right.$$

$$\left. \times \left[k_l^{(1)}(\kappa b_i) R^{i'}_{L''L'}(b_i) - \kappa k_l^{(1)\prime}(\kappa b_i) R^i_{L''L'}(b_i) \right] \right\}$$

$$= -\kappa b_i^2 \sum_L (-1)^l i_l(\kappa r_i) Y_L(\hat{r}_i) \sum_{L'} W[k^{(i)}, R^i]_{LL'} C^i_{L'} \qquad (3.25),$$

where, in the last step, we have used the orthonormality of the spherical harmonics to get rid of the summation over L'' and we have defined the matrix Wronskian

$$W[k^{(i)}, R^i]_{LL'} \equiv k_l^{(i)}(\kappa b_i) R^{i\prime}_{LL'}(b_i) - \kappa k_l^{(i)\prime}(\kappa b_i) R^i_{LL'}(b_i) \qquad (3.26).$$

Sub-case (iii): $\vec{s} \in \partial\tau_j$ for $j \neq i$:- From Fig. 3.1(b) we see that $\vec{r} - \vec{s} = \vec{r}_i - (\vec{s}_j - \vec{R}_{ij})$, $|\vec{s}_j - \vec{R}_{ij}| > r_i$ and $R_{ij} > s_j$, since the atomic spheres are assumed to be non-overlapping. We may thus express (A33) as

$$G_o^+(\vec{r},\vec{s}) = -\kappa \sum_L (-1)^l i_l(\kappa r_i) k_l^{(i)}(\kappa|\vec{s}_j - \vec{R}_{ij}|) Y_L(\hat{r}_i) Y_L(\widehat{\vec{s}_j - \vec{R}_{ij}}) \qquad (3.27).$$

At this point we must use the re-expansion formula (A41) in the form

$$k_l^{(i)}(\kappa|\vec{s}_j - \vec{R}_{ij}|) Y_L(\widehat{\vec{s}_j - \vec{R}_{ij}}) = \sum_{L'} H^{ij}_{LL'} (-1)^{l'} i_{l'}(\kappa s_j) Y_{L'}(\hat{s}_j) \qquad (3.28),$$

where we have defined the energy-dependant structure factors

$$H^{ij}_{LL'} \equiv 4\pi \sum_{L''} (-1)^l I(L,L',L'') k_{l''}^{(i)}(\kappa R_{ij}) Y_{L''}(R_{ij}) \qquad (3.29).$$

Putting (3.27) and (3.28) together and following through the algebra as in (3.25) we find

$$\text{Term}(i,j) \equiv \int_{\partial\tau_j} [G_o^+(\vec{r},\vec{s}) \nabla\psi(\vec{s}) - \psi(\vec{s}) \nabla_s G_o^+(\vec{r},\vec{s})] \cdot \hat{s}_j b_j^2 \, d\Omega_j$$
$$= -\kappa b_j^2 \sum_L (-1)^l i_l(\kappa r_i) Y_L(\hat{r}_i) \sum_{L'} H^{ij}_{LL'} (-1)^{l'} \sum_{L''} W[i, R^j]_{LL''} C^j_{L''} \qquad (3.30),$$

with the further definition

$$W[i, R^j]_{LL'} \equiv i_l(\kappa b_j) R^{j\prime}_{LL'}(b_j) - \kappa i_l'(\kappa b_j) R^j_{LL'}(b_j) \qquad (3.31).$$

Sub-case (iv): $\vec{s} \in \partial\tau_o$:- Fig. 3.1(c) shows that $\vec{r} - \vec{s} = \vec{r}_i - (\vec{s}_o - \vec{R}_{io})$ with $|\vec{s}_o - \vec{R}_{io}| > r_i$ and $s_o > R_{io}$. We must again use the re-expansion formula (A41) in the Green function expansion (A33) to get

$$G_o^+(\vec{r},\vec{s}) = -\kappa \sum_L (-1)^l i_l(\kappa r_i) Y_L(\hat{r}_i) \sum_{L'} H^{io}_{LL'} (-1)^{l'} k_{l'}^{(i)}(\kappa s_o) Y_{L'}(\hat{s}_o) \qquad (3.32),$$

where $$H^{io}_{LL'} \equiv 4\pi \sum_{L''} (-1)^l I(L,L',L'') i_{l''}(\kappa R_{io}) Y_{L''}(\hat{R}_{io}) \qquad (3.33).$$

This gives

$$\text{Term}(i,o) \equiv \int_{\partial\tau_o} [G_o^+(\vec{r},\vec{s}) \nabla\psi(\vec{s}) - \psi(\vec{s}) \nabla_s G_o^+(\vec{r},\vec{s})] \cdot (-\hat{s}_o) b_o^2 \, d\Omega_o$$
$$= -(-\kappa b_o^2) \sum_L (-1)^l i_l(\kappa r_i) Y_L(\hat{r}_i) \sum_{L'} H^{io}_{LL'} (-1)^{l'} \sum_{L''} W[k^{(i)}, R^o]_{LL''} C^o_{L''} \qquad (3.34),$$

the extra minus sign coming from the fact that the outward pointing normal of $\overline{\tau}_c$ is $-\hat{s}_o$ and the Wronskian is defined similarly to (3.26).

Case 2: $\vec{r} \in \overline{\tau}_o$:-

Sub-case (i): $\vec{s} \in \bar{I}$:- As before we leave it as

$$\text{Term}\ (o, I) \equiv \int_I G_o^+(\vec{r},\vec{s})\, V(\vec{s})\, \Psi(\vec{s})\, d^3s \qquad (3.35).$$

Sub-case (ii): $\vec{s} \in \partial\overline{\tau}_o$:- Fig. 3.1(d) shows that $\vec{r} - \vec{s} = \vec{r}_o - \vec{s}_c$ and $r_o > s_o$. The Green function (A33) is now

$$G_o^+(\vec{r},\vec{s}) = -\kappa \sum_L (-1)^l h_l^{(1)}(\kappa r_o)\, i_l(\kappa s_o)\, Y_L(\hat{r}_o)\, Y_L(\hat{s}_o) \qquad (3.36).$$

We then get

$$\text{Term}\ (o,o) \equiv \int_{\partial\overline{\tau}_o} [G_o^+(\vec{r},\vec{s})\nabla\Psi(\vec{s}) - \Psi(\vec{s})\nabla_s G_o^+(\vec{r},\vec{s})]\cdot(-\hat{s}_o)\, b_o^2\, d\Omega_o$$
$$= -(-\kappa b_o^2)\sum_L (-1)^l h_l^{(1)}(\kappa r_c)\, Y_L(\hat{r}_c) \sum_{L'} W[i,R^o]_{LL'}\, C^o_{L'} \qquad (3.37)$$

with the Wronskian defined like (3.31).

Sub-case (iii): $\vec{s} \in \partial\tau_i$ for $i = 1,2,\ldots,N$:- Fig. 3.1(e) shows that $\vec{r} - \vec{s} = (\vec{r}_o - \vec{R}_{io}) - \vec{s}_i$ with $|\vec{r}_o - \vec{R}_{io}| > s_i$ and $r_o > R_{io}$. Hence, with the use of (A41) and the definition

$$H^{oi}_{LL'} \equiv 4\pi \sum_{L''} (-1)^{l'} I(L,L',L'')\, i_{l''}(\kappa R_{io})\, Y_{L''}(\hat{R}_{io}) \qquad (3.38),$$

the Green function (A33) becomes

$$G_o^+(\vec{r},\vec{s}) = -\kappa \sum_L (-1)^l h_l^{(1)}(\kappa r_o)\, Y_L(\hat{r}_o) \sum_{L'} H^{io}_{LL'} (-1)^{l'} i_{l'}(\kappa s_i)\, Y_{L'}(\hat{s}_i) \qquad (3.39).$$

The result is then

$$\text{Term}\ (o,i) \equiv \int_{\partial\tau_i} [G_o^+(\vec{r},\vec{s})\nabla\Psi(\vec{s}) - \Psi(\vec{s})\nabla_s G_o^+(\vec{r},\vec{s})]\cdot\hat{s}_i\, b_i^2\, d\Omega_i$$
$$= -\kappa b_i^2 \sum_L (-1)^l h_l^{(1)}(\kappa r_o)\, Y_L(\hat{r}_o) \sum_{L'} H^{oi}_{LL'} (-1)^{l'} \sum_{L''} W[i,R^i]_{L'L''}\, C^i_{L''} \qquad (3.40).$$

Case 3: $\vec{r} \in I$:-

Sub-case (i): $\vec{s} \in I$:- The integral is unaltered as

$$\text{Term}\ (I,I) \equiv \int_I G_o^+(\vec{r},\vec{s})\, V(\vec{s})\, \Psi(\vec{s})\, d^3s \qquad (3.41).$$

Sub-case (ii): $\vec{s} \in \partial\tau_i$ for $i = 1,2,\ldots,N$:- From Fig. 3.1(f) we see that $\vec{r} - \vec{s} = \vec{r}_i - \vec{s}_i$ with $r_i > s_i$, so that

$$G_o^+(\vec{r},\vec{s}) = -\kappa \sum_L (-1)^l h_l^{(1)}(\kappa r_i)\, i_l(\kappa s_i)\, Y_L(\hat{r}_i)\, Y_L(\hat{s}_i) \qquad (3.42)$$

and

$$\text{Term}\ (I,i) \equiv \int_{\partial\tau_i} [G_o^+(\vec{r},\vec{s})\nabla\Psi(\vec{s}) - \Psi(\vec{s})\nabla_s G_o^+(\vec{r},\vec{s})]\cdot\hat{s}_i\, b_i^2\, d\Omega_i$$

$$= -\kappa b_i^2 \sum_L (-1)^\ell h_\ell^{(1)}(\kappa r_i) Y_L(\hat{r}_i) \sum_{L'} W[i, R^i]_{LL'} C_{L'}^i, \qquad (3.43).$$

Sub-case (iii): $\vec{s} \in \partial\bar{\tau}_o$:- From Fig. 3.1(g) we see that $\vec{r} - \vec{s} = \vec{r}_o - \vec{s}_o$ with $s_o > r_o$ and so

$$G_o^+(\vec{r}, \vec{s}) = -\kappa \sum_L (-1)^\ell i_\ell(\kappa r_o) h_\ell^{(1)}(\kappa s_o) Y_L(\hat{r}_o) Y_L(\hat{s}_o) \qquad (3.44),$$

giving

$$\text{Term}\,(I, o) \equiv \int_{\partial\bar{\tau}_o} [G_o^+(\vec{r}, \vec{s}) \nabla\psi(\vec{s}) - \psi(\vec{s}) \nabla_s G_o^+(\vec{r}, \vec{s})] \cdot (-\hat{s}_o) b_o^2 \, d\Omega_o$$

$$= -(-\kappa b_o^2) \sum_L (-1)^\ell i_\ell(\kappa r_o) Y_L(\hat{r}_o) \sum_{L'} W[h^{(1)}, R^o]_{LL'} C_{L'}^o, \qquad (3.45).$$

At this point we have completed the evaluation of the terms in (3.16).

Before collecting up the widely scattered parts of (3.16) we make some simplifying definitions. Firstly,

$$B_L^i \equiv -\kappa b_i^2 (-1)^\ell \sum_{L'} W[i, R^i]_{LL'} C_{L'}^i, \qquad (3.46)$$

and $$B_L^o \equiv \kappa b_o^2 (-1)^\ell \sum_{L'} W[h^{(1)}, R^o]_{LL'} C_{L'}^o, \qquad (3.47);$$

which (assuming invertibility of the Wronskian matrices) imply

$$-\kappa b_i^2 C_L^i = \sum_{L'} W[i, R^i]^{-1}_{LL'} (-1)^{\ell'} B_{L'}^i, \qquad (3.48)$$

and $$\kappa b_o^2 C_L^o = \sum_{L'} W[h^{(1)}, R^o]^{-1}_{LL'} (-1)^{\ell'} B_{L'}^o, \qquad (3.49).$$

Secondly, we define the t-matrices for the SSRs by

$$(t^i)^{-1}_{LL'} \equiv \sum_{L''} W[h^{(1)}, R^i]_{LL''} W[i, R^i]^{-1}_{L''L'} (-1)^{\ell'} \qquad (3.50)$$

and $$(t^o)^{-1}_{LL'} \equiv \sum_{L''} W[i, R^o]_{LL''} W[h^{(1)}, R^o]^{-1}_{L''L'} (-1)^{\ell'} \qquad (3.51).$$

Collecting up (3.23,25,30,34,35,37,40,41,43,45) and using (3.46-51), we find that (3.16) becomes, in the three cases for $E < V_o$,

$$0 = \int_I G_o^+(\vec{r}, \vec{s}) V(\vec{s}) \psi(\vec{s}) d^3s + \sum_L (-1)^\ell i_\ell(\kappa r_i) Y_L(\hat{r}_i) \Big\{ \sum_{L'} (t^i)^{-1}_{LL'} B_{L'}^i + \sum_{\substack{j=0 \\ j\neq i}}^{N} \sum_{L'} H^{ij}_{LL'} B_{L'}^j \Big\}$$

(for $\vec{r} \in \tau_i$ and $i = 1, 2, \ldots, N$) (3.52),

$$0 = \int_I G_o^+(\vec{r}, \vec{s}) V(\vec{s}) \psi(\vec{s}) d^3s + \sum_L (-1)^\ell h_\ell^{(1)}(\kappa r_o) Y_L(\hat{r}_o) \Big\{ \sum_{L'} (t^o)^{-1}_{LL'} B_{L'}^o + \sum_{j=1}^{N} \sum_{L'} H^{oj}_{LL'} B_{L'}^j \Big\}$$

(for $\vec{r} \in \bar{\tau}_o$) (3.53)

and

$$\psi(\vec{r}) = \int_I G_o^+(\vec{r}, \vec{s}) V(\vec{s}) \psi(\vec{s}) d^3s + \sum_{i=1}^{N} \sum_L h_\ell^{(1)}(\kappa r_i) Y_L(\hat{r}_i) B_L^i + \sum_L i_\ell(\kappa r_o) Y_L(\hat{r}_o) B_L^o$$

(for $\vec{r} \in I$) (3.54).

If we complete the definition of the coefficients $H^{ij}_{LL'}$ by

$$H^{ii}_{LL'} \equiv 0 \qquad (\text{for } i = 0,1,\ldots,N) \quad (3.55),$$

then we find, using (3.29,33,38,55) together with (A20,28) and the properties of the $I(L,L',L'')$ in App. A, that they have the symmetry

$$H^{ij}_{LL'} = H^{ji}_{L'L} \qquad (3.56).$$

In fact the atomic t-matrices defined in (3.50,51) are also symmetric. In Natoli et al. (1986) it is shown that the analogous quantities (for positive energies) are indeed closely related to the usual atomic t-matrices from scattering theory for the atomic sphere potentials. Since the potential is real we have time-reversal invariance (see e.g. Taylor (1972)) and in the angular momentum representation the matrices are symmetric. Looking at (3.50) for example, this symmetry is not obvious, but is demonstrated in our following, new result.

For a given atomic sphere τ_i we define matrices $\underset{\sim}{u}$, $\underset{\sim}{k}$, $\underset{\sim}{i}$, $\underset{\sim}{R}$, $\underset{\sim}{s}$, $\underset{\sim}{X}$ and $\underset{\sim}{I}$, by

$$u_{LL'} \equiv (t^i)^{-1}_{LL'} \quad k_{LL'}(r) \equiv k^{(1)}_l(\varkappa r)\delta_{LL'} \quad i_{LL'}(r) \equiv i_l(\varkappa r)\delta_{LL'}$$

$$R_{LL'}(r) \equiv R^i_{LL'}(r) \quad s_{LL'} \equiv (-1)^l \delta_{LL'} \quad \underset{\sim}{X}(r) \equiv r\underset{\sim}{R}(r) \quad I_{LL'} \equiv \delta_{LL'} \quad (3.57).$$

These matrices satisfy the following relations (with $b \equiv b_i$)

$$\underset{\sim}{u} = \left(\underset{\sim}{k}(b)\underset{\sim}{R}'(b) - \underset{\sim}{k}'(b)\underset{\sim}{R}(b)\right)\left(\underset{\sim}{i}(b)\underset{\sim}{R}'(b) - \underset{\sim}{i}'(b)\underset{\sim}{R}(b)\right)^{-1} \text{ (from (3.50))} \quad (3.58),$$

$$\underset{\sim}{i}(r)\underset{\sim}{k}'(r) - \underset{\sim}{i}'(r)\underset{\sim}{k}(r) = \left(\tfrac{-1}{\varkappa r^2}\right)\underset{\sim}{s} \quad \text{(from (A12))} \quad (3.59)$$

and

$$\underset{\sim}{X}''(r) = \underset{\sim}{G}(r)\underset{\sim}{X}(r) \qquad (3.60);$$

where, from (3.21), $\underset{\sim}{G}$ is the symmetric matrix defined by

$$G_{LL'}(r) \equiv U^i_{LL'}(r) + \frac{l(l+1)}{r^2}\delta_{LL'} - E\,\delta_{LL'} \qquad (3.61)$$

and, for small r, $\underset{\sim}{X}$ is given by

$$X_{LL'}(r) \approx r^{l+1}\delta_{LL'} \qquad (3.62).$$

We wish to show that $\underset{\sim}{u}$ is symmetric, i.e. $\underset{\sim}{u} = \underset{\sim}{u}^T$. Multiplying both sides of (3.58) on the left by $(\underset{\sim}{i}\underset{\sim}{R}' - \underset{\sim}{i}'\underset{\sim}{R})^T\underset{\sim}{s}^T$ and on the right by $\underset{\sim}{s}(\underset{\sim}{i}\underset{\sim}{R}' - \underset{\sim}{i}'\underset{\sim}{R})$, and using $\underset{\sim}{s}^2 = \underset{\sim}{I}$, gives us

$$(\underset{\sim}{i}\underset{\sim}{R}' - \underset{\sim}{i}'\underset{\sim}{R})^T \underset{\sim}{s}^T \underset{\sim}{u}\, \underset{\sim}{s}\, (\underset{\sim}{i}\underset{\sim}{R}' - \underset{\sim}{i}'\underset{\sim}{R}) = (\underset{\sim}{i}\underset{\sim}{R}' - \underset{\sim}{i}'\underset{\sim}{R})^T \underset{\sim}{s}^T (\underset{\sim}{k}\underset{\sim}{R}' - \underset{\sim}{k}'\underset{\sim}{R}) \qquad (3.63),$$

in which the dropping of the radial dependence of the matrices is intended to imply that $r = b$. If we consider the LHS of (3.63), we see that its symmetry is equivalent to that of $\underset{\sim}{u}$. So our effort will go into proving the symmetry of the RHS of (3.63), i.e.

$$\underset{\sim}{v} \equiv (\underset{\sim}{i}\underset{\sim}{R}' - \underset{\sim}{i}'\underset{\sim}{R})^T \underset{\sim}{s}^T (\underset{\sim}{k}\underset{\sim}{R}' - \underset{\sim}{k}'\underset{\sim}{R}) \qquad (3.64).$$

This is done by first expanding it out and using the diagonality of $\underset{\sim}{i}$, $\underset{\sim}{k}$ and $\underset{\sim}{s}$, so that

$$\begin{aligned}\underset{\sim}{v} &= (\underset{\sim}{R}'^T \underset{\sim}{i} - \underset{\sim}{R}^T \underset{\sim}{i}')\, \underset{\sim}{s}\, (\underset{\sim}{k}\underset{\sim}{R}' - \underset{\sim}{k}'\underset{\sim}{R}) \\ &= [\underset{\sim}{R}'^T \underset{\sim}{i}\, \underset{\sim}{s}\, \underset{\sim}{k}\, \underset{\sim}{R}'] + [\underset{\sim}{R}^T \underset{\sim}{i}' \underset{\sim}{s}\, \underset{\sim}{k}'\underset{\sim}{R}] - \underset{\sim}{R}'^T \underset{\sim}{i}\, \underset{\sim}{s}\, \underset{\sim}{k}'\underset{\sim}{R} - \underset{\sim}{R}^T \underset{\sim}{i}' \underset{\sim}{s}\, \underset{\sim}{k}\, \underset{\sim}{R}' \\ &= [\underset{\sim}{R}'^T \underset{\sim}{i}\, \underset{\sim}{s}\, \underset{\sim}{k}\, \underset{\sim}{R}'] + [\underset{\sim}{R}^T \underset{\sim}{i}' \underset{\sim}{s}\, \underset{\sim}{k}'\underset{\sim}{R}] - [\underset{\sim}{R}'^T \underset{\sim}{i}\, \underset{\sim}{s}\, \underset{\sim}{k}'\underset{\sim}{R} + \underset{\sim}{R}^T \underset{\sim}{i}\, \underset{\sim}{s}\, \underset{\sim}{k}'\underset{\sim}{R}'] + \left(\frac{-1}{\kappa b^2}\right)\underset{\sim}{R}^T \underset{\sim}{R}' \qquad (3.65),\end{aligned}$$

where, in the last step, we have used (3.59). Now each of the terms in square brackets on the RHS of (3.65) is manifestly symmetric, so our task is reduced to showing the symmetry of the term $\underset{\sim}{R}^T \underset{\sim}{R}'$. This is best done by considering instead the combination $\underset{\sim}{X}^T(r)\, \underset{\sim}{X}'(r)$. From (3.57) this is just

$$\underset{\sim}{X}^T(r)\, \underset{\sim}{X}'(r) = r\, \underset{\sim}{R}^T(r)\, \underset{\sim}{R}(r) + r^2\, \underset{\sim}{R}^T(r)\, \underset{\sim}{R}'(r) \qquad (3.66),$$

and its symmetry is thus equivalent to that of $\underset{\sim}{R}^T(r)\, \underset{\sim}{R}'(r)$. Now consider its derivative

$$\begin{aligned}\left(\underset{\sim}{X}^T(r)\, \underset{\sim}{X}'(r)\right)' &= \underset{\sim}{X}^{T\prime}(r)\, \underset{\sim}{X}'(r) + \underset{\sim}{X}^T(r)\, \underset{\sim}{X}''(r) \\ &= \underset{\sim}{X}'^T(r)\, \underset{\sim}{X}'(r) + \underset{\sim}{X}^T(r)\, \underset{\sim}{G}(r)\, \underset{\sim}{X}(r) \quad \text{(from (3.60))} \qquad (3.67).\end{aligned}$$

This is obviously symmetric because of the symmetry of $\underset{\sim}{G}(r)$. Therefore, since its derivative is symmetric for all r, and since it is diagonal at $r = 0$ (by (3.62)), then $\underset{\sim}{X}^T(r)\, \underset{\sim}{X}'(r)$ itself is symmetric for all r. So our result is obtained and we have

$$\underset{\sim}{u} = \underset{\sim}{u}^T \qquad (3.68).$$

At this stage we have, as unknowns in (3.52-54), the coefficients B_L^i and the wavefunction $\Psi(\vec{r})$ for $\vec{r} \in I$. If, as in the MT case, the potential were zero in the IR, then the integrals would disappear and we could use (3.52,53) to determine the B_L^i

and then via (3.54) the $\Psi(\vec{r})$ for $\vec{r} \in I$. In the general potential case Natoli et al. (1986) point out that (3.54) is the Lippmann-Schwinger equation relative to a potential which is the real potential in the IR and zero outside, with an inhomogeneous part corresponding to the second and third terms on the RHS. They then introduce a T-matrix relative to this potential which transforms (3.54) into a closed expression for $\Psi(\vec{r})$ in the IR. This is then used to evaluate the remaining integrals in (3.52,53). The difficult part now comes in evaluating this T-matrix and, at present, we have not found a practicable and accurate method of doing this evaluation.

Our approach has been to use the Born approximation for the interstitial T-matrix, i.e. we approximate it with the potential operator. This will be reasonable provided that the reset IR potential is weak; in other words, the true IR potential does not vary too much from its average over too large a volume. (In actual fact, because of our resetting of the reference zero of the potential to the value in (3.11), this is a variety of distorted-wave Born approximation.) The approximation is equivalent to ignoring the integral on the RHS of (3.54) and using the resulting expression for Ψ in the integrals of (3.52,53).

So, for $\vec{r} \in \tau_i$, we take

$$\begin{aligned}
&\int_I G_o^+(\vec{r},\vec{s})\, V(\vec{s})\, \Psi(\vec{s})\, d^3s \\
&= \int_I \Big\{-\kappa \sum_L (-1)^\ell i_\ell(\kappa r_i) k_\ell^{(i)}(\kappa s_i) Y_L(\hat{r}_i) Y_L(\hat{s}_i)\Big\} V(\vec{s}) \Big\{\sum_{j=1}^{N} \sum_{L'} k_{\ell'}^{(j)}(\kappa s_j) Y_{L'}(s_j)\, B_{L'}^{j} \\
&\qquad + \sum_{L'} i_{\ell'}(\kappa s_o) Y_{L'}(\hat{s}_o)\, B_{L'}^{o} \Big\}\, d^3s \\
&= \sum_L (-1)^\ell i_\ell(\kappa r_i) Y_L(\hat{r}_i) \Big\{ \sum_{j=0}^{N} \sum_{L'} T_{LL'}^{ij}\, B_{L'}^{j} \Big\}
\end{aligned} \tag{3.69}$$

where we have defined

$$T_{LL'}^{ij} \equiv -\kappa \int_I k_\ell^{(i)}(\kappa s_i) Y_L(\hat{s}_i)\, V(\vec{s})\, k_{L'}^{(j)}(\kappa s_j) Y_{L'}(\hat{s}_j)\, d^3s \quad (j=1,\ldots,N) \tag{3.70}$$

and $$T^{io}_{LL'} \equiv -\kappa \int_I k_l^{(1)}(\kappa s_i) Y_L(\hat{s}_i) V(\vec{s}) j_{l'}(\kappa s_o) Y_{L'}(\hat{s}_o) d^3s \qquad (3.71).$$

For $\vec{r} \in \tau_o$ we obtain, in a like manner,

$$\int_I G_o^+(\vec{r},\vec{s}) V(\vec{s}) \Psi(\vec{s}) d^3s = \sum_L (-1)^l k_l^{(1)}(\kappa r_o) Y_L(\hat{r}_o) \left\{ \sum_{j=0}^{N} \sum_{L'} T^{oj}_{LL'} B^j_{L'} \right\} \qquad (3.72),$$

where

$$T^{oj}_{LL'} \equiv -\kappa \int_I j_l(\kappa s_o) Y_L(\hat{s}_o) V(\vec{s}) k_{l'}^{(1)}(\kappa s_j) Y_{L'}(\hat{s}_j) d^3s \quad (j = 1,\ldots,N) \qquad (3.73)$$

and $$T^{oo}_{LL'} \equiv -\kappa \int_I j_l(\kappa s_o) Y_L(\hat{s}_o) V(\vec{s}) j_{l'}(\kappa s_o) Y_{L'}(\hat{s}_o) d^3s \qquad (3.74).$$

It may be easily seen from these definitions that

$$T^{ij}_{LL'} = T^{ji}_{L'L} \qquad (3.75).$$

The equations (3.52,53) may now be written

$$\sum_L (-1)^l j_l(\kappa r_i) Y_L(\hat{r}_i) \sum_{j=0}^{N} \sum_{L'} S^{ij}_{LL'} B^j_{L'} = 0 \quad (\vec{r} \in \tau_i \; i = 1,\ldots,N) \qquad (3.76)$$

and $$\sum_L (-1)^l k_l^{(1)}(\kappa r_o) Y_L(\hat{r}_o) \sum_{j=0}^{N} \sum_{L'} S^{oj}_{LL'} B^j_{L'} = 0 \quad (\vec{r} \in \tau_o) \qquad (3.77),$$

and the secular matrix $S^{ij}_{LL'}$ is defined by

$$S^{ij}_{LL'} \equiv (t^i)^{-1}_{LL'} \delta_{ij} + H^{ij}_{LL'} + T^{ij}_{LL'} \quad (i,j = 0,1,\ldots,N) \qquad (3.78)$$

(or, in matrix form, by

$$\underset{\sim}{S} \equiv \underset{\sim}{t}^{-1} + \underset{\sim}{H} + \underset{\sim}{T} \qquad (3.79)).$$

Considering the orthonormality of the spherical harmonics, the equations (3.76,77) imply the "secular equation"

$$\sum_{j=0}^{N} \sum_{L'} S^{ij}_{LL'} B^j_{L'} = 0 \qquad (3.80).$$

This has non-zero solution vectors B^i_L only when the determinant of the secular matrix is zero. Thus a search for bound states involves looking for those energies at which the secular determinant is zero and then using (3.80) to find the B^i_L, and (3.48,49) to get the coefficients C^i_L of the wavefunction expansions inside the SSRs. We do not treat the normalization of the wavefunction since it is not necessary for the purposes of this thesis. An efficient method of normalization has been under investigation by CRN (pers. com.), within the framework of the FP-SW method, and is of course essential for the further development of the method.

For the energy range $V_o < E < 0$ an almost identical procedure is followed. In this case we define $k \equiv \sqrt{E - V_o}$ and use the

standing-wave Green function (A34) with the re-expansion formula (A43). We obtain

$$\sum_L j_\ell(kr_i) Y_L(\hat{r}_i) \sum_{j=0}^{N}{}' \sum_{L'} S^{ij}_{LL'} B^j_{L'} = 0 \quad (\vec{r} \in \tau_i \quad i = 1, \ldots, N) \tag{3.81}$$

and

$$\sum_L n_\ell(kr_0) Y_L(\hat{r}_0) \sum_{j=0}^{N}{}' \sum_{L'} S^{0j}_{LL'} B^j_{L'} = 0 \quad (\vec{r} \in \overline{\tau}_0) \tag{3.82}.$$

The secular equation (3.80) still holds, with the definition in (3.78), but the individual parts of the secular matrix are given by the following formulae

$$(t^i)^{-1}_{LL'} \equiv \sum_{L''} W[m, R^i]_{LL''} W[j, R^i]^{-1}_{L''L'} \quad (i = 1, \ldots, N) \tag{3.83}$$

and

$$(t^0)^{-1}_{LL'} \equiv \sum_{L''} W[j, R^0]_{LL''} W[m, R^0]^{-1}_{L''L'} \tag{3.84};$$

$$B^i_L \equiv k b_i^2 \sum_{L'} W[j, R^i]_{LL'} C^i_{L'} \tag{3.85}$$

and

$$B^0_L \equiv -k b_0^2 \sum_{L'} W[m, R^0]_{LL'} C^0_{L'} \tag{3.86};$$

$$H^{ij}_{LL'} \equiv \begin{cases} 0 & (i = j) \\ 4\pi \sum_{L''} i^{\ell' - \ell - \ell''} I(L, L', L'') n_{\ell''}(kR_{ij}) Y_{L''}(\hat{R}_{ij}) & (0 \neq i \neq j \neq 0) \\ 4\pi \sum_{L''} i^{\ell' - \ell - \ell''} I(L, L', L'') j_{\ell''}(kR_{i0}) Y_{L''}(\hat{R}_{i0}) & (i \neq 0 \quad j = 0) \\ 4\pi \sum_{L''} i^{\ell - \ell' - \ell''} I(L, L', L'') j_{\ell''}(kR_{j0}) Y_{L''}(\hat{R}_{j0}) & (i = 0 \quad j \neq 0) \end{cases} \tag{3.87};$$

and finally

$$T^{ij}_{LL'} \equiv \begin{cases} k \int_I n_\ell(ks_i) Y_L(\hat{s}_i) V(\vec{s}) n_{\ell'}(ks_j) Y_{L'}(\hat{s}_j) d^3s & (i \neq 0 \quad j \neq 0) \\ k \int_I n_\ell(ks_i) Y_L(\hat{s}_i) V(\vec{s}) j_{\ell'}(ks_0) Y_{L'}(\hat{s}_0) d^3s & (i \neq 0 \quad j = 0) \\ k \int_I j_\ell(ks_0) Y_L(\hat{s}_0) V(\vec{s}) n_{\ell'}(ks_j) Y_{L'}(\hat{s}_j) d^3s & (i = 0 \quad j \neq 0) \\ k \int_I j_\ell(ks_0) Y_L(\hat{s}_0) V(\vec{s}) j_{\ell'}(ks) Y_{L'}(\hat{s}) d^3s & (i = 0 \quad j = 0) \end{cases} \tag{3.88}.$$

The equation corresponding to (3.54) for $\vec{r} \in I$ is

$$\psi(\vec{r}) = \int_I G_0^+(\vec{r}, \vec{s}) V(\vec{s}) \psi(\vec{s}) d^3s + \sum_{i=1}^{N}{}' \sum_L n_\ell(kr_i) Y_L(\hat{r}_i) B^i_L + \sum_L{}' j_\ell(kr_0) Y_L(\hat{r}_0) B^0_L \tag{3.89}.$$

It is not difficult to show that the separate parts of the secul-

ar matrix for $V_o < E < 0$ have the same symmetry properties as those referred to in (3.56,68,75).

Section 3.3: Secular Equation in the Continuum Case and the Calculation of Photoionization Cross-Sections.

For $0 < E$ we have a continuum of states and, having chosen a particular energy, we find the wavefunction for that energy. Using this wavefunction we then evaluate the photoionization cross-section. In this situation we must use the Green function (A35) in the Lippmann-Schwinger equation

$$\Psi(\vec{r}) = \phi_o(\vec{r}) + \int G_o^+(\vec{r},\vec{s})V(\vec{s})\Psi(\vec{s})d^3s \qquad (3.90)$$

in which $\phi_o(\vec{r}) = \exp(i\vec{k}\cdot\vec{r})$ (with $k \equiv \sqrt{E}$) is included to impose the correct boundary conditions at infinity, i.e. those of an asymptotically free electron ejected by the absorbed photon. This case is treated in detail in Natoli et al. (1986) for the situation in which there is no OS and the IR extends to infinity. In this work we have an OS and can thus drop the inhomogeneous term $\phi_o(\vec{r})$ from (3.90) since we can impose the appropriate boundary conditions directly on the radial solution of the coupled Schrödinger equations in the EMR. Furthermore, we again reset the zero of the potential energy to V_o as in (3.11) so that $k \equiv \sqrt{E - V_o}$.

Inside an ASR the wavefunction is given, as before, by (3.20). However, in the EMR we must write the wavefunction as

$$\Psi(\vec{r}) = \sum_L \sum_{L'} (A_{L'} Q_{LL'}(r_o) + C^o_{L'} R^o_{LL'}(r_o)) Y_L(\hat{r}_o) \qquad (3.91),$$

where A_L and C^o_L are constants, and $Q_{LL'}$ and $R^o_{LL'}$ are separately solutions of the radial equations, normalized to one state per Ryd., with the asymptotic behaviour

$$Q_{LL'}(r) \approx \delta_{LL'} \left(\frac{1}{k\pi}\right)^{1/2} \frac{1}{r} \sin\left(kr - \tfrac{1}{2}l\pi + \omega_l\right) \quad (r \to \infty) \qquad (3.92)$$

and $$R^o_{LL'}(r) \approx -\delta_{LL'} \left(\frac{1}{k\pi}\right)^{1/2} \frac{1}{r} \exp\left(i\left(kr - \tfrac{1}{2}l\pi + \omega_l\right)\right) \quad (r \to \infty) \qquad (3.93).$$

The extra phase-shift ω_l is introduced to deal with long-range

(e.g. Coulombic) potentials, and depends on r. (Schiff (1968) p. 142.)

With the application of the partition and the use of the re-expansion formula (A44), (3.90) may be rewritten similarly to the $V_o < E < 0$ case. One finds, for $\vec{r} \in I$, the equation

$$\psi(\vec{r}) = \int_I G_o^+(\vec{r},\vec{s})V(\vec{s})\psi(\vec{s})d^3s + \sum_{i=1}^{N}\sum_L -ik_\ell^{(1)}(kr_i)Y_L(\hat{r}_i)B_L^i + \sum_L j_\ell(kr_o)Y_L(\hat{r}_o)B_L^o \quad (3.94).$$

Here we have defined

$$B_L^i \equiv kb_i^2 \sum_{L'} W[j,R^i]_{LL'} C_{L'}^i, \quad (3.95)$$

and

$$B_L^o \equiv -kb_o^2 \sum_{L'} \left(W[-ik^{(1)},R^o]_{LL'} C_{L'}^o + W[-ik^{(1)},Q]_{LL'} A_{L'}\right) \quad (3.96).$$

As usual, ignoring the first term in the RHS of (3.94) and using the remaining expression to dispose of the integrals over the IR (in the Born approximation) for the other regions of the partition, we get

$$\sum_L j_\ell(kr_i)Y_L(\hat{r}_i)\left\{\sum_{j=0}^{N}\sum_{L'} S_{LL'}^{ij} B_{L'}^j\right\} = 0 \quad (\vec{r}\in\tau_i \;\; i=1,\ldots,N) \quad (3.97)$$

and

$$\sum_L -ik_\ell^{(1)}(kr_o)Y_L(\hat{r}_o)\left\{\sum_{j=0}^{N}\sum_{L'} S_{LL'}^{oj} B_{L'}^j - \sum_{L'} D_{LL'} A_{L'}\right\} = 0 \quad (\vec{r}\in\tau_o) \quad (3.98).$$

The secular matrix is defined as in (3.78), but the individual parts are now given by

$$(t^i)^{-1}_{LL'} \equiv \sum_{L''} W[-ik^{(1)},R^i]_{LL''} W[j,R^i]^{-1}_{L''L'} \quad (3.99)$$

and

$$(t^o)^{-1}_{LL'} \equiv \sum_{L''} W[j,R^o]_{LL''} W[-ik^{(1)},R^o]^{-1}_{L''L'} \quad (3.100);$$

$$H_{LL'}^{ij} \equiv \begin{cases} 0 & (i=j) \\ 4\pi \sum_{L''} i^{\ell'-\ell-\ell''} I(L,L',L'')(-ik_{\ell''}^{(1)}(kR_{ij}))Y_{L''}(\hat{R}_{ij}) & (i\neq 0 \neq j\neq 0) \\ 4\pi \sum_{L''} i^{\ell'-\ell-\ell''} I(L,L',L'') j_{\ell''}(kR_{io})Y_{L''}(\hat{R}_{io}) & (i\neq 0 \;\; j=0) \\ 4\pi \sum_{L''} i^{\ell-\ell'-\ell''} I(L,L',L'') j_{\ell''}(kR_{jo})Y_{L''}(R_{jo}) & (i=0 \;\; j\neq 0) \end{cases} \quad (3.101);$$

and

$$T_{LL'}^{ij} \equiv \begin{cases} k\int_I (-ik_\ell^{(1)}(ks_i))Y_L(\hat{s}_i)V(\vec{s})(-ik_{\ell'}^{(1)}(ks_j))Y_{L'}(\hat{s}_j)d^3s & (i\neq 0 \;\; j\neq 0) \\ k\int_I (-ik_\ell^{(1)}(ks_i))Y_L(\hat{s}_i)V(\vec{s}) j_{\ell'}(ks_o)Y_{L'}(\hat{s}_o)d^3s & (i\neq 0 \;\; j=0) \\ k\int_I j_\ell(ks_o)Y_L(\hat{s}_o)V(\vec{s})(-ik_{\ell'}^{(1)}(ks_j))Y_{L'}(\hat{s}_j)d^3s & (i=0 \;\; j\neq 0) \\ k\int_I j_\ell(ks_o)Y_L(\hat{s}_o)V(\vec{s}) j_{\ell'}(ks_o)Y_{L'}(\hat{s}_o)d^3s & (i=0 \;\; j=0) \end{cases} \quad (3.102).$$

The inhomogeneous term is

$$D_{LL'} \equiv kb_c^2 \Big\{ W[j,Q]_{LL'} - \sum_{L''} \sum_{\underline{L}} W[j,R^o]_{LL''} W[-ik^{(1)},R^o]^{-1}_{L''\underline{L}} W[-ik^{(1)},Q]_{\underline{L}L'} \Big\} \qquad (3.103).$$

This expression may be considerably simplified with a recent result of C.R. Natoli (pers. com.). In matrix notation

$$\begin{aligned}
(1/kb_c^2)\underset{\sim}{D} &= \underset{\sim}{W}[j,Q] - (\underset{\sim}{W}[j,R^o]\underset{\sim}{W}[-ik^{(1)},R^o]^{-1})\underset{\sim}{W}[-ik^{(1)},Q] \\
&= \underset{\sim}{W}[j,Q] - \underset{\sim}{W}[-ik^{(1)},R^o]^{-1\,T}\underset{\sim}{W}[j,R^o]^T\underset{\sim}{W}[-ik^{(1)},Q] \qquad \text{as in (3.68)} \\
&= \underset{\sim}{W}[-ik^{(1)},R^o]^{-1\,T}\Big\{\underset{\sim}{W}[-ik^{(1)},R^o]^T\underset{\sim}{W}[j,Q] - \underset{\sim}{W}[j,R^o]^T\underset{\sim}{W}[-ik^{(1)},Q]\Big\} \\
&\equiv \underset{\sim}{W}[-ik^{(1)},R^o]^{-1\,T}\underset{\sim}{M} \qquad (3.104).
\end{aligned}$$

If we expand the Wronskians in $\underset{\sim}{M}$ and rearrange, we get

$$\begin{aligned}
\underset{\sim}{M} &= -ik\Big\{\underset{\sim}{R}^o(b_c)^T\big(\underset{\sim}{h}^{(1)}(kb_o)\underset{\sim}{j}'(kb_o) - \underset{\sim}{h}^{(1)\prime}(kb_o)\underset{\sim}{j}(kb_o)\big)\underset{\sim}{Q}'(b_o) \\
&\qquad - \underset{\sim}{R}^{o\prime}(b_o)^T\big(\underset{\sim}{h}^{(1)}(kb_o)\underset{\sim}{j}'(kb_o) - \underset{\sim}{h}^{(1)\prime}(kb_o)\underset{\sim}{j}(kb_o)\big)\underset{\sim}{Q}(b_o)\Big\} \\
&= \left(\frac{-1}{kb_o^2}\right)\Big\{\underset{\sim}{R}^{o\,T}\underset{\sim}{Q}' - \underset{\sim}{R}^{o\prime\,T}\underset{\sim}{Q}\Big\} \qquad (3.105).
\end{aligned}$$

Now $\underset{\sim}{R}^o(r)$ and $\underset{\sim}{Q}(r)$ satisfy the same set of coupled equations (3.21) in the EMR.

$$\Big[\frac{d^2}{dr^2} + \frac{2}{r}\frac{d}{dr} - \underset{\sim}{G}(r)\Big]\underset{\sim}{R}^o(r) = 0 \qquad (3.106)$$

and

$$\Big[\frac{d^2}{dr^2} + \frac{2}{r}\frac{d}{dr} - \underset{\sim}{G}(r)\Big]\underset{\sim}{Q}(r) = 0 \qquad (3.107),$$

where $\underset{\sim}{G}(r)$ is defined in (3.61). If we now multiply (3.106) on the left by $\underset{\sim}{Q}(r)^T$, multiply (3.107) on the left by $\underset{\sim}{R}^o(r)^T$ and subtract the latter from the transpose of the former, then we get (using the symmetry of $\underset{\sim}{G}(r)$)

$$\begin{aligned}
0 &= \Big[\Big(\frac{d^2}{dr^2} + \frac{2}{r}\frac{d}{dr}\Big)\underset{\sim}{R}^o(r)^T\Big]Q(r) - \underset{\sim}{R}^o(r)^T\Big[\Big(\frac{d^2}{dr^2} + \frac{2}{r}\frac{d}{dr}\Big)\underset{\sim}{Q}(r)\Big] \\
&= \Big(\frac{d}{dr} + \frac{2}{r}\Big)\Big[\underset{\sim}{R}^o(r)^T\underset{\sim}{Q}'(r) - \underset{\sim}{R}^{o\prime}(r)^T\underset{\sim}{Q}(r)\Big] \\
&\equiv \Big(\frac{d}{dr} + \frac{2}{r}\Big)\underset{\sim}{P}(r) \qquad (3.108).
\end{aligned}$$

The general solution of the matrix differential equation is

$$\underset{\sim}{P}(r) = \frac{i}{r^2}\underset{\sim}{\Pi} \qquad \text{(for some constant matrix } \underset{\sim}{\Pi}\text{)} \qquad (3.109).$$

To determine the constant matrix we must use the asymptotic behaviour of $\underset{\sim}{Q}(r)$ and $\underset{\sim}{R}^o(r)$ given by (3.92,93). Therefore

$$\Pi_{LL'} = \left(-\frac{1}{\pi}\right)\delta_{LL'} \qquad (3.110).$$

Finally, from (3.104,105,108,109,110) we get

$$D_{LL'} = \frac{1}{\pi b_0^2}\left(W[-ik^{(i)}, R^0]^{-1}\right)^T_{LL'} \qquad (3.111).$$

Now because of the orthonormality of the spherical harmonics we get from (3.97,98) the secular equation

$$\sum_{j=0}^{N}\sum_{L'} S^{ij}_{LL'} B^j_{L'} = \delta_{i0}\sum_{L'} D_{LL'} A_{L'} \qquad (3.112).$$

In this equation A_L represents the exciting amplitude and we set it equal to $\delta_{LL''}$ so that, for each L'', we solve (3.112) to obtain $B^i_L(L'')$. With this set of vector solutions, relative to each particular exciting wave L'', we are in a position to calculate the photoionization cross-section.

In the interests of simplicity we restrict our calculation to the case where the photoabsorbing atom is at the centre of the cluster with $i = 1$. We calculate only the K-edge cross-sections, so that the initial state is a spherically symmetric 1s state $|\Psi_{in}\rangle$ which lies so deep in energy that the spatial extent of the wavefunction is effectively entirely bounded by the atomic sphere. This means that the integral in the dipole transition matrix element need only be performed in that sphere.

From Natoli et al. (1986) we have that the cross-section, for electromagnetic radiation polarized in the $\hat{\varepsilon}$ direction, is given by

$$\sigma(E;\hat{\varepsilon}) = 4\pi^2\alpha\hbar\omega\sum_{L''}\left|D^-_{L''}(E;\hat{\varepsilon})\right|^2 \qquad (3.113),$$

where α is the fine-structure constant, $\hbar\omega$ is the photon energy and

$$D^-_{L''}(E;\hat{\varepsilon}) \equiv \langle \Psi^-_{L''}(E)|\vec{r}.\hat{\varepsilon}|\Psi_{in}\rangle \qquad (3.114).$$

In this last expression $\Psi^-_{L''}(E)$ is our solution of the Lippmann-Schwinger equation (3.90) relative to the exciting wave L''. Now, for $\vec{r}\in\tau_1$, we have from (3.20) that

$$\Psi^-_{L''}(E;\vec{r}) = \sum_{L}\sum_{L'} C^1_{L'}(L'')R^1_{LL'}(r)Y_L(\hat{r}) \qquad (3.115)$$

and from (3.95) that

$$C'_{L}(L'') = \frac{1}{kb_i^2} \sum_{L'} W[j,R']^{-1}_{LL'} B'_{L'}(L'') \qquad (3.116).$$

Also,

$$\Psi_{in}(\vec{r}) \equiv \phi(r) Y_{001}(\hat{r}) = \frac{1}{\sqrt{4\pi}} \phi(r) \qquad (3.117).$$

Now, we shall further specialize our calculation to an average cross-section over all orientations of the molecule. Since the propagation vector of the radiation does not appear in (3.113), this average is equivalent to averaging over all polarization directions $\hat{\varepsilon}$. The result is well known to be

$$\begin{aligned}\sigma(E) &= 4\pi^2\alpha\hbar\omega \sum_{L''} \frac{1}{3} \sum_{i=1}^{3} \left| \langle \Psi^-_{L''}(E) | x_i | \Psi_{in} \rangle \right|^2 \\ &= \left(\tfrac{4}{3}\pi^2\alpha\hbar\omega\right)\left(\tfrac{4\pi}{3}\right) \sum_{L''} \sum_{m\alpha} \left| \int \Psi^-_{L''}(E;\vec{r})\, r\, Y_{1m\alpha}(\hat{r})\, \Psi_{in}(\vec{r})\, d^3r \right|^2 \\ &= \left(\tfrac{4}{9}\pi^2\alpha\hbar\omega\right) \sum_{L''} \sum_{m\alpha} \left| \sum_{L'} C'_{L'}(L'') \int R'_{1m\alpha,L'}(r)\, \phi(r)\, r^3 dr \right|^2 \end{aligned} \qquad (3.118).$$

(Here the x_i are the three components of the position operator.) Since the initial 1s state in an atom is usually populated by two electrons, the total cross-section (3.118) has to be doubled.

Section 3.4: Inclusion of Molecular Point Symmetry.

The dimension of the secular matrix (3.78) is in principle infinite; however, for practical calculations, it must be made finite. This is done by truncating the angular momentum indices $L \equiv (\ell, m, \alpha)$ in the expansions of the wavefunction for each SSR to some maximum allowed ℓ-value (which may vary from sphere to sphere). The dimension is then roughly proportional to the number of atoms in the cluster times $(\ell(\max)+1)^2$; and the total number of matrix elements is the square of this. Fortunately, the convergence in ℓ is quite rapid - $\ell(\max) = 4$ being quite adequate for most atomic spheres. Even so, for clusters of ten or more atoms say, we are looking at matrices with dimensions in the region of 100 and upwards. The main burden of the calculations of

Secs. 3.2,3 is in the construction of the secular matrix and the subsequent matrix manipulations, i.e. finding inverses or determinants; so large matrices are rather undesirable.

One method of reducing the work involved arises if the molecule has some point symmetry; that is to say, if the molecular potential is invariant under some non-trivial subgroup of the group O(3) of orthogonal transformations about a fixed point. In this case, as is well known (see e.g. Tinkham (1964)), the wavefunctions may be chosen to transform according to the irreducible representations (irreps) of the point group.

Specifically we consider the case where the molecule is invariant under the finite group of transformations $\mathcal{G}$ relative to the molecular centre $\vec{R}_o$. This group has a finite number of finite-dimensional irreps $\Gamma^{(\gamma)}$ (for $\gamma = 1,2,\ldots,g$). Because of the symmetry, the molecule will consist of P groups of equivalent atoms (transforming into each other under the group); and for each group $p = 1,2,\ldots,P$ there are N_p atoms. (We index the OS by $p = 0$ so that $N_o = 1$.) For a given group p, the individual atoms are labelled $q = 1,2,\ldots,N_p$ so that our usual atomic index i becomes composite $i \equiv (p,q)$. Note that $N = \sum_{p=1}^{P} N_p$.

It is shown in Diamond (1973) for the MT case, that a wavefunction transforming according to column λ of an irrep $\Gamma^{(\gamma)}$ may be constructed by expanding in terms of linear combinations of spherical harmonics at the atomic sites with the correct transformation properties built in. Although the extension to the full-potential case is not straightforward, we do not describe it here, since it would be a too complicated digression from our line of argument; and the result is the same as for the MT case anyway.

In particular, we expand in the symmetrized combinations

$$X^{pq}_{ln}(\hat{r}_{pq}) \equiv \sum_{m\alpha} K^{\gamma\lambda pq}_{lnm\alpha}\, Y_{lm\alpha}(\hat{r}_{pq}) \qquad (3.119),$$

where n runs through the combinations that may arise for a given l on a given set of equivalent atoms p (possibly there are none such). The constants $K^{\gamma\lambda pq}_{lnm\alpha}$ form a unitary transformation from the spherical harmonic bases on the atoms, which block diagonalizes the secular equation according to the irreps. We can then restrict our attention to a particular block which is of a smaller, more manageable size. The symmetrized secular matrix is then

$$\bar{S}^{pp'}_{\Lambda\Lambda'} \equiv \sum_{q}\sum_{m\alpha}\sum_{q'}\sum_{m'\alpha'} K^{pq}_{lnm\alpha}\, S^{pq\;p'q'}_{lm\alpha\, l'm'\alpha'}\, K^{p'q'}_{l'n'm'\alpha'} \qquad (3.120),$$

where $\Lambda \equiv (l, n)$ and we have dropped the γ and λ indices since these are fixed. The parts of the secular matrix in (3.78) are given by similar expressions to (3.120) and the symmetrized secular matrix is then given by

$$\bar{S}^{pp'}_{\Lambda\Lambda'} = (\bar{t}^{\,p})^{-1}_{\Lambda\Lambda'}\,\delta_{pp'} + \bar{H}^{pp'}_{\Lambda\Lambda'} + \bar{T}^{pp'}_{\Lambda\Lambda'} \qquad (3.121).$$

The secular equation is now

$$\sum_{p'\Lambda'} \bar{S}^{pp'}_{\Lambda\Lambda'}\,\bar{B}^{p'}_{\Lambda'} = \begin{cases} 0 & (E<0) \\ \delta_{p0}\sum_{\Lambda'} \bar{D}_{\Lambda\Lambda'}\,\bar{A}_{\Lambda'} & (0<E) \end{cases} \qquad (3.122).$$

Note that the symmetrized basis functions are normalized to

$$\sum_{q}\int X^{pq}_{ln}(\hat{r}_{pq})\, X^{pq}_{l'n'}(\hat{r}_{pq})\, d\Omega_{pq} = \delta_{ll'}\,\delta_{nn'} \qquad (3.123),$$

which implies that

$$\sum_{q}\sum_{m\alpha} K^{pq}_{lnm\alpha}\, K^{pq}_{ln'm\alpha} = \delta_{nn'} \qquad (3.124).$$

We introduce also

$$\hat{X}^{pq}_{ln}(\hat{r}_{pq}) \equiv \sqrt{N_p}\; X^{pq}_{ln}(\hat{r}_{pq}) \qquad (3.125)$$

purely for the purpose of the symmetrized expansion of the potential, since it is thus normalized to unity on individual atoms.

Now the $(\bar{\underset{\sim}{t}}^{\,p})^{-1}$ may be calculated directly without calculating the $(\underset{\sim}{t}^{\,i})^{-1}$ and invoking the transformation as in (3.120). For a given group of equivalent atoms p, we represent the potential by

$$V(\vec{r}) = \sum_{i=1}^{N_p}\sum_{\Lambda} V^{p}_{\Lambda}(r_i)\,\hat{X}^{i}_{\Lambda}(\hat{r}_i)\;\theta(b_p - r_i) \qquad (3.126).$$

We note that the molecular potential must transform according to

the totally symmetric irrep $\Upsilon = 1$ of $\mathcal{G}$. We shall denote this implicitly by using the $\hat{X}$ for the potential and the X for the wavefunction which may belong to any of the irreps. So the wavefunction in group P may be written

$$\psi(\vec{r}) = \sum_{q=1}^{N_P} \sum_{\Lambda} \phi_{\Lambda}^{P}(r_i) X_{\Lambda}^{i}(\hat{r}_i)\, \theta(b_P - r_i) \qquad (3.127),$$

where

$$\phi_{\Lambda}^{P}(r_i) \equiv \sum_{\Lambda'} C_{\Lambda'}^{P}\, R_{\Lambda\Lambda'}^{P}(r_i) \qquad (3.128).$$

Now ψ is a solution of the Schrödinger equation

$$(\nabla^2 + E)\,\psi(\vec{r}) = V(\vec{r})\,\psi(\vec{r}) \qquad (3.129),$$

so that

$$\sum_{q}\sum_{\Lambda}\left[\frac{1}{r_i^2}\frac{d}{dr_i}\left(r_i^2\frac{d}{dr_i}\right) + E - \frac{l(l+1)}{r_i^2}\right]\phi_{\Lambda}^{P}(r_i)\, X_{\Lambda}^{i}(\hat{r}_i)\,\theta(b_P - r_i)$$
$$= \sum_{q}\sum_{\Lambda'}\sum_{\Lambda''} V_{\Lambda'}^{P}(r_i)\,\phi_{\Lambda''}^{P}(r_i)\, X_{\Lambda''}^{i}(\hat{r}_i)\,\hat{X}_{\Lambda'}^{i}(\hat{r}_i)\,\theta(b_P - r_i) \qquad (3.130).$$

Since $\hat{X}$ transforms as $\Upsilon = 1$ and X as some general irrep, their product must transform as X. Therefore there exist constants $J_P(\Lambda, \Lambda'; \Lambda'')$ such that

$$X_{\Lambda'}^{i}(\hat{r}_i)\,\hat{X}_{\Lambda''}^{i}(\hat{r}_i) = \sum_{\Lambda} J_P(\Lambda, \Lambda'; \Lambda'')\, X_{\Lambda}^{i}(\hat{r}_i) \qquad (3.131).$$

Using (3.123) we get

$$J_P(\Lambda, \Lambda'; \Lambda'') = \sum_{q} \int X_{\Lambda}^{i}(\hat{r}_i)\, X_{\Lambda'}^{i}(\hat{r}_i)\,\hat{X}_{\Lambda''}^{i}(\hat{r}_i)\, d\Omega_i$$
$$= \sum_{q} \sum_{m\alpha} \sum_{m'\alpha'} \sum_{m''\alpha''} K_{lm\alpha}^{Pq}\, K_{l'm'\alpha'}^{Pq}\, K_{l''m''\alpha''}^{Pq}\, I(L, L', L'') \qquad (3.132).$$

If we now define

$$U_{\Lambda\Lambda'}^{P}(r) \equiv \sum_{\Lambda''} J_P(\Lambda, \Lambda'; \Lambda'')\, V_{\Lambda''}^{P}(r) \qquad (3.133),$$

then, putting (3.131) into (3.130) and using (3.133), together with the isolating property of the δ functions, we get

$$\sum_{\Lambda}\left[\frac{1}{r_i^2}\frac{d}{dr_i}\left(r_i^2\frac{d}{dr_i}\right) + E - \frac{l(l+1)}{r_i^2}\right]\phi_{\Lambda}^{P}(r_i) X_{\Lambda}^{i}(\hat{r}_i) = \sum_{\Lambda\Lambda'} U_{\Lambda\Lambda'}^{P}(r_i)\,\phi_{\Lambda'}^{P}(r_i)\, X_{\Lambda}^{i}(\hat{r}_i) \qquad (3.134).$$

Multiplying both sides of (3.134) by $X_{\Lambda''}^{i}(\hat{r}_i)$, integrating with respect to $\hat{r}_i$ and summing over q, gives by (3.123,128)

$$\left[\frac{1}{r^2}\frac{d}{dr}\left(r^2\frac{d}{dr}\right) + E - \frac{l(l+1)}{r^2}\right] R_{M'}^{P}(r) = \sum_{\Lambda''} U_{\Lambda M''}^{P}(r)\, R_{\Lambda''\Lambda'}^{P}(r) \qquad (3.135).$$

With the $R_{\Lambda\Lambda'}^{P}(r)$ one may create symmetrized versions of the Wronskian matrices used in the definitions of the SSR t-matrices.

Using the symmetrized basis, all relations involving unsymmetrized quantities are also valid for the corresponding symmetrized quantities.

The use of a symmetric basis alters the expression for the photoabsorption cross-section (3.118). The dipole-allowed final states that can be excited from an initial 1s state will only belong to a few of the irreps. Furthermore, the degeneracy of an irrep means that, for the average over orientations, we need to consider only one of the columns of the irrep. The final result is then

$$\sigma(E) = \left(\frac{4}{9}\pi^2\alpha\hbar\omega\right)\sum_{\gamma} d(\gamma)\sum_{\Lambda''}\left|\sum_{\Lambda'} C'_{\Lambda'}(\Lambda'')\int R'_{11,\Lambda'}(r)\phi(r)r^3dr\right|^2 \quad (3.136),$$

where $d(\gamma)$ is the dimension of the irrep γ.

Chapter 4. MODELLING THE POTENTIAL.

Section 4.1: Initial Potential Generating Program MLPSHX.

Since the central point of this work is the removal of an approximation to the one-electron potential, we shall devote some space to the development of an accurate representation of the potential in the form required by the FP-SW formalism of the previous chapter. As is seen from (3.19-22), the potential in each SSR must be represented by a spherical harmonic expansion (SHX) about the centre of the region. The formulae (3.70,71,73,74,88, 102) which use the potential in the IR do not seem to favour any particular type of representation for that potential. The original idea for evaluating these integrals was to use a SHX of the potential around the molecular centre and then to re-expand the atom-centred (and OS-centred) partial waves about the molecular centre using (A40-44). The SHX would be that of a potential which was the true potential in the IR and zero elsewhere. Consequently the IR integrals could be extended to the whole interior of the OS and reduce to the sum of a set of radial integrals multiplied by the Gaunt-like coefficients of (A30) and some structure factors like (3.29) etc.

The choice of a scheme to evaluate the IR integrals (3.70) etc., proved to be the most troublesome and difficult part of the work. In the end, the scheme just outlined was deemed unsatisfactory and we abandoned it for several reasons. These centred around the considerable algebraic complexity involved (particularly in the symmetrized form described in Sec. 3.4), and doubts about what degree of accuracy could be expected with the ℓ-truncation in the re-expansions and the SHX of a discontinuous potential. While continuing investigations into similar schemes, we have

settled temporarily on a brute-force three-dimensional numerical quadrature scheme which we describe in Sec. 5.1. In this scheme the potential values are stored on the grid points of the quadrature mesh and no questions of convergence arise. Nevertheless, with an eye to future possibilities, we consider in this section the SHX of the IR potential about the centre of the molecule and what difficulties are encountered.

Before becoming involved in the expansion of the potential, a question immediately arises about which potential to use. Following the discussion of Sec. 2.1, we should use a potential which is the sum of the Coulomb potential of the ground-state electron density of the cluster plus the nuclei, and Slater's $X\alpha$ approximation to the exchange-correlation potential. Initially however, we usually do not have the true electron density, so we approximate it by a superposition of the electron densities of the free atoms. These last may be obtained from independant calculations whose results are tabulated (e.g. Clementi and Roetti (1974) or Herman and Skillman (1963)). In this thesis we use only potentials derived from such superpositions. Presumably, if one wishes to approach experimental results as closely as possible, one should use self-consistent electron densities. However, for the purpose of determining the size and nature of the effects of including non-MT corrections to the potential, such superimposed potentials are probably quite adequate. One requires at least that they model, in an approximate way, the potential variations of a real molecule that the MT potential lacks.

We describe now the details of the generation of the potential representation in the form used by the FP-SW method. A program called MLPSHX was written to carry out the generation of such representations for arbitrary clusters. The notation is that of

Now we seek the superimposed potential of a cluster of N atoms with nuclei at sites $\vec{R}_i$ for $i = 1,2,\ldots,N$. With each atom i is associated a nucleus of charge Z_i and an electron cloud of density $\rho_i(r_i)$ (spherically symmetric), such that

$$\int_0^\infty 4\pi r^2 \rho_i(r)\,dr \equiv Z_i^e \qquad (= Z_i \text{ if atom neutral}) \quad (4.1).$$

The potential energy of the electron, that we seek is

$$V(\vec{r}) \equiv V_{CN}(\vec{r}) + V_{CE}(\vec{r}) + V_{X\alpha}(\vec{r}) \qquad (4.2),$$

where V_{CN} is the Coulomb potential energy due to the nuclei, V_{CE} is the Coulomb potential energy due to the electrons and $V_{X\alpha}$ is the exchange-correlation potential energy.

We know that V_{CN} is a solution of Poisson's equation (note V is an energy in Rydbergs)

$$\nabla^2 V_{CN}(\vec{r}) = 8\pi \rho_N(\vec{r}) \qquad (4.3),$$

where

$$\rho_N(\vec{r}) \equiv -\sum_{i=1}^{N} Z_i\, \delta^3(\vec{r} - \vec{R}_i) \qquad (4.4);$$

so that

$$V_{CN}(\vec{r}) = -\sum_{i=1}^{N} 2Z_i / |\vec{r} - \vec{R}_i| \qquad (4.5).$$

Likewise V_{CE} is a solution of

$$\nabla^2 V_{CE}(\vec{r}) = -8\pi \rho(\vec{r}) \qquad (4.6)$$

and the total superimposed electron density is

$$\rho(\vec{r}) \equiv \sum_{i=1}^{N} \rho_i(|\vec{r} - \vec{R}_i|) \qquad (4.7).$$

Let us consider for the moment the general problem of solving Poisson's equation in multipoles. Thus, for some general charge density $\rho(\vec{r})$ expanded as

$$\rho(\vec{r}) \equiv \sum_L \rho_L(r)\, Y_L(\hat{r}) \qquad (4.8),$$

we wish to find $V(\vec{r})$, satisfying Poisson's equation, and expanded as

$$V(\vec{r}) \equiv \sum_L V_L(r)\, Y_L(\hat{r}) \qquad (4.9).$$

As is well known, we may write the solution using (A37) as

$$V(\vec{r}) = \int (\rho(\vec{s})/|\vec{r}-\vec{s}|)\, d^3s \qquad (4.10).$$

Using the expansion formula in (A37), and the spherical harmonic addition theorem, this is

$$V(\vec{r}) = \iint \left[\sum_L \left(\frac{4\pi}{2l+1}\right) \xi_l\left(\frac{s}{r}\right)\left(\frac{1}{s}\right) Y_L(\hat{r})\, Y_L(\hat{s}) \right] s^2 \rho(\vec{s})\, d\Omega(\hat{s})\, ds \qquad (4.11),$$

where ξ_l is defined by

$$\xi_l(x) \equiv \begin{cases} x^{l+1} & (x < 1) \\ x^{-l} & (x > 1) \end{cases} \qquad (4.12).$$

If we now put (4.8,9) into (4.11) and use the orthonormality of the spherical harmonics, we find

$$V_L(r) = \frac{4\pi}{2l+1} \int \xi_l\left(\frac{s}{r}\right) \rho_L(s)\, s\, ds \qquad (4.13)$$

or, more explicitly,

$$V_L(r) = \frac{4\pi}{2l+1} \left\{ \frac{1}{r^{l+1}} \int_0^r \rho_L(s) s^{l+2} ds + r^l \int_r^\infty \rho_L(s) s^{-l+1} ds \right\} \qquad (4.14).$$

Returning to our main development (where ρ is the electron density again and V is the potential energy of a given electron) we may use the $l = 0$ case in (4.14), along with the linearity of Poisson's equation and (4.7), to write

$$V_{CE}(\vec{r}) = \sum_{i=1}^{N} V_i^e(|\vec{r} - \vec{R}_i|) \qquad (4.15),$$

with

$$V_i^e(r_i) \equiv 8\pi \left\{ \frac{1}{r_i} \int_0^{r_i} \rho_i(s) s^2 ds + \int_{r_i}^\infty \rho_i(s) s\, ds \right\} \qquad (4.16).$$

Thus we can set

$$V_c(\vec{r}) \equiv V_{CN}(\vec{r}) + V_{CE}(\vec{r}) = \sum_{i=1}^{N} V_i(|\vec{r} - \vec{R}_i|) \qquad (4.17),$$

where

$$V_i(r_i) \equiv -\frac{2Z_i}{r_i} + 8\pi \left\{ \frac{1}{r_i} \int_0^{r_i} \rho_i(s) s^2 ds + \int_{r_i}^\infty \rho_i(s) s\, ds \right\} \qquad (4.18).$$

The Xα potential we shall take to be

$$V_{X\alpha}(\vec{r}) = -6\alpha \left[(3/8\pi) \rho(\vec{r}) \right]^{1/3} \qquad (4.19),$$

where α is taken to be the average of the atomic values given by Schwarz (1972) for the atoms in the cluster. In the MT version of the SW-X method (Johnson (1973)) each separate atomic potential uses its own appropriate α_i. In our case this would cause potential discontinuities, which we are trying to avoid; so we take a

single value. In any case the differences are only a few percent of the Xα potential and this itself is a small fraction of the total potential.

We now need to find the SHX of the electron density in (4.7) about a particular atomic site i. The general problem of spherical harmonic re-expansions is treated by Löwdin (1956), although we do not use his full machinery, since we can take advantage of the fact that we are superimposing spherical functions at the different sites.

Thus, within atomic sphere τ_i, we write

$$\rho(\vec{r}) \equiv \sum_L \rho_L^{(i)}(r_i)\, Y_L(\hat{r}_i) \qquad (4.20),$$

so that

$$\begin{aligned}\rho_L^{(i)}(r_i) &= \int \rho(\vec{r})\, Y_L(\hat{r}_i)\, d\Omega_i \\ &= \sum_{j=1}^{N} \int \rho_j(|\vec{r}_i - \vec{R}_{ji}|)\, Y_L(\hat{r}_i)\, d\Omega_i \quad (\text{using } (3\cdot8,9),(4\cdot7)) \\ &= \sqrt{4\pi}\, \rho_i(r_i)\, \delta_{L,(001)} + \sum_{\substack{j=1 \\ j\neq i}}^{N} \int \rho_j(|\vec{r}_i - \vec{R}_{ji}|)\, Y_L(\hat{r}_i)\, d\Omega_i \end{aligned} \qquad (4.21).$$

The individual integrals in (4.21) may be evaluated as follows. First we note that the function $\rho_j(|\vec{r}_i - \vec{R}_{ji}|)$, considered as a function of $\vec{r}_i$, is axially symmetric about the direction of $\vec{R}_{ji}$. Therefore it may be expanded in Legendre polynomials thus:

$$\rho_j(|\vec{r}_i - \vec{R}_{ji}|) \equiv \sum_l \left(\frac{2l+1}{4\pi}\right) \beta_l^{ji}(r_i)\, P_l(\hat{r}_i \cdot \hat{R}_{ji}) \qquad (4.22)$$

for some as yet unknown β_l^{ji}. Using the addition theorem (A24) in (4.22) and then putting the result into (4.21) gives

$$\rho_L^{(i)}(r_i) = \sqrt{4\pi}\, \rho_i(r_i)\, \delta_{L,(001)} + \sum_{\substack{j=1 \\ j\neq i}}^{N} \beta_l^{ji}(r_i)\, Y_L(\hat{R}_{ji}) \qquad (4.23).$$

If we consider a fixed r_i in (4.22) and denote $w \equiv \hat{r}_i \cdot \hat{R}_{ji}$, then

$$|\vec{r}_i - \vec{R}_{ji}| = \sqrt{r_i^2 + R_{ji}^2 - 2 r_i R_{ji} w} \qquad (4.24)$$

and the use of the well-known orthogonality integral for Legendre polynomials gives

$$\beta_l^{ji}(r_i) = 2\pi \int_{-1}^{1} \rho_j\left(\sqrt{r_i^2 + R_{ji}^2 - 2 r_i R_{ji} w}\right) P_l(w)\, dw \qquad (4.25).$$

At this point Löwdin (1956) introduces his recurrence-relation

method for the calculation of (4.25). Our earlier experiments with this method led to large integration errors at high l, presumably related to the high polynomial powers that appear as weight factors in the separate sub-integrals. Although a recasting of the recurrence relations in some manner may provide more stable results, we abandoned the method in favour of a direct evaluation of (4.25) using a 48-point Gauss-Legendre mesh on the interval (-1,1).

Although we have only calculated the expansion of the electron density in (4.23,25), the result also applies to the potential energy (4.17) once the radial forms (4.18) have been calculated and stored away. While the method gives smooth and accurate radial functions for the expansion in an atomic region, some problems arise when the expansion is around the molecular centre. This is because of the cusps in the electron density at the atomic nuclei and the Coulomb singularities in the potential, both of which give rise to slowly convergent SHXs, whose radial functions are not smooth.

For an ASR these problems do not matter because the required radial extent of the SHX does not reach as far as neighbouring nuclei. For the IR however, it extends past all atomic centres. Fortunately, the SHX for the IR is only required to give a good approximation of the potential in the IR, and does not really need to model the Coulomb singularities or density cusps in the ASRs. These are already well modelled by their own SHXs and thus, via (3.21), are completely accounted for in the solution of the Schrödinger equation. In extracting the SHX for the IR electron density and potential we can replace the singularities by "caps" in the ASRs that fit smoothly to the values at the sphere boundaries.

The beneficial effects of this approach may be seen for a simple situation in Fig. 4.1. Here we model the potential energy (= 2/R) of a proton in the field of another proton fixed at the position P = (0,0,2) Bohr. The SHX of the potential is about the origin O and is truncated at $l = 9$. In the first case we show the truncation error when the potential singularity is included (and the expansion (A37) is used); and in the second we have replaced the potential, within 1 Bohr of the fixed proton, by a quadratic smoothly fitting cap. The specification of the contour intervals shows first the lowest contour, then the contour interval (in brackets) and finally the highest contour. Notice that in the second case the contour intervals are twenty times as fine as in the first.

In our electron density and potential expansions we use quartic caps. Instead of (4.21) we have for the IR

$$\rho_L^{(o)}(r_o) = \sum_{j=1}^{N} \int \tilde{\rho}_j(|\vec{r}_o - \vec{R}_{jo}|)\, Y_L(\hat{r}_o)\, d\Omega \qquad (4.26),$$

where

$$\tilde{\rho}_j(r) \equiv \begin{cases} a_0 + a_1 r + a_2 r^2 + a_3 r + a_4 r^4 & (r < b_j) \\ \rho_j(r) & (r > b_j) \end{cases} \qquad (4.27).$$

The a_n are chosen so that $\tilde{\rho}_j$ is smooth at $r = 0$ and matches up to the second derivative at $r = b_j$. This means

$$a_1 = a_3 = 0 \qquad a_0 = \rho_j(b_j) - \tfrac{5}{8} b_j \rho_j'(b_j) + \tfrac{1}{8} b_j^2 \rho_j''(b_j)$$

$$a_2 = \tfrac{3}{4} b_j^{-1} \rho_j'(b_j) - \tfrac{1}{4} \rho_j''(b_j) \qquad a_4 = -\tfrac{1}{8} b_j^{-3} \rho_j'(b_j) + \tfrac{1}{8} b_j^{-2} \rho_j''(b_j) \qquad (4.28).$$

Note that the re-expansions we have described so far apply only to the electron density and to the Coulomb part of the potential. This is because of the linear superposition property associated with these quantities. Unfortunately, the Xα potential (4.19) does not have this property so we must find other means of generating the SHXs. At first sight (4.19) suggests that there might exist some direct algebraic means of using the SHXs for ρ

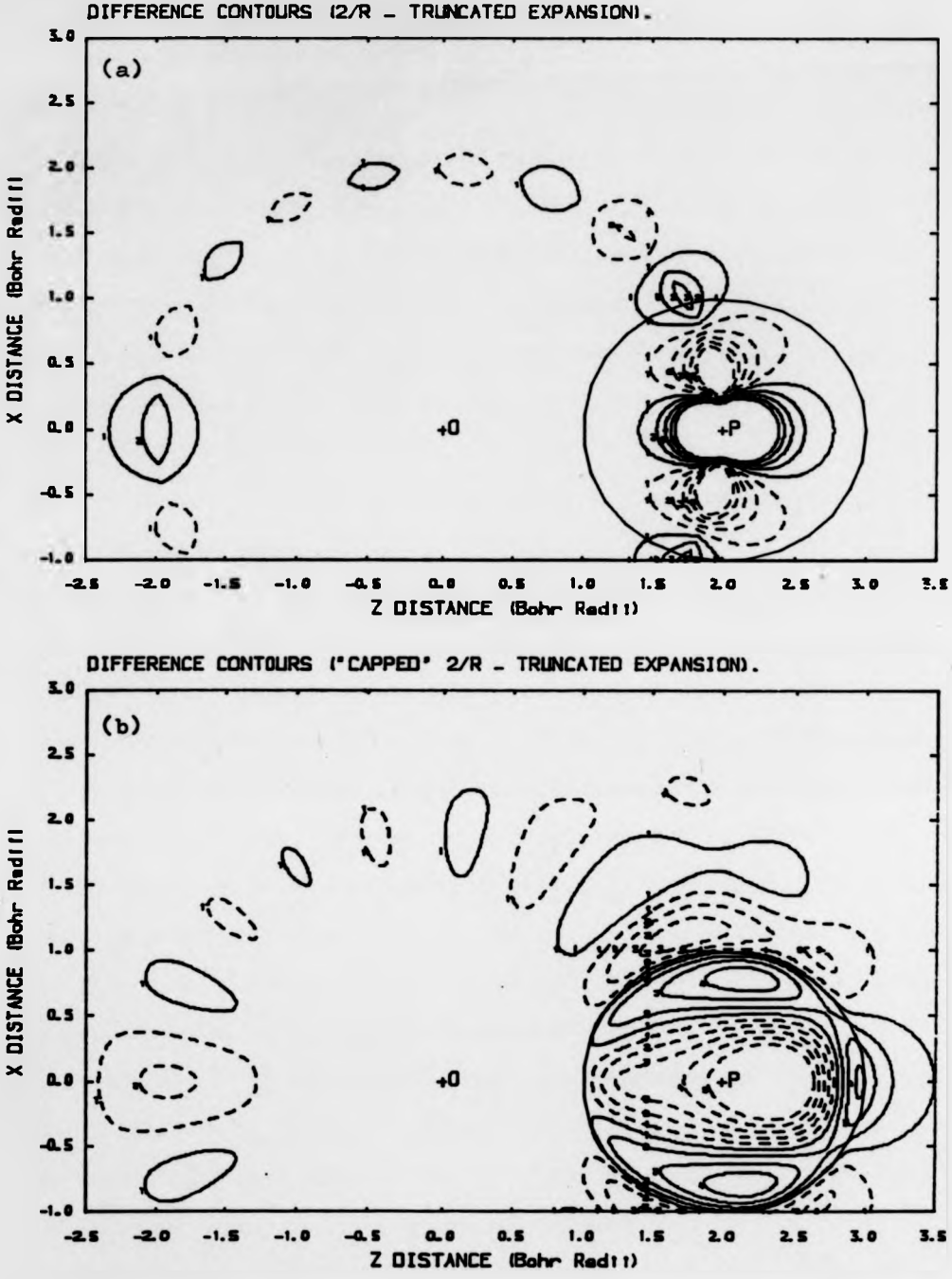

Figure 4.1: Truncation error for l=9 SHXs of 2/R potential: (a) unaltered, (b) quadratically capped. Contours full (+), broken (-): spacing (a) -0.9(0.2)0.9, (b) -0.045(0.01)0.045 Rydbergs.

(which we have already obtained) to obtain the SHXs of its cube root, and thus $V_{X\alpha}$; however, no such mathematical means appear to exist. Alternatively we might consider the inverse direction; expressing ρ in terms of its cube root and trying to solve the implicit equations that result (by iterative methods etc.). While the latter possibility seems promising, its implementation was deemed too complicated because of the double products of Gaunt coefficients (A30) that appear in the expressions. Nevertheless, a fresh attack on the problem may reopen the possibility of using this potentially fast method.

For the present we have resorted to direct evaluation of the surface integrals

$$V_L^{i(X\alpha)}(r_i) \equiv -6\alpha \left(\frac{3}{8\pi}\right)^{1/3} \int \rho(\vec{r}_i + \vec{R}_i)^{1/3} Y_L(\hat{r}_i)\, d\Omega_i \qquad (4.29).$$

The main difficulty here is that we must find a numerical quadrature for the surface of the sphere, which is accurate and yet does not require too many points. Since the region of integration is fixed, we might hope to use some two-dimensional analogue of the one-dimensional Gaussian quadrature formulae. These latter are well known for their great efficiency. Unfortunately, no comparable general scheme is known for generating efficient spherical formulae of arbitrarily high degree (see Stroud (1971)). One possible method is to use a product of two one-dimensional formulae for the θ and ϕ parts of the surface integral. While this gives reasonable results, the uneven distribution of points over the sphere surface means that, for a given final accuracy, more points are required than is strictly necessary.

There are available in the literature a variety of schemes for integration over a spherical surface that are much better than product formulae. (Stroud (1971) contains a large collection and McLaren (1963) gives a more detailed exposition.) One measure of

the efficiency E_f of such formulae is

$$E_f \equiv (\ell(max)+1)^2/3N_p \qquad (4.30),$$

where ℓ(max) refers to the highest order spherical harmonic which is integrated exactly by the formula; $(\ell(max)+1)^2$ then being the total number of such functions. N_p is the total number of points in the formula ($3N_p$ accounting for the two positional degrees and one weight degree of freedom for each point). For highly efficient formulae E_f may be about 1. We have found in Lebedev (1977) a 302-point formula with ℓ(max) = 29 (giving an E_f of about 0.993). The formula is based on the use of a set of points and weights invariant under the octahedral group with inversion O_h. By considering combinations of spherical harmonics that transform according to the totally symmetric irrep of O_h only, the size of the equations that need to be solved to provide the positions and weights of points is greatly reduced (functions in the other irreps automatically giving zero sums by virtue of the orthogonality of irreps). Although such a method is applicable in principle to arbitrarily high ℓ(max), it is pointed out by Lebedev (1977) that the size and complexity of the equations increase rapidly with ℓ(max).

The ℓ(max) of 29 in our 302-point formula is easily adequate for our purposes. This may be seen from a consideration of (3.22) together with the properties of the Gaunt coefficients in App. A2 which show that the highest ℓ-component in the potential that is used is double that of the wavefunction. Since, even for the continuum wavefunctions of Sec. 3.3, we would take a wavefunction ℓ(max) of 10 or so (related to the XANES energy range and the cluster size - see Sec. 5.5), then the potential ℓ(max) is not too great for our formula. And in fact, using this formula in MLPSHX to evaluate (4.29) has produced good results as we show in

the next section.

Note that MLPSHX was written to take account of molecular symmetry following the discussion of Sec. 3.4. The results of the program are thus the symmetrized potential radial components that appear in (3.126). We do not give the details since it is only a minor extension to the formalism of this section.

Section 4.2: Full Potential for Chromium Hexacarbonyl and Discussion.

We now use MLPSHX to generate a full potential for our model system chromium hexacarbonyl. First of all let us see the electron density that results from the superposition of free atoms. This is shown in Fig. 4.2. Note particularly the build-up of density around the CO ligand in contrast with the relatively low density between the Cr and C atoms. Given the large fraction of the C and O valence electrons involved in the triple carbonyl bond, one might expect that the actual density is significantly different from our free-atom superposition. One therefore suspects that a self-consistent density for the CO ligand would be more appropriate here.

The total potential from (4.2) that this density gives may be seen in Fig. 4.3. By considering this figure in conjunction with Fig. 2.1 we may estimate that the typical error of the MT potential is of the order of half a Rydberg over much of the IR volume, rising to two or more Rydbergs at the carbon and oxygen sphere boundaries.

As a first test we ran MLPSHX with the same sphere radii as was used for the MT case. (Remember that these were chosen with touching spheres so that the C and O potentials matched at their contact point.) The ℓ-truncations were chosen to be roughly dou-

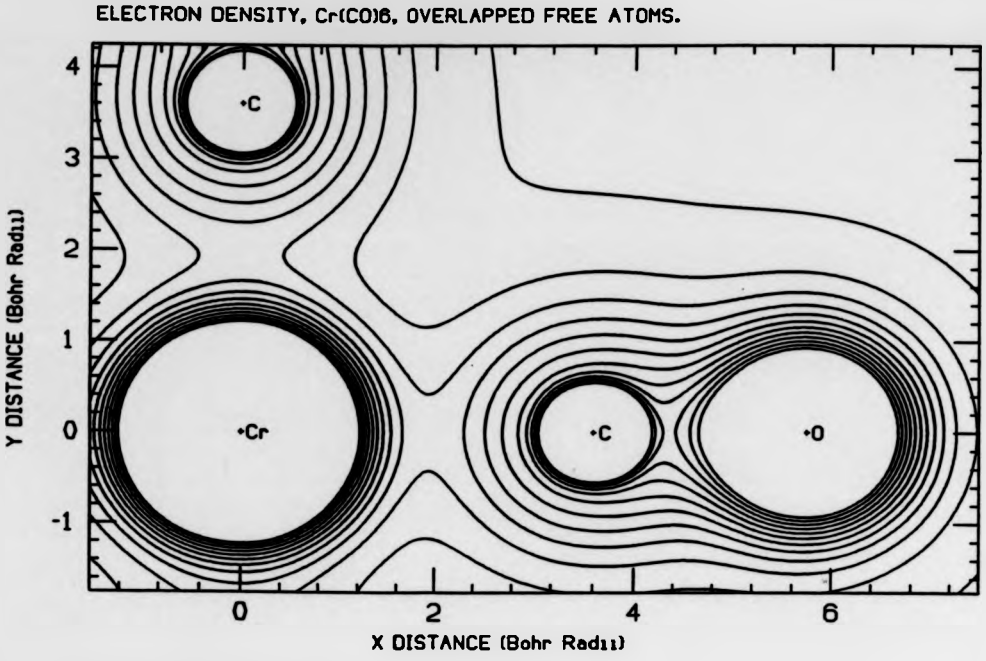

Figure 4.2: Chromium hexacarbonyl electron density resulting from the superposition of the free-atom densities. Plane of contour plot intersects four of the CO ligands. Contour interval is 0.04 Bohr^{-3} with the highest contour at 0.45 Bohr^{-3} (closest to the atomic nuclei), and the lowest at 0.01 Bohr^{-3}. (This is summarized as 0.01(0.04)0.45 Bohr^{-3}.)

---

ble the typical wavefunction values for the reasons described above. Thus l (max) = 20(IR/EMR), 10(Cr), 5(C) and 5(O). When the potential was reconstructed from the SHX radial functions the results were very good, with the values in the SSRs and most of the IR within 0.05 Ryd. of the actual values. The greatest inaccuracies occurred in the vicinity of the oxygen sphere in the IR. The worst was a discontinuity of about 0.6 Ryd. on a small part of the oxygen sphere surface; the average magnitude over the whole surface being about a quarter of this. The discontinuities at the other sphere surfaces, closer to the molecular centre, were

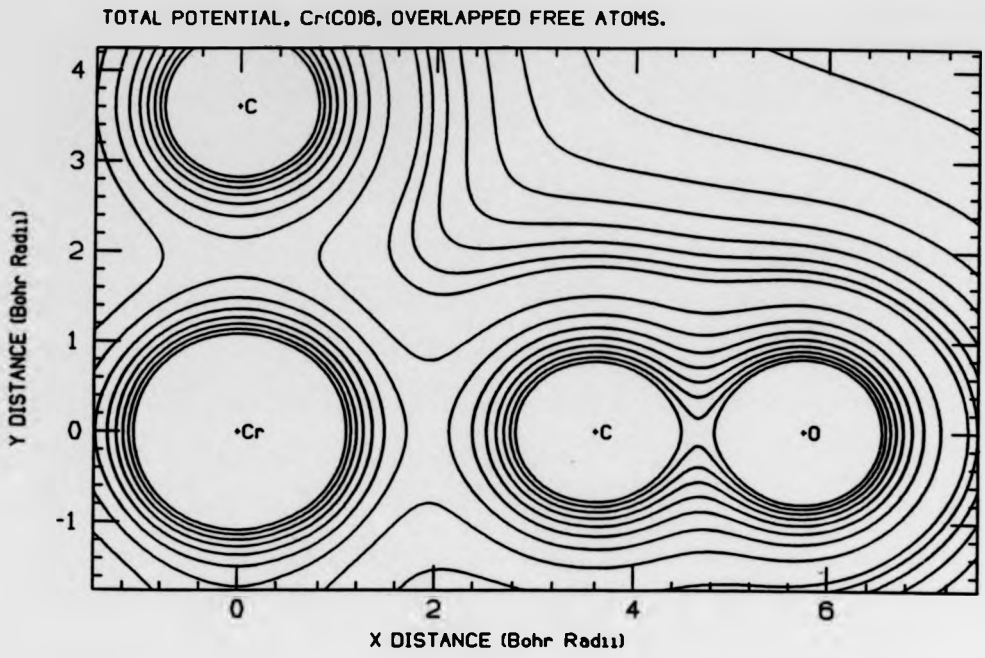

Figure 4.3: Chromium hexacarbonyl total potential from the superimposed free-atom electron densities. There are two contour intervals for the sixteen contours whose values are then summarized as -6.0(0.6)-1.2(0.15)-0.15 Ryd., with the lowest value nearest to the atomic nuclei.

less than a tenth of this. The decline in accuracy of the expansions is of course directly related to the distance from the expansion centre (for fixed l(max)).

At this point we realize that the considerations that are taken into account when choosing sphere radii for the FP, are significantly different from the MT case. The main consideration in the latter case is to reduce the IR volume as much as possible. This requires the various spheres to be touching and leaves little room for manoeuvre when trying to minimize potential discontinuities at sphere boundaries. Although in the FP case we wish also to reduce the IR volume, it is not such a pressing requirem-

ent, since our potential model there is reasonable. The necessity of having touching spheres can then be relaxed and we can adapt the individual radii to ameliorate the local inaccuracies of the SHXs.

Therefore, in our final model for the chromium hexacarbonyl potential, we expand the oxygen spheres by 15% at the expense of the carbon spheres (keeping them touching). This increases the angle subtended by the oxygen spheres as seen from the molecular centre and, considering the relationship between the number of lobes and the order of a spherical harmonic, we might hope that the l-truncation that we used above for the IR will give a better representation. We also reduce the chromium sphere radius by about 12%. This enlarges the IR volume, but that particular region is more accurately represented by the higher l-truncation of the SHX in the IR.

The parameters of the partition are now as follows. The Cr-C distance is 3.6075 Bohr and the C-O distance is 2.1486 Bohr. The oxygen sphere radii are increased to 1.2176 Bohr while the chromium and carbon spheres are reduced to 2.2000 and 0.9309 Bohr respectively. The OS touches the oxygen spheres and is thus 3.074 Bohr. The l-truncation is the same as given earlier except that the larger sphere radii for the oxygens require an increase of the associated l(max) to 6. The symmetrized basis functions for the potential have l-values, in consecutive order for each region; 0, 4, 6, 8, 10, 12, 12, 14, 16, 16, 18, 18, 20, 20 (IR+EMR); 0, 4, 6, 8, 10 (Cr); 0, 1, 2, 3, 4, 4, 5, 5 (C) and 0, 1, 2, 3, 4, 4, 5, 5, 6, 6 (O).

The residual truncation error for this model is seen in Fig. 4.4. We note that, for a small trade-off of accuracy near the carbon spheres, we have reduced the worst errors of the previous

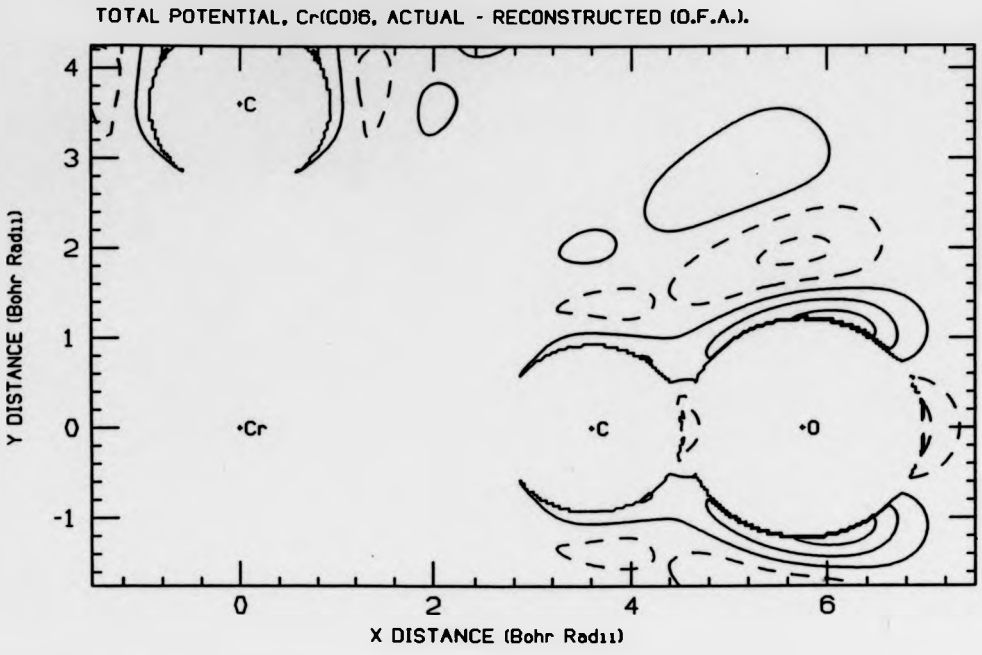

Figure 4.4: Residual truncation error for expansion of chromium hexacarbonyl potential. Positive contours are full and negative contours are broken. Contour values are -0.75(0.1)0.75 Ryd.

model by a half. In general we note that the inaccuracies of our model are from one to three orders of magnitude smaller than the MT case. We therefore feel that this is a sufficient foundation on which to base our test of the FP-SW theory of Chap. 3. Let us stress that, from now on, the partition and its various parameters will be held constant; and we reiterate the fact that the values of these parameters result solely from the accuracy requirements of the potential model.

Let us finally look at the actual radial functions that MLPSHX gives for the potential expansions. These may be seen in Figs. 4.5 and 4.6. Note the smooth behaviour of the IR functions especially in the neighbourhood of the C and O radii. In the region of $r = 0$ the behaviour of the ASR radial functions should be propo-

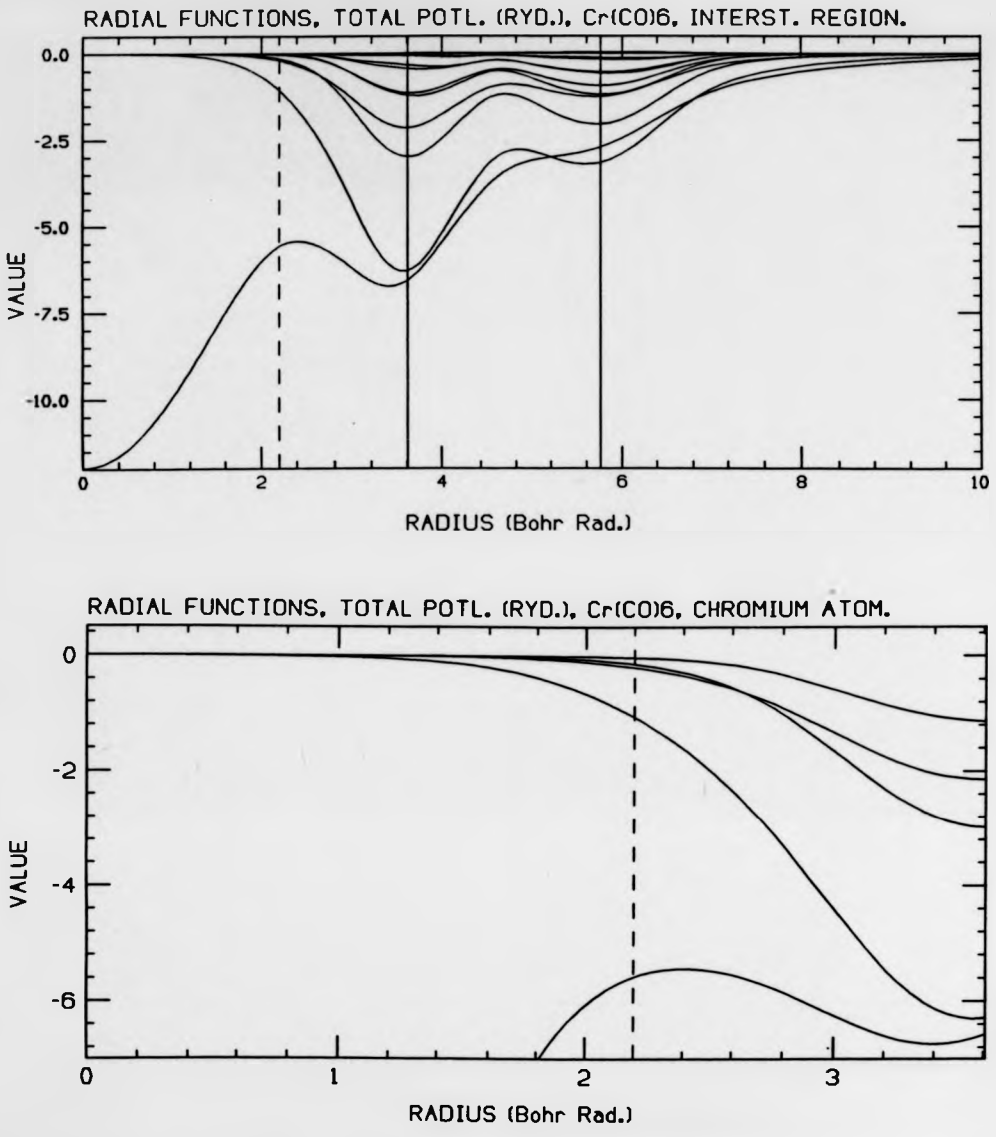

Figure 4.5: Chromium hexacarbonyl potential radial functions for the IR(+EMR) and the Cr atom. In the IR plot the left edge is the Cr nucleus, the two full vertical lines correspond to the C and O distances and the vertical broken line (both plots) is the Cr sphere radius. In ascending order the curves correspond to the symmetrized functions (see text); (IR, at r=3.6 Bohr) 1,2,4,3,6,5,8,9,13,14,7,10,12; (Cr, at r=2.2 Bohr) 1,2,3,4,5.

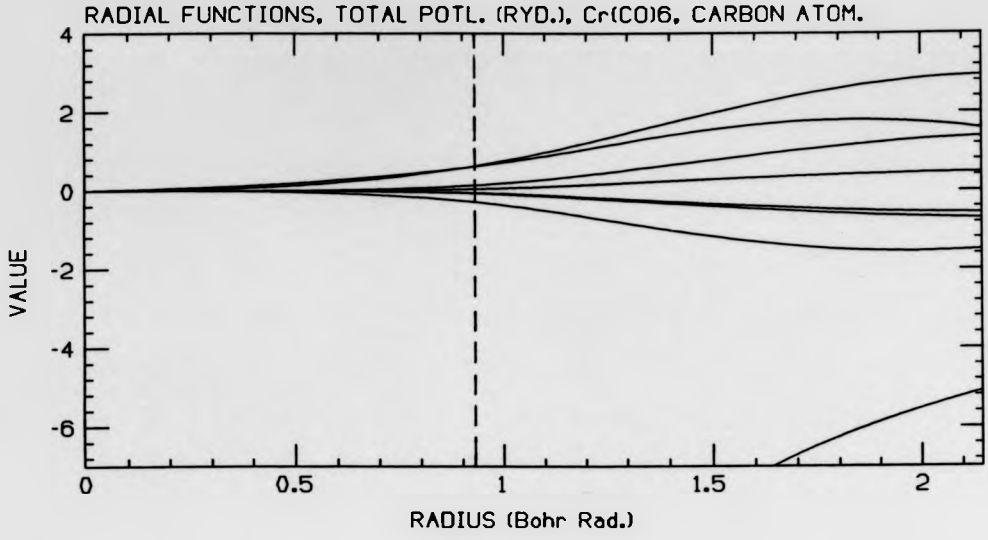

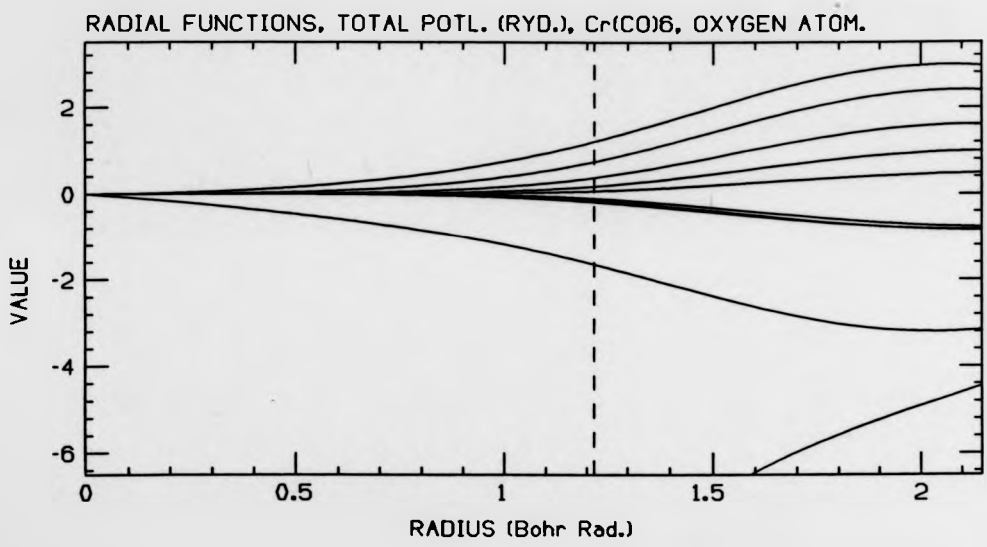

Figure 4.6: Chromium hexacarbonyl potential radial functions for the C and O atoms. The broken vertical lines correspond to the sphere radii for each atom. In ascending order, at the sphere radii, the curves correspond to the symmetrized functions; (C) 1,4,5,8,7,6,2,3; (O) 1,2,5,7,10,9,8,6,4,3. Note that each radial function is multiplied by the appropriate linear combination of spherical harmonics to give its actual contribution.

rtional to r^{ℓ} (except for $\ell = 0$ and the Coulomb singularities). The limited precision of the computer arithmetic means that this behaviour is not accurately reproduced for the higher ℓ-values. Because of concern over what this inaccuracy might do to the integration of the coupled radial Schrodinger equations, we have written a program called INPSHX which, among other things, smooths the radial functions by using a Chebyshev polynomial approximation for the part remaining when the original function is divided by r^{ℓ}. (These radial functions for the potential are analogous to those in (4.20).)

Chapter 5. FULL-POTENTIAL SCATTERED-WAVE PROGRAMS.

Section 5.1: The Energy Eigenvalue Search Program ENESHX.

The ultimate aim of the programming task is to produce computer code that will calculate the XANES of an arbitrary cluster. Since our main purpose at present is to explore the effects of full-potential (FP) calculations and their computational feasibility, our immediate goal is less ambitious. Nevertheless, we wish to produce code that will have a useful life significantly beyond our initial investigations, and general enough to be usable for a wide variety of physically interesting molecules or clusters. Also it should be amenable to further development and to incorporation into more advanced programs. A further desirable feature is that it produce results in a reasonable time even on relatively small computers.

With these general requirements in mind we have decided to restrict the calculations to K-edge XANES in the dipole approximation, for symmetric molecules with say three shells of coordinating atoms. The code is designed to be as fast and as accurate as possible at the expense of storage space.

From a practical point of view we must also arrange the programming so that it can be easily debugged. We need to be able to tell the difference between mere programming errors and fundamental deficiencies of the theory. This is partly achieved by following the basic plan of the old programs (described in Sec. 2.4) and using as much of the actual code as possible. This has been done with the special function, interpolation, integration and matrix manipulation subroutines, all of which are well tested and quite flexible. Other than these, the code is almost entirely new.

With the necessity of testing in mind we have decided to write the code in two stages. Firstly we wrote an energy eigenvalue search program called ENESHX (analogous to ENERGY of Sec. 2.4) which realizes the theory of Sec. 3.2 for bound states. This is much simpler than the full continuum photoionization program (that we called CNTSHX in analogy with CONTNM) and would be an important part of a future FP self-consistent field program. ENESHX can then be tested separately and, once this has been done it may be adapted to make CNTSHX by taking advantage of the great similarity of the important parts.

We now describe the writing of ENESHX. This program takes a non-MT potential from MLPSHX and INPSHX and searches for one-electron eigenstates in that potential. In particular, given a range of energies in which to search, and an irreducible representation of the point group of the cluster to which the eigenstates belong, it looks for those energies at which the (symmetrized) secular matrix $\overline{\underset{\sim}{S}}$ (from (3.120)) has zero determinant. The search procedure tests the determinant on an evenly spaced mesh in the energy range and having found a change in sign it refines the zero position with a binary search. The details need not concern us here since it is similar to that of the old ENERGY. Also, when the energy is very deep, the electron is confined in an atomic core and the wavefunction may be treated quite simply. The effects of non-sphericity of the potential have negligible consequences for deep core levels so we do not include it. The most important new feature of the code in the FP case is the construction of the secular matrix for a valence eigenstate, and we describe here the important details.

It was shown in Sec. 3.2 that the secular matrix may be written as a sum of three parts

$$\underset{\sim}{\bar{S}} = \underset{\sim}{\bar{t}}^{-1} + \underset{\sim}{\bar{H}} + \underset{\sim}{\bar{T}} \qquad (5.1)$$

each of which is constructed in a very different way. The block diagonal matrix $\underset{\sim}{\bar{t}}$ gives the scattering behaviour of each atom, while $\underset{\sim}{\bar{H}}$ describes the propagation of the electron between atoms and $\underset{\sim}{\bar{T}}$ includes the effects of the non-constant interstitial potential on this propagation.

The propagators (or "structure factors") $\underset{\sim}{\bar{H}}$ are in fact identical to those of the MT program ENERGY. Our evaluation of the summation in (3.120) follows that of ENERGY in general outline, but we have modified some of the important details like the storage and retrieval of the Gaunt coefficients of (A23). The summation is quite complicated and we do not reproduce the details here.

The first novel feature is the calculation of the atomic scattering matrices in $\underset{\sim}{\bar{t}}$. Since the atomic potentials have non-spherical components, the solutions of the radial Schrödinger equation are now coupled (as described earlier) and we must deal with matrices. We then need the matrix solution and its derivative at the sphere boundary to put into (3.50,51,83,84) to get the individual diagonal blocks of $\underset{\sim}{\bar{t}}$. Following (3.21,22,57) we put the radial equation into the form

$$\frac{d^2}{dr^2}\underset{\sim}{X} = \underset{\sim}{G}\,\underset{\sim}{X} \qquad (5.2),$$

where

$$G_{\Lambda\Lambda'}(r) \equiv U_{\Lambda\Lambda'}(r) + \frac{l(l+1)}{r^2}\delta_{\Lambda\Lambda'} - E\,\delta_{\Lambda\Lambda'} \qquad (5.3),$$

$$\underset{\sim}{X} \equiv r\,\underset{\sim}{R}(r) \qquad (5.4)$$

and $\underset{\sim}{R}$ is the desired matrix solution.

From (5.2) it is not difficult to show that

$$\left(\underset{\sim}{I} - \frac{h^2}{12}\underset{\sim}{G}(r+h)\right)\underset{\sim}{X}(r+h) = 2\left(\underset{\sim}{I} + \frac{5}{12}h^2\underset{\sim}{G}(r)\right)\underset{\sim}{X}(r) - \left(\underset{\sim}{I} - \frac{h^2}{12}\underset{\sim}{G}(r)\right)\underset{\sim}{X}(r-h) + O(h^6) \qquad (5.5).$$

On dropping terms of order h^6 and higher one obtains the recurrence relation for the matrix Numerov method. By defining

$$\underset{\sim}{Y}(r) \equiv \left(\underset{\sim}{I} - \frac{h^2}{12}\underset{\sim}{G}(r)\right)\underset{\sim}{X}(r) \tag{5.6}$$

the recurrence relation takes the simpler form

$$\underset{\sim}{Y}(r+h) = 12\,\underset{\sim}{X}(r) - 10\,\underset{\sim}{Y}(r) - \underset{\sim}{Y}(r-h) \tag{5.7}.$$

At each step of the recurrence procedure one obtains $\underset{\sim}{Y}(r+h)$ using (5.7) then, performing a matrix inversion in (5.6), one obtains $\underset{\sim}{X}(r+h)$.

To use the matrix Numerov procedure in practice for the atomic spheres and for the outer sphere, it is necessary to provide two initial solution matrices for the first two points of the integration mesh. For an atom the asymptotic form of the solution near the origin is (Natoli et al. (1986))

$$X_{\lambda\lambda'}(r) \longrightarrow r^{\ell+1}\delta_{\lambda\lambda'} \tag{5.8}.$$

Furthermore, the monopole part of the potential, i.e. the Coulomb singularity dominates near the origin and the radial Schrödinger equation becomes effectively decoupled. Thus we can take the solution matrices for small r to be those of the uncoupled equations, using a power series expansion and putting them on the matrix diagonal according to (5.8).

For the EMR we use a similar argument, since the monopole part of the potential dies away most slowly (in the absence of a non-zero dipole moment). Thus we take $\underset{\sim}{X}$ to be diagonal at infinity (or some sufficiently large starting radius) and use the diagonal part of $\underset{\sim}{G}$. We then use the WKB approximation to obtain each of the diagonal elements in the asymptotic region and then use the Numerov method to integrate inwards.

It will have been seen that the Numerov method depends on the equal spacing of the mesh points. However, in the ASRs the potential is varying rapidly in the region of the nucleus and the mesh points need to be closer together in that region. This is done using a scheme of mesh doubling in which, every twenty (equally

spaced) mesh points, the mesh increment doubles in size. The handling of the recurrence relation across these jumps (especially in the inward recurrence used for the EMR) requires some extra manipulations, but poses no real problems.

The most complicated and difficult part of the program is the evaluation of the matrix $\underset{\sim}{\overline{\overline{T}}}$ for the IR, given by (3.70,71,73,74) or (3.88). This matrix may be written, for $V_o < E < 0$ say, as

$$\overline{\overline{T}}^{pp'}_{\Lambda\Lambda'} = k \int_I F^p_\Lambda(\vec{s})\, V(\vec{s})\, F^{p'}_{\Lambda'}(\vec{s})\, d^3s \qquad (5.9);$$

where

$$F^p_\Lambda(\vec{s}) \equiv \sum_q f^p_l(ks_{pq})\, X^{pq}_{lm}(\hat{s}_{pq}) \qquad (5.10),$$

$$f^p_l(ks_{pj}) \equiv \begin{cases} n_l(ks_{pq}) & (p \neq 0) \\ j_l(ks_{pq}) & (p = 0) \end{cases} \qquad (5.11)$$

and

$$X^{pq}_{lm}(\hat{s}_{pq}) \equiv \sum_{m\alpha} K^{pq}_{lnm\alpha}\, Y_{lm\alpha}(\hat{s}_{pq}) \qquad (5.12).$$

The integral in (5.9) is over the IR and we need to find a scheme of numerical integration which is flexible enough to cope with different geometries and yet still be accurate. The general problem of finding Gaussian quality points and weights for numerical quadrature in three-dimensional regions of arbitrary shape remains unsolved, although efficient formulae for regions with special shapes are known (Stroud (1971)).

Although the shape of the IR itself is rather inconvenient, it is made up from the interior of the sphere τ_o minus the volumes of the atomic spheres τ_i. Efficient quadrature formulae are known for spherical surfaces and it is easy to combine them with Gaussian line formulae to give accurate formulae for spherical volumes. Thus our choice of integration method is to first integrate over the whole sphere with a large, accurate formula and then use smaller formulae for the atoms, subtracting their individual contributions. We took the formula for τ_o to be a product

of the 302-point spherical surface formula of Lebedev (1977) (see Sec. 4.1) and a Gauss-Legendre formula for the radius with the number of points chosen according to the radius of the OS. (This was one point for each half Bohr of radius.) Since the size of atoms does not vary too widely, we have fixed the atomic sphere formulae to be products of a 32-point surface formula with a five point Gauss-Jacobi radial formula (of order 2). In practice the points and weights are lumped together in one formula, with some of the weights being negative. For the clusters studied so far one typically requires between 1500 and 6000 points.

Stroud (1971) comments that an efficient quadrature formula tends to have all its points inside the region of integration and to have all its weights positive. Our general formula falls down in these respects and is a compromise forced upon us by the lack of better methods. Nevertheless, provided that the integrand is smooth over the whole interior of the OS, we should expect to obtain high accuracy. The existence of the spherical Neumann function in (5.11) however, creates a problem since this function has a pole of order $l+1$ at the atomic centre and would upset the numerical quadrature. Since the contribution of the integrand inside the atomic spheres is first added then subtracted away, its precise behaviour is unimportant as long as it is smooth, so that the two numerical quadratures see no discontinuities or singularities. We dispose of the singularity by matching the Neumann function outside the sphere to a smooth continuation inside the sphere:

$$g_l(r) \equiv \begin{cases} a_0 + a_1 r^2 + a_2 r^4 & (l=0) \\ r^l (a_0 + a_1 r + a_2 r^2) & (l>0) \end{cases} \qquad (5.13),$$

so that the value, first and second derivatives are matched at the sphere boundary; i.e.

$$g_l(b_i) = n_l(kb_i) \quad g_l'(b_i) = kn_l'(kb_i) \quad g_l''(b_i) = k^2 n_l''(kb_i) \qquad (5.14).$$

The small r behaviour in (5.13) is chosen so that the function is smooth near the origin when multiplied by the appropriate spherical harmonic (see (5.12)).

The procedure we have described for the integration in (5.9) is rather cumbersome and its potential accuracy may be somewhat questionable. However, numerical tests with simple geometries, involving spheres cut from larger spheres and known functions with singularities smoothed away, indicated that accuracies of three to five significant figures were possible. On the other hand it was not known whether such results would be obtained in the more complicated situation of (5.9) and we were forced to just try it and see.

It is obvious from (5.9-12) that the calculation of $\underset{\sim}{\overline{T}}$ will use a lot of time and space because of the large and complicated arrays used, especially since there are several thousand points in the integration mesh. What we did with EMESHX was to calculate as much as possible at the beginning and to store it for later use during the program running time. In particular, we store $X_{lm}^{p\rho}(\hat{s}_{p\rho}^{a})$ and $w_a V(\vec{s}^a)$, where a is an index that runs over all the integration mesh points and w_a is the weight for a given mesh point. The first of these is a particularly large array and can occupy typically several megabytes (Mbytes) of computer memory. Now the variation of $\underset{\sim}{\overline{T}}$ with energy resides only in k in (5.9,10) so, at a new energy point, one recalculates an array containing $F_\Lambda^p(\vec{s}^a)$ and then performs a summation

$$\overline{T}_{\Lambda\Lambda'}^{pp'} = k \sum_a F_\Lambda^p(\vec{s}^a)\,(w_a V(\vec{s}^a))\,F_{\Lambda'}^{p'}(\vec{s}^a) \qquad (5.15).$$

The three parts of the secular matrix are then added together and the determinant is calculated.

Section 5.2: Testing ENESHX with the Hydrogen Molecular Ion.

The program ENESHX is quite large and algebraically very complicated. It is important at this stage, bearing in mind that it will form the basis for the development of CNTSHX, that we find an unequivocal way of testing it. A particularly clear test is provided by the hydrogen molecular ion H_2^+. This system is a bound state of one electron and two protons, and we thus do not have to worry about exchange, multi-electron effects or self-consistency. Furthermore, the exact analytic solution (in the Born-Oppenheimer approximation for fixed proton separation R) has been known for a long time (Bates et al. (1953) and references therein). Smith and Johnson (1969) used it as one of the first tests for their program ENERGY and we shall refer to their results. Pettifor (1973) has demonstrated analytically for H_2^+ that the inclusion of the non-spherical components of the potential in the atomic spheres appreciably modifies the wavefunctions.

We perform our calculations with R = 2.0 Bohr, very close to the known equilibrium separation of the protons. The initial partition (denoted A) is as follows. The protons are placed on the z-axis at $\frac{1}{2}R$ and $-\frac{1}{2}R$, and are each enclosed by spheres of radius $\frac{1}{2}R$ centred on their positions; while the whole molecule is enclosed in an outer sphere of radius R centred on the origin. The potential seen by the electron (and also the partition that we have constructed) has a point symmetry $D_{\infty h}$ with respect to the origin. As mentioned in the discussion of Sec. 3.4 the wavefunctions will transform according to the irreps of this group. $D_{\infty h}$ is a continuously infinite group and has an infinite number of irreps; A_{1g}, A_{1u}, A_{2g} and A_{2u} being one-dimensional; while E_{mg} and E_{mu} are two-dimensional (where m = 1,2,3,....). Following Smith and Johnson (1969) and Bates et al. (1953) we shall search

for the ten lowest-lying eigenstates in the irreps A_{1g}, A_{2u}, E_{1g} and E_{1u}.

Smith and Johnson (1969) have taken the truncation of the allowed ℓ-values at $\ell = 1$ for the atomic spheres and $\ell = 3$ for the EMR. We take the truncation much higher to try to minimize the errors resulting from the use of a finite number of partial waves. (See Tab. 5.3 for details.) The ℓ-truncation for the potential is taken at twice the values used for the wavefunctions.

As in Bates et al. (1953) we label the eigenstates by integer quantum numbers n, l and m, such that $n-1 \geqslant l \geqslant m \geqslant 0$. If $m = 0$, the state belongs to A_{1g} or A_{2u}, while if $m > 0$, then it is in E_{mg} or E_{mu}. The parity of ℓ determines whether the state is "gerade" or "ungerade". Note that in the limit $R \rightarrow 0$, the quantum numbers would correspond in meaning to the usual ones for the hydrogen-like wavefunctions of He^+ and the eigen-energies would approach $-4/n^2$.

For the purposes of our initial investigations of FP calculations, the program was written so that it may be run in three modes. The first, denoted "L=0" corresponds to the MT version of the potential, in which only the monopole part of the potential is used in the ASRs and the EMR, and the potential in the IR is reset to the constant value V_o (its average); the second, denoted "+L>0", then introduces the higher multipole parts of the potential in the ASRs and the EMR; and the third, denoted "+IR", intr-oduces the true non-constant potential in the IR. In this way we can separate the effects of the different non-MT parts of the potential.

The results of our calculations with ENESHX on partition A may be seen in Tab. 5.1. Before considering them in detail we should mention several preliminary tests that were made. Firstly, we

Table 5.1: Comparison of exact eigenvalues (h) in Rydbergs (from Bates et al. (1953)) for H_2^+ with those calculated by the programs ENERGY and ENESHX. The ten states are specified by their Mulliken (1955) designations (a) and, as in the Bates et al. paper, the united atom designations (b) and the quantum numbers (c). The ENERGY results (d) are those of Smith and Johnson (1969). The ENESHX results (e), (f) and (g) correspond to the successive introduction (as described in the main text) of the non-MT components of the potential.

State			ENERGY	ENESHX			Exact
(a)	(b)	(c)	(d)	(e)	(f)	(g)	(h)
Mul.	U.a.	Q.no.	S. & J.	L=0	+L > 0	+IR	Bates et
des.	des.	n l m	paper	(MT ap.)	on atoms	varying	al.paper
$1a_{1g}$	$1s\sigma_g$	1 0 0	-2.0716	-2.07196	-2.10906	-2.18973	-2.20525
$2a_{1g}$	$2s\sigma_g$	2 0 0	-0.70738	-0.70412	-0.70769	-0.72093	-0.72173
$3a_{1g}$	$3d\sigma_g$	3 2 0	-0.45574	-0.45597	-0.47330	-0.47102	-0.47155
$4a_{1g}$	$3s\sigma_g$	3 0 0	-0.34859	-0.34873	-0.35123	-0.35525	-0.35536
$1a_{2u}$	$2p\sigma_u$	2 1 0	-1.2868	-1.28795	-1.31151	-1.33426	-1.33507
$2a_{2u}$	$3p\sigma_u$	3 1 0	-0.49722	-0.49752	-0.50696	-0.51085	-0.51083
$3a_{2u}$	$4p\sigma_u$	4 1 0	-0.26979	-0.26973	-0.27310	-0.27466	-0.27463
$4a_{2u}$	$4f\sigma_u$	4 3 0	-0.24997	-0.24994	-0.25329	-0.25329	-0.25329
$1e_{1g}$	$3d\pi_g$	3 2 1	-0.44646	-0.44646	-0.45397	-0.45333	-0.45340
$1e_{1u}$	$2p\pi_u$	2 1 1	-0.88866	-0.88867	-0.86514	-0.85585	-0.85755

checked whether our copy of the Smith and Johnson program ENERGY gave the results quoted in Tab. 5.1(d). This was in fact the case except for the $2a_{1g}$ state which we found at -0.70377 Ryd. We therefore suspect the value quoted in Smith and Johnson (1969) to be a misprint. We then ran ENESHX in the L=0 mode for the same ℓ-truncation and found the same results, confirming that those parts of ENESHX which correspond to ENERGY, but which were programm-

ed differently, have been done correctly. Note that the differences between Tab. 5.1(d) and (e) result from the higher ℓ-truncation used in the latter. Because of the simple analytic form of the potential we can use (A37) to obtain an exact multipole expansion and bypass the program MLPSHX. Comparing the results from ENESHX using both potentials (and INPSHX with and without smoothing) shows no differences, at least in the first five significant figures.

If we consider the results of ENESHX shown in Tab. 5.1, we see that the successive introduction of the non-MT components of the potential (going from column (e) to (f) and then to (g)) gives improved eigenvalues for all ten states. Looking more closely we see that the remaining error in the FP case, considered as a fraction of that in the MT case (and defined by (E(g)-E(h))/(E(e)-E(h))) ranges from about 11.6% for the $1a_{1g}$ level (the ground state) down to less than 0.2% for the highest levels (with the $4a_{2u}$ level virtually exact). Also the relative sizes of the effects of the non-spherical potential components in the ASRs and the EMR, and of the non-constant IR potential, vary among the states. Contrary to a conjecture of Pettifor (1973) (at the end of his Sec. III), the greater part of the improvement in the $1a_{1g}$ level results from the proper treatment of the IR potential rather than the higher multipoles of the sphere potentials. This variation of the two corrections comes from the different apportionment of the electron density between the different regions of the partition; as may be seen physically by considering the first-order energy shift in perturbation theory, given by

$$\Delta E = \langle \Psi | \Delta V | \Psi \rangle \qquad (5.16).$$

If a larger part of the electron density is in one of the regions then the difference between the full and MT potentials in that

region will have a greater effect on the energy shift. This may be seen for the $4a_{2u}$ level in which the great bulk of the electron density is in the EMR so that, even in the $+L>0$ mode, the eigenvalue is exact. This shows incidently that the integration of the coupled radial equations in (3.21) is quite accurate. Hence we can say that the remaining error in, for example, the $1a_{1g}$ state is due to the deficiencies of our treatment of the IR potential effect by the Born approximation. In this state the Born approximation has given 84% of the correction that should have come from the IR (defined by $(E(g)-E(f))/(E(h)-E(f))$).

We see that even in the worst case the Born approximation is quite reasonable and a great improvement over the MT case. One suspects that if we had calculated the full $\underset{\sim}{T}$ in (3.73) the remaining error would disappear. As we pointed out earlier the practical difficulties in realizing this full calculation have yet to be resolved. However, noting the accuracy of the radial solutions for the ASRs and the EMR, we are led to reconsider the use of empty interstitial spheres so that for some of the IR we have a more accurate solution and the remaining IR is smaller.

It is not difficult to see that a ring of six empty spheres may be inserted around the "equator" of our earlier partition (A) so that each sphere touches two others, the OS and both hydrogen spheres. Let us denote this new partition B. It may be further seen that two more rings of six smaller empty spheres may be placed above and below the first in a staggered configuration such that each sphere touches the OS, one hydrogen sphere and two of the larger empty spheres. Let us denote this partition C. The symmetry of these two new partitions is now D_{6h} with the six-fold axis along the z-axis. This group has twelve irreps, but the four irreps of $D_{\infty h}$ that we consider are not split by the lowering of

symmetry.

The energy eigenvalues calculated with these two partitions may be seen in Tab. 5.2. As before, for a fixed partition, the

Table 5.2: ENESHX energy eigenvalues in Rydbergs for H_2^+ with the two empty-sphere partitions B and C. In both cases values are given for all three program modes.

State	Molecular partition B (1 shell empty spheres)			Molecular partition C (2 shells empty spheres)		
(a)	(b) L=0	(c) +L>0	(d) +IR	(e) L=0	(f) +L>0	(g) +IR
$1a_{1g}$	-2.07376	-2.13616	-2.19780	-2.07376	-2.13987	-2.19847
$2a_{1g}$	-0.70426	-0.71198	-0.72123	-0.70425	-0.71221	-0.72119
$3a_{1g}$	-0.45621	-0.47254	-0.47130	-0.45621	-0.47244	-0.47131
$4a_{1g}$	-0.34878	-0.35247	-0.35524	-0.34878	-0.35249	-0.35522
$1a_{2u}$	-1.28385	-1.30953	-1.33406	-1.28384	-1.31165	-1.33425
$2a_{2u}$	-0.49721	-0.50703	-0.51082	-0.49721	-0.50745	-0.51085
$3a_{2u}$	-0.26982	-0.27332	-0.27465	-0.26982	-0.27347	-0.27465
$4a_{2u}$	-0.24999	-0.25332	-0.25329	-0.24999	-0.25331	-0.25329
$1e_{1g}$	-0.44610	-0.45355	-0.45334	-0.44610	-0.45348	-0.45335
$1e_{1u}$	-0.88966	-0.86363	-0.85699	-0.88969	-0.86353	-0.85711

successive improvement of the potential gives uniformly better eigenvalues. When we compare among partitions the results are somewhat equivocal. For the full calculation (the +IR mode) there is a general improvement as one goes from partition A to B to C. When the eigenvalues are better it is by a greater margin than when they are worse. However, for the L=0 and +L>0 modes it is less clear. By the time we get to partition C the calculations have become very time-consuming and cumbersome, and it is clear that a point of diminishing returns has been reached. (For details of the parameters used in constructing the partitions see Tab.

Table 5.3: Summary of details of the partitions used for the H_2^+ system. For each partition is given its point symmetry with respect to the origin of coordinates, with the main symmetry axis taken to be along the z-axis. The details of the numbers, positions and radii of the spherical regions are given together with the ℓ-truncations used for the potential and the wavefunctions, and the resulting dimensions of the secular matrices for each irrep. (Note that the partitions are chosen so that one of the mirror planes is the xz-plane.) For the IR we show the number of mesh points used by ENESHX to perform the numerical quadrature given by Eqn. 5.15, together with the fraction of the outer sphere volume in the IR.

Molecular partition						A	B	C
Point symmetry						$D_{\infty h}$	D_{6h}	D_{6h}
Group of	No. SRs	Rad. (au)	Prototype posn. (x,y,z) (au)	ℓ(max) W.	P.			
equivalent	1	2	(0 , 0 , 0)	6	12	+	+	+
spheres used	2 H	1	(0 , 0 , 1)	3	6	+	+	+
in partition	6	2/3	(4/3 , 0 , 0)	2	4		+	+
	12	2/5	(6/5,2$\sqrt{3}$/5,4/5)	2	4			+
Secular matrix dimensions, by irrep					A_{1g}	8	13	19
					A_{2u}	7	9	15
					E_{1g}	6	10	19
					E_{1u}	6	13	22
Details of IR	Number of integration mesh points					1830	2790	4710
	Percentage of OS volume					75.0	52.8	43.2

5.3.)

So far the eigenvalues have been above the average interstitial potential $V_o \equiv \overline{V}_I$, and thus we have not tested the equations (3.29,33,38,50,51,55,70,71,73 or 74). This may be done in two

ways. Firstly, we can change R to a different value (re-scaling partition A appropriately). For example, if R = 2.8 Bohr, then $\overline{V}_I$ becomes -5/3 Ryd. which is above the new $1a_{1g}$ energy (from Bates et al. (1953)) of -1.88299 Ryd. ENESHX gives in this case for the three modes $E(1a_{1g})$ = -1.77562 (L=0), -1.80732 (+L>0) and -1.87130 (+IR). Otherwise we can observe that V_o is to some extent an arbitrary parameter, and we can reset it to, say, V_o = -1.9 Ryd. (keeping R = 2.0 Bohr). ENESHX now gives $E(1a_{1g})$ = -1.91990 (L=0), -1.95748 (+L>0) and -2.14185 (+IR). Either way the results are good.

The latter example raises a question about the suitability of using $V_o \equiv \overline{V}_I$ as the zero of the interstitial potential. As we have said, this zero may be set arbitrarily. The reason for our choice is to reduce the strength of the interstitial potential so that the Born approximation is reasonably good. In effect this means reducing the size of the matrix elements of $\overline{\overline{T}}$. Experimenting with different values for V_o in the H_2^+ case shows that more accurate eigenvalues may be obtained when V_o is a few tenths of a Rydberg below $\overline{V}$. For example, if V_o is reset from V_o = -7/3 Ryd. (its value in partition A in Tab. 5.3) to V_o = -2.56 Ryd., then $E(1a_{1g})$ = -2.19888 (in the +IR mode, i.e. with the full potential). However, different states achieve their optimum accuracy at different values of V_o. Nevertheless, it is possible that some different a priori choice of V_o (other than $\overline{V}_I$) might give a general improvement in accuracy. Consideration of the form of the integrands in (3.70,71,73,74,88) suggests that some weighted average of the interstitial potential might be more appropriate.

An important part of the research concerns the computational feasibility and general practicability of the theory. These depend of course on the computing power available. (We note that this

power is currently increasing rapidly.) All the non-MT calculations reported here were performed on a VAX 8650 running under version 4.7 of the VMS operating system. The main processor runs at 6 mega-instructions per second (Mips) (although in comparing this with other computers one should take into account the sizes of their respective "instruction sets"). The central memory has 32 mega-bytes (Mbyte) of storage; although any one program may use at most 3.91 Mbyte of this. Since the computer is a "virtual memory" machine, any program requiring more storage must leave the excess on the much slower mass-storage disks, "swapping" the information in and out of the CPU as required. Once this happens the computer time rises sharply.

In Tab. 5.4 we see details of computing requirements for the runs of ENESHX whose results were shown in Tabs. 5.1 and 5.2. It is seen that, when the true IR potential is used, it is by far the greatest user of CPU-time and storage space. The small differences between the L=0 and +L>0 modes arise because in the L=0 mode the atomic t-matrices are diagonal and hence the matrix inv-

Table 5.4: CPU-times and memory requirements for ENESHX with the H_2^+ ion for the different partitions and program modes. For a given energy the times are those for the evaluation of a single secular determinant. Virtually all of this time is taken in constructing the secular matrix itself.

Molecular partition		A			B			C		
Program mode		L=0	+L>0	+IR	L=0	+L>0	+IR	L=0	+L>0	+IR
Memory used (Mbyte)		0.7	0.7	1.9	0.8	0.8	3	1	1	6
CPU-time per energy point by irrep (sec)	A_{1g}	0.32	0.34	1.78	0.63	0.69	5.99	1.85	2.02	23.1
	A_{2u}	0.25	0.26	1.51	0.33	0.35	4.19	1.33	1.45	20.0
	E_{1g}	0.20	0.20	1.85	0.41	0.44	5.32	2.64	2.73	23.5
	E_{1u}	0.19	0.20	1.83	0.74	0.81	7.27	3.10	3.34	30.3

ersion routine takes less time. It should be noted that the L=0 calculation with ENERGY for partition A is about ten times as fast as ENESHX (although the latter would not normally be used in that mode).

It is clear that more may be made of the H_2^+ test. In particular, it would be interesting to know how good the wavefunctions are. Since Bates et al. (1953) give the algebraic form of the exact solutions and the FP-SW theory gives the wavefunctions via (3.20,48,49,54,80,85,86,89), they may be easily compared. For now we shall be satisfied with the results obtained which show that the program is working correctly; that the inclusion of non-MT parts of the potential is correctly described by the extended SW theory of Sec. 3.2; and that even with the use of the Born approximation for the IR the eigenvalues produced are much more accurate than in the MT case. Finally we note that the results of Tabs. 5.1 and 5.2 came from the first runs of ENESHX without experimenting with any of the free parameters in the partitions. We believe ENESHX to be the first general-purpose full-potential scattered-wave program in existence.

Section 5.3: ENESHX Results for Chromium Hexacarbonyl.

While the H_2^+ system provides an excellent test of ENESHX, it is interesting to try it for a more realistic cluster. We therefore used it for our model compound chromium hexacarbonyl whose MT potential is quite bad, so that we could get an idea of the sizes of the improvements that might result when the full potential is used. Unfortunately, there are no exact calculations for this system and, since we use the non-self-consistent potential of Sec. 4, the results will only be an approximation to the real case. A comparison with experiment is possible, but in this case

would not serve to distinguish between errors of the basic one-electron (RHF) hamiltonian or those stemming from the MT approximation.

We denote the partition of Sec. 4 as A and let the ℓ-truncation for the wavefunction be ℓ(max) = 6 (OS), 6 (Cr), 3 (C) and 3 (O). With this partition the IR makes up 92.2% of the OS volume (a very open cluster) and 4638 points are required for the IR integration. The values of the core-level energies are shown in Tab. 5.5. The dividing line between core and valence levels was chosen as -3.0 Ryd. (in accordance with the normal practice in the old SW programs). However, the real valence states will lie much higher than this. Since the core states do not use the non-MT components of the potential they are of minor interest.

Table 5.5: Core levels for $Cr(CO)_6$ from ENESHX. In principle some of these levels should be split by the ligand field into different irreps of the point group. In practice this splitting is very small, so we denote the states by their atomic designations as well. In the ground state all of these levels are filled and we give the number of electrons in each.

State		Occupation	Energy
(a)	(b)	(c)	(d)
Atomic level	Molecular equivalents	(electrons)	(Rydbergs)
Cr-1s	$1a_{1g}$	2	-429.537
Cr-2s	$2a_{1g}$	2	-48.6462
Cr-2p	$1t_{1u}$	6	-41.5189
O-1s	$3a_{1g}$ $1e_g$ $2t_{1u}$	12	-38.0756
C-1s	$4a_{1g}$ $2e_g$ $3t_{1u}$	12	-20.2651
Cr-3s	$5a_{1g}$	2	-5.33918
Cr-3p	$4t_{1u}$	6	-3.36219

Table 5.6: Filled valence levels for $Cr(CO)_6$ from ENESHX using the partition of Chap. 4 (that we denote partition A).

L=0		+L > 0		+IR	
State	Energy (Ryd.)	State	Energy (Ryd.)	State	Energy (Ryd.)
$6a_{1g}$	-1.72652	$6a_{1g}$	-1.81470	$5t_{1u}$	-2.14461
$5t_{1u}$	-1.72616	$3e_g$	-1.81454	$3e_g$	-2.14357
$3e_g$	-1.72442	$5t_{1u}$	-1.81325	$6a_{1g}$	-2.14288
$7a_{1g}$	-0.74040	$4e_g$	-0.79972	$4e_g$	-1.07651
$6t_{1u}$	-0.73079	$7a_{1g}$	-0.79862	$7a_{1g}$	-1.07075
$4e_g$	-0.72064	$6t_{1u}$	-0.79256	$6t_{1u}$	-1.06873
$1t_{2g}$	-0.65852	$1t_{2g}$	-0.63395	$1t_{2g}$	-1.01230
$7t_{1u}$	-0.65260	$7t_{1u}$	-0.62691	$1t_{1g}$	-0.99529
$1t_{2u}$	-0.64503	$1t_{2u}$	-0.61518	$7t_{1u}$	-0.99467
$1t_{1g}$	-0.63683	$1t_{1g}$	-0.60679	$1t_{2u}$	-0.98927
$8a_{1g}$	-0.49500	$8a_{1g}$	-0.51319	$8a_{1g}$	-0.64514
$5e_g$	-0.33564	$5e_g$	-0.35640	$5e_g$	-0.56278
$8t_{1u}$	-0.31078	$8t_{1u}$	-0.30836	$8t_{1u}$	-0.43661
$2t_{2g}$	-0.30296	$2t_{2g}$	-0.28727	$2t_{2g}$	-0.43587

In Tab. 5.6 we see the ENESHX results for partition A in each of the program modes. The inclusion of non-MT components of the potential has a marked effect on the eigenvalues, particularly that of the IR. The general trend is a drop in energy by about 0.1 to 0.4 Ryd. Note that the $6a_{1g}$, $3e_g$ and $5t_{1u}$ levels stem primarily from the oxygen 2s levels on the six atoms, while the $7a_{1g}$, $4e_g$ and $6t_{1u}$ are largely carbon 2s in origin. The splitting of these levels is quite small and they can be still thought of as core levels, with the true valence levels starting at higher energy. It will have been seen that, although the general ordering of the eigenvalues has remained the same, some of the closely

lying eigenvalues have changed position. The reasons for these changes seem to lie in a subtle balance of competing effects, whose elucidation requires a much more penetrating analysis than is available to us at present.

We can also include empty spheres in our partition to reduce the size of the IR. It is possible to put eight spheres at the corners of a cube (as in Sec. 2.4) to maintain the octahedral symmetry of the partition. In particular, the prototype for this group of spheres has its centre at (d,d,d) where d = 2.648 Bohr, and the radius is 2.387 Bohr (touching the Cr sphere and the OS). The IR is thus reduced to 60.2% of the OS volume, but the IR integration now requires 5918 points. The ℓ-truncation for the empty spheres is $\ell(\max) = 2$ for the wavefunctions and $\ell(\max) = 4$ for the potential. This partition (denoted B) represents the biggest cluster treated so far, with a central atom and three shells of coordinating spheres.

The results for partition B may be seen in Tab. 5.7 and they appear to be qualitatively not very much different from those for partition A. In general they are a few hundredths of a Rydberg deeper in energy, and there has been a slight change in the balance between the SSR and IR corrections. What is quite obvious from both of these runs is that the proper treatment of the IR is essential for all of the filled levels that we show. Although the higher virtual levels may be well treated in the $+L > 0$ mode because they spread significantly into the EMR, the important electronic states require the full potential. This fact will presumably be important for the development of a fully self-consistent FP-SW program.

The details of the computer runs may be seen in Tab. 5.8. The CPU-times are not prohibitive although, in the +IR mode for part-

ition B, it can be seen that the "swapping" mentioned earlier is starting to take a serious toll.

Table 3.7: Filled valence levels for $Cr(CO)_6$ from ENESHX using empty interstitial spheres (partition B).

L=0		+L>0		+IR	
State	Energy (Ryd.)	State	Energy (Ryd.)	State	Energy (Ryd.)
$6a_{1g}$	-1.75559	$6a_{1g}$	-1.84393	$5t_{1u}$	-2.15650
$5t_{1u}$	-1.75514	$3e_g$	-1.84384	$3e_g$	-2.15549
$3e_g$	-1.75332	$5t_{1u}$	-1.84267	$6a_{1g}$	-2.15462
$7a_{1g}$	-0.76113	$7a_{1g}$	-0.82439	$4e_g$	-1.08182
$6t_{1u}$	-0.75514	$4e_g$	-0.82282	$7a_{1g}$	-1.07729
$4e_g$	-0.74423	$6t_{1u}$	-0.81746	$6t_{1u}$	-1.07570
$1t_{2g}$	-0.68982	$1t_{2g}$	-0.66908	$1t_{2g}$	-1.02344
$7t_{1u}$	-0.68477	$7t_{1u}$	-0.66143	$1t_{1g}$	-1.00547
$1t_{2u}$	-0.68049	$1t_{2u}$	-0.65328	$7t_{1u}$	-1.00515
$1t_{1g}$	-0.67187	$1t_{1g}$	-0.64360	$1t_{2u}$	-1.00091
$8a_{1g}$	-0.47423	$8a_{1g}$	-0.57560	$8a_{1g}$	-0.71964
$5e_g$	-0.35103	$5e_g$	-0.38306	$5e_g$	-0.58161
$2t_{2g}$	-0.29165	$8t_{1u}$	-0.33315	$8t_{1u}$	-0.48866
$8t_{1u}$	-0.27907	$2t_{2g}$	-0.31148	$2t_{2g}$	-0.45336

Table 5.3: CPU-times and memory requirements for ENESHX with the $Cr(CO)_6$ molecule and the two partitions A (from Chap. 4) and B (as A but with empty spheres). We show times for eight of the ten irreps of O_h. For the irreps A_{1u} and A_{2g} no appropriate basis functions were found. For each of the irreps shown we give also the dimensions of the secular matrices.

Molecular partition		A				B			
Program mode			L=0	+L>0	+IR		L=0	+L>0	+IR
		dim S				dim S			
	A_{1g}	14	0.73	0.77	10.3	17	1.76	1.94	25.4
	A_{2u}	6	0.23	0.23	7.4	9	0.77	0.78	18.0
CPU-times	E_g	18	1.40	1.44	12.3	21	3.21	3.34	32.0
per energy point	E_u	6	0.24	0.24	7.5	9	0.87	0.88	18.4
for each irrep	T_{1g}	12	0.54	0.58	9.6	15	1.39	1.44	24.3
(sec)	T_{1u}	24	1.77	1.86	16.3	30	4.75	5.28	51.4
	T_{2g}	20	1.14	1.20	13.4	26	3.37	3.92	41.3
	T_{2u}	16	1.02	1.06	11.7	19	2.33	2.39	31.5
Memory used (Mbytes)			0.9	0.9	3.5		1.1	1.1	6.5

Section 5.4: The Continuum Photo-Absorption Cross-Section Program CNTSHX.

Having confidence that the programming of ENESHX had been done correctly, the coding of CNTSHX followed. Furthermore, the good results from ENESHX, particularly for H_2^+, show that our approach to non-MT calculations was fundamentally correct and that we might expect similar results in the continuum case.

As in ENESHX the most difficult part of CNTSHX lay in the creation of the secular matrix. The solution of the secular equation and the consequent evaluation of the photoabsorption cross-section (following (3.136)) required no new programming innovations

and loosely follows CONTIM. The major new feature of the continuum secular matrix is that it is complex. It is possible to treat the real and imaginary parts separately even when solving the secular equation, but this requires a doubling of the dimensions and added complication. So we decided to use explicitly the complex variables available in the FORTRAN language. This has the advantage of clarity and leaves us in a position to be able to introduce complex potentials easily when we come to treat inelastic loss mechanisms more appropriately.

The secular matrix in CNTSHX is made using adapted versions of the routines in ENESHX. For $\underset{\sim}{\bar{H}}$ and $\underset{\sim}{\bar{T}}$, the differences arise only from the appearance of the spherical Hankel function rather than the spherical Neumann function, and involve no great difficulties. For $\underset{\sim}{\bar{t}}$ we can still perform the integrations for $\underset{\sim}{R}(r)$ in real algebra, the introduction of complex arising only when we construct the matrix Wronskians. The major difference here arises when we consider the EMR, since both the regular and irregular solutions are present. In this case we call the Numerov integration routine for each solution separately, imposing the appropriate boundary condition at infinity through the choice of the first two values in the Numerov recurrence formula. This choice will be the values of the regular and irregular Coulomb wavefunctions for a cluster with residual charge Z, since at large distance the potential will have settled down very close to a -2Z/r tail. (Note that, for photoionization Z will be usually 1 au(C), although we will also use a neutral cluster for which the Coulomb wavefunctions degenerate into the spherical Bessel and Neumann functions.)

Compared to the original writing of ENESHX, the above modifications to produce CNTSHX were not very difficult and did not take

long to complete. Providing an absolute test for CNTSHX was however not so easy. Unfortunately, there seems to exist no analytic formula for the continuum states of H_2^+. The only such formula that we know of is that for hydrogen-like atoms, which can be used to calculate exact photoabsorption cross-sections (see Bethe and Salpeter (1957)). The result is

$$\sigma(k) = \left\{(4\pi^2\alpha)\left(\frac{2^7}{3}\right)\right\}\left(\frac{1}{Z^2}\right)\left(\frac{1}{1+\left(\frac{k}{Z}\right)^2}\right)^4\left(\frac{e^{-4\left(\frac{Z}{k}\right)\tan^{-1}\left(\frac{k}{Z}\right)}}{1-e^{-2\pi Z/k}}\right) \qquad (5.17).$$

This is the cross-section for photoionization from the 1s ground state, of an electron on the field of a nucleus of charge Z, to a continuum final state of wave-number k (with energy k^2).

Although this system has only one atom and a spherically symmetric potential, it is possible to use it as a test for CNTSHX. To make it a meaningful test of the effects of non-MT potentials requires however careful consideration. It is possible to represent the potential exactly by a MT potential with no IR and obtain a result arbitrarily close to (5.17). But this would not be very useful for our purpose. We can however make a "pseudo-cluster" in which the central atom is coordinated by, say, six empty spheres in an octahedral configuration. In this way the MT approximation is not so good and we might expect to see differences as the non-spherical components in the empty spheres and the potential variation in the IR are introduced.

There are some difficulties that necessitate a judicious choice of the various parameters. As we have said in Sec. 3.3, the integration for the dipole matrix elements is performed only in the sphere of the photoionized atom, on the assumption that the initial-state wavefunction is effectively zero outside the sphere. Bearing in mind that the radial integral has a factor r^3 in it, we must be careful to ensure that the initial wavefunction

has become small enough at the sphere boundary so that the asymptotic tail does not contribute significantly. Of course this will also depend on the range of energies under consideration.

We chose $Z = 3$ (a doubly ionized lithium atom), with the sphere radii being b(Li) = 4 Bohr, b(ES) = 1.5 Bohr and b(OS) = 7 Bohr. Typical potential discontinuities for the MT potential are of the order of half a Rydberg. In Fig. 5.1 we see the CNTSHX results for this pseudo-cluster compared with the exact values of (5.17).

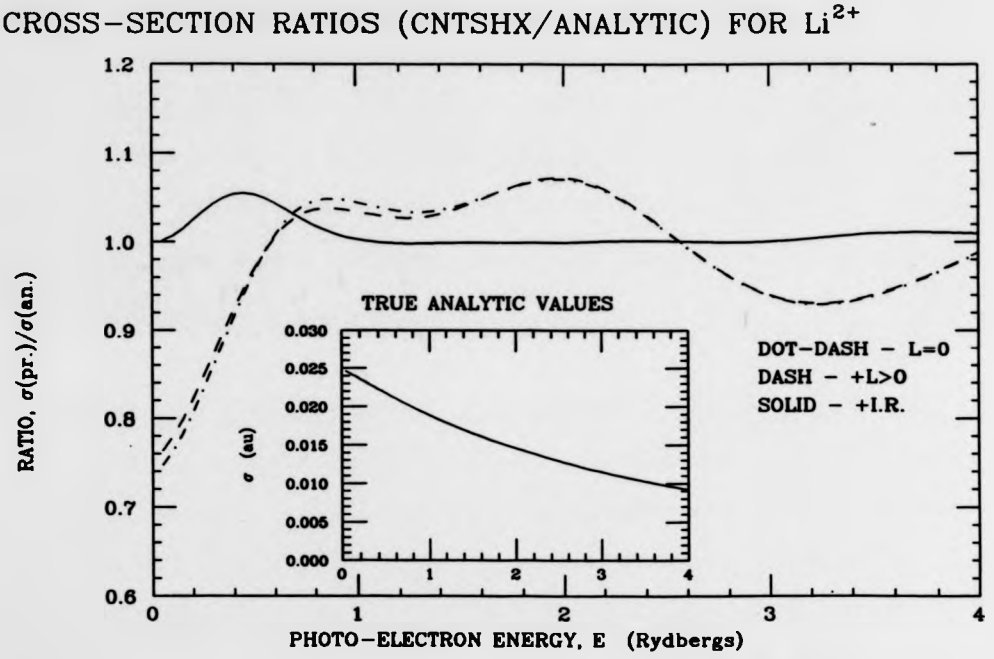

Figure 5.1: Photoionization cross-sections for Li^{2+} from CNTSHX compared with the analytic values. The CNTSHX values are shown for the three program modes as ratios of the exact formula of equation (5.17) which is shown inset.

Firstly, we see that the inclusion of non-spherical components in the SSR potentials (+L > 0 mode) gives only a slight improvement over the MT case (L=0 mode). This is because they exist only

in the empty spheres whose total volume is small in comparison with the IR. The inclusion of the influence of the non-constant IR potential produces the main improvement, and above 1 Ryd. the residual error is reduced to less than 1%. Below 1 Ryd. it seems reasonable to conclude that the error of up to 5% results from the use of the Born approximation. In actual fact at higher energies, the underlying improvement is probably better than that shown here. A little experimentation indicates that the error above 3 Ryd. arises from the truncation of the radial integral within the lithium sphere rather than the Born approximation.

In summary, we can be confident that CNTSHX is programmed correctly and that the inclusion of non-MT corrections to the potential produces significant improvements in the calculated cross-sections. In the next section we see how large the improvements are for a realistic cluster such as our model system chromium hexacarbonyl.

Section 5.5: CNTSHX Results for Chromium Hexacarbonyl.

We perform our first CNTSHX calculations with the two partitions (A and B of Sec. 5.3) for chromium hexacarbonyl. In the continuum case however, it is necessary to increase the maximum l-values allowed in the truncation, particularly those in the EMR. Although the excitation of an s-state would normally give a p-wave final state, the non-central nature of the molecular potential gives rise to higher order partial waves. The maximum l necessary may be found crudely by $l(\max) \approx kR$, where k is the photoelectron wave-number and R is a measure of the range of the molecular potential (which we can take to be the radius of the OS). Thus if we wish to calculate cross-sections up to four Rydbergs above the ionization threshold (so that $k \leq 2$ au(L^{-1})),

then we should go up to $\ell \approx 14$. In practice the higher components are still quite small even at the top of this energy range, so that we can get way with $\ell(\max) = 9$. Our ℓ-truncation was then chosen to be $\ell(\max) = 9$ (OS), 9 (Cr), 4 (C), 4 (O) and (for the empty spheres in partition B) 3 (ES).

Recalling that our calculations give only the continuum cross-sections and that transitions to bound final states are not included, we note that the two small bound-state peaks at 6018 and 6023 eV in the experimental spectrum of chromium hexacarbonyl (in Fig. 2.2) will not be reproduced. For the purpose of determining the effects of the use of full potentials, we shall ignore them and concentrate on the features of the continuum spectrum for our analysis.

The results from CNTSHX for these two partitions may be seen in Figs. 5.2 and 5.3. Note that the potentials from MLPSHX use

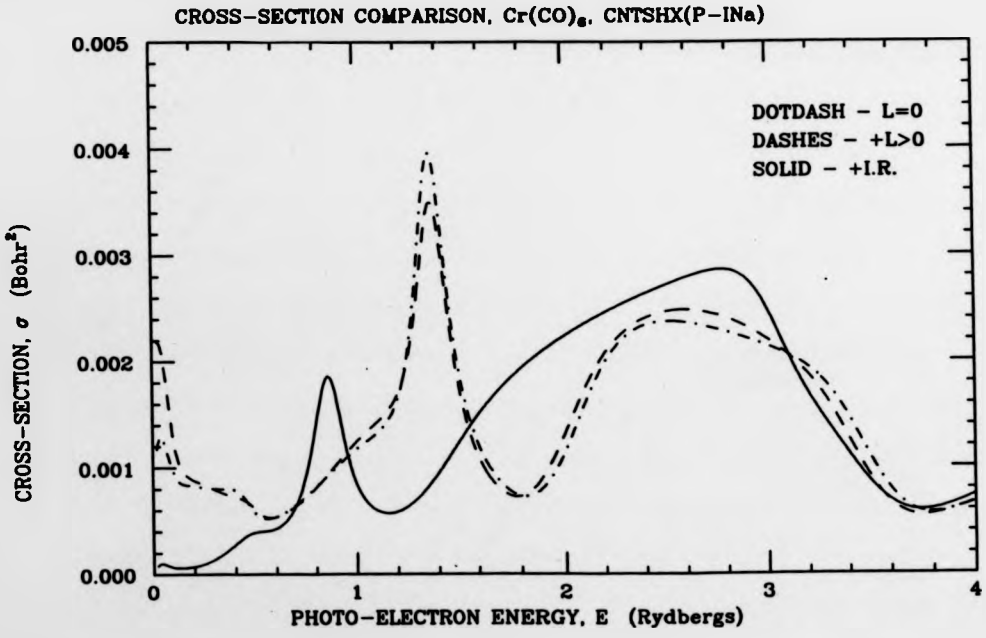

Figure 5.2: CNTSHX results with INa potential for chromium hexac-

arbonyl. This uses partition A with the free-atom densities for all atoms.

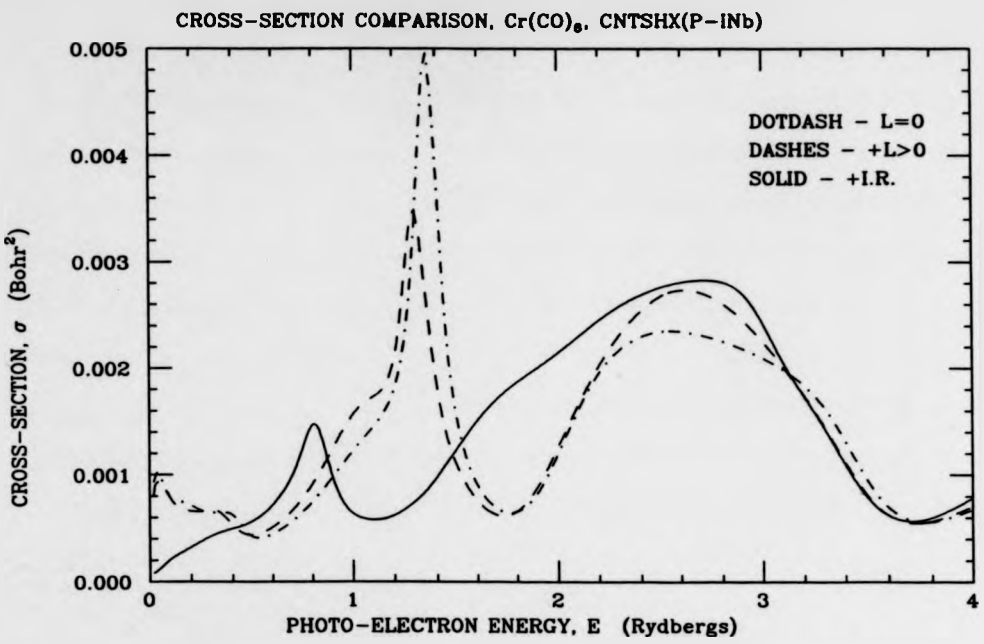

Figure 5.3: CNTSHX results with INb potential for chromium hexacarbonyl. This uses partition B with the free-atom densities for all atoms.

the atoms in their ground states with the wavefunctions from Clementi and Roetti (1974) in the configurations Cr: $1s^2 2s^2 2p^6 3s^2 3p^6 4s^1 3d^5$, C: $1s^2 2s^2 2p^2$ and O: $1s^2 2s^2 2p^4$. The first thing we see is that the differences between the full-potential spectra and the MT spectra (+IR and L=0 respectively) are rather large, especially in the lower part of the energy range. By comparison, the inclusion of the non-spherical components in the SSRs (+L>0 mode) had relatively little effect, although in partition B the effects are noticeably larger. Comparing the full calculation in each case, we see only small differences indicating that the Born approximation is indeed giving the majority of the correction due to

the IR potential.

The computing performance is summarized in Tab. 5.9. The large increase in storage requirements over ENESHX is due to the use of complex variables for the arrays used to calculate the interstitial $\underset{\sim}{T}$, in conjunction with the higher ℓ-truncation. The large amount of storage required for partition B causes much swapping between the disk and the main memory, and thus a considerable time penalty. For the computer that we used, the INb calculation probably represents the limits of practicability, especially in a multi-user environment.

Table 5.9: CPU-times and memory requirements for CNTSHX with chromium hexacarbonyl for the different program modes and partitions. The dipole-allowed final states lie only in the T_{1u} irreducible representation of O_h.

Molecular partition		A		B	
		CPU-time (sec)	Memory (Mbyte)	CPU-time (sec)	Memory (Mbyte)
Program mode	L=0	7.5	1.8	14.4	2.4
	+L > 0	8.0	1.8	15.9	2.4
	+IR	110	7.1	214	10.5

As far as the comparison with experiment goes, the results still leave much to be desired. The two continuum "shape resonances" are found in all cases although with considerable variation of detail. The most encouraging improvement of the +IR case is in the separation of the minima following the two main peaks. Experimentally this is 2.5 Ryd., but for the L=0 and +L > 0 modes (in both INa and INb) it is found to be 2.0 Ryd. In the +IR mode in both cases we find it to be 2.6 Ryd. On the negative side the +IR mode gives too small a magnitude to the first peak and the wrong shape to the broader second peak. For all modes the general size

of the oscillations is too large. In the L=0 and +L > 0 modes we see some extra structure within the first half Rydberg above threshold. This seems to stem from the two bound-state transitions becoming resonances in the continuum. The potentials of the L=0 and +L > 0 modes are not deep enough to bind these states so they have become embedded in the continuum. This is partly borne out by a search with ENESHX for virtual T_{1u} levels. Only in the +IR mode do they turn up as bound states.

Although the results are in poor agreement with experiment, they are undoubtedly telling us something important about the physics of the situation. One immediate response might be to vary the available free parameters in the partition, in the hope of more closely approaching experiment. As with the MT case, this path is sterile and devoid of physical meaning, and is completely at variance with the ab initio approach. It seems likely that the answer lies in the physical considerations that we set aside earlier. Of these a more realistic potential appears to be the most pressing immediate requirement. While the inelastic loss and the exchange may be of comparable importance, they are beyond the scope of this work.

In using the potentials INa and INb we took no account of the effects of the redistribution of electron density in bonds, or of the core hole and consequent partial relaxation of the electronic levels in its presence. Since we have no self-consistent full-potential final state available, we must see what can be done with the formalism that we have assembled. Virtually the only thing that remains to us is some variation on the Z+1 approximation introduced earlier.

We retain the partition A and vary the electronic structure on the central chromium atom. As before we take the orbitals of man-

ganese, which lies just above chromium in the periodic table; removing an electron from the 1s orbital to create the core hole. With a chromium nucleus and the remaining 24 electrons in the manganese orbitals, this leaves us with a neutral system in the configuration $1s^1 2s^2 2p^6 3s^2 3p^6 4s^2 3d^5$. In theory we should remove one of the electrons in the highest levels to give the fully ionized system. However, it is not physically obvious as to which one we should remove and furthermore, the possibility of shielding of the core hole by other mobile electrons in the solid state suggests that the ionized state may not be appropriate.

We therefore tried three further calculations, denoted Z+1a, Z+1b and Z+1c, in which the configuration of the outer orbitals is $4s^2 3d^5$, $4s^1 3d^6$ and $4s^1 3d^5$ respectively (the last being completely ionized). The results are shown in Figs. 5.4, 5.5 and 5.6, and one is immediately struck by the sensitivity of the +IR resu-

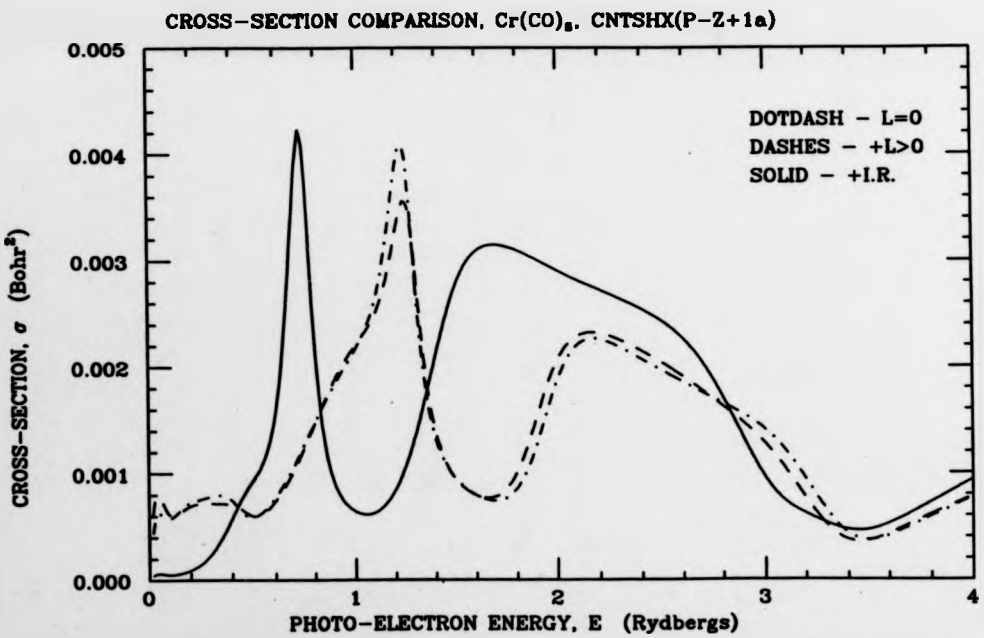

Figure 5.4: CNTSHX results with Z+1a potential for $Cr(CO)_6$. Uses partition A with Mn orbitals in configuration $1s^1 \ldots 4s^2 3d^5$.

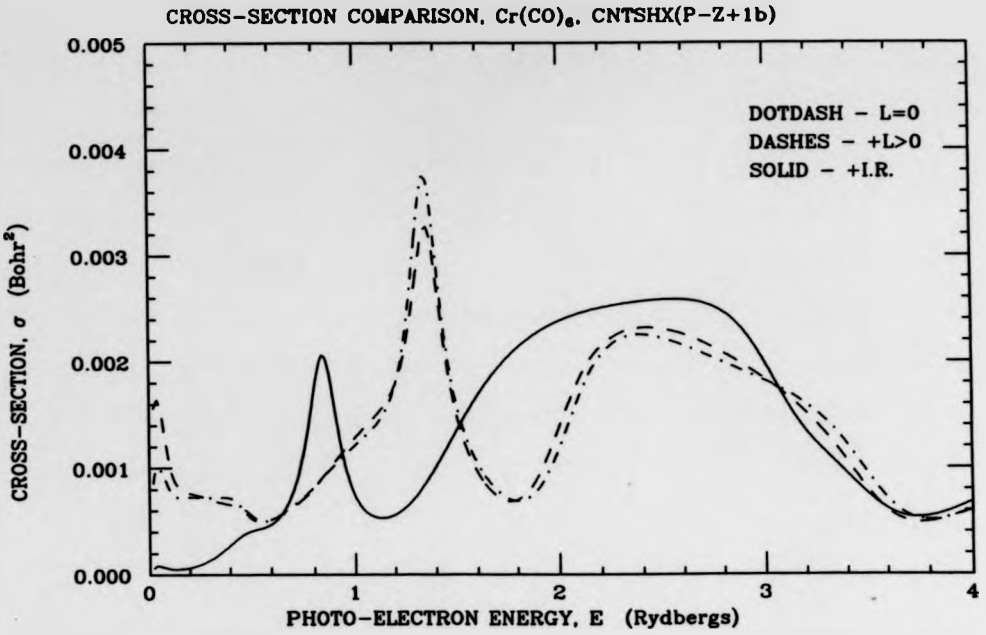

Figure 5.5: CNTSHX results with Z+1b potential for $Cr(CO)_6$. Uses partition A with Mn orbitals in configuration $1s^1 \ldots 4s^1 3d^6$.

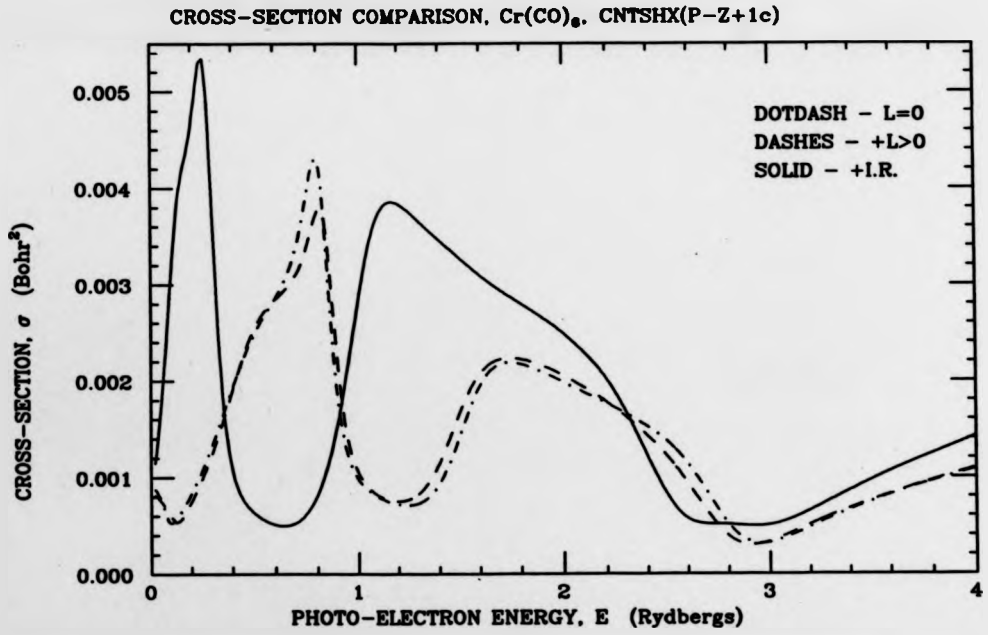

Figure 5.6: CNTSHX results with Z+1c potential for $Cr(CO)_6$. Uses partition A with Mn orbitals in configuration $1s^1 \ldots 4s^1 3d^5$.

lts to the changes in the configuration of the outer electrons. By comparison, the MT results (L=0 mode) vary relatively little and mainly in the position of the main features on the energy axis. Clearly the MT averaging process is acting to nullify the variation in the charge density between the three cases.

Of all our calculations to date, the Z+1a case seems closest to experiment. The first peak is a more reasonable size and the asymmetry of the second peak is better. The overall magnitude of the structure is still too large and it is presumably here that the correct treatment of inelastic loss will be required.

Chapter 6. CONCLUSIONS.

Section 6.1: Main Results, Discussion and Future Directions.

We have shown that it is possible, even using modest computing resources, to remove the muffin-tin approximation in scattered-wave Xα calculations of one-electron energy eigenvalues and core level photoionization cross-sections. The results obtained show that the non-constant components of the interstitial region potential are as important as, if not more important than, the non-spherical components of the atomic sphere potentials, especially for open, covalently bonded systems. It is a necessary prerequisite of any XANES calculation for these systems to remove the MT approximation prior to discussing other physical effects, such as the correct modelling of the core hole, the appropriate exchange-correlation potential, inelastic loss and self-consistency. Indeed in the last case it may be that the MT approximation causes the SCF iterations to give potentials even further removed from reality than the superimposed free-atom potentials; so that the benefits of real self-consistency have been masked.

It is also clear that the XANES calculations are very sensitive, both in the energy-separation of spectral features and in their shape and magnitude, to the choice of potential adopted. As a consequence this work raises serious questions about the significance and quantitative accuracy of previous ab initio XANES calculations for similar open systems based on MT potentials. (It is conceivable that MT potentials adjusted to fit model-compound spectra may be transferrable to unknown materials, but this is by no means obvious.)

Having settled on the FP-SW theory developed by Natoli et al. (1986), for the reasons given in Chap. 2, we derived the bound-

state version (in the Born approximation for the IR) for the first time (applying the general scheme given in Natoli at al. (1986)). It was shown in a new result that the expressions (3.50) etc. for the atomic t-matrices do imply symmetry of the matrices even though this is not readily apparent.

In Chap. 4 we showed that the potential can be modelled to an adequate degree of accuracy, by spherical harmonic expansions, so that meaningful tests of non-MT corrections were possible. Altho the modelling of the IR potential was treated, it was not used in the later development of the FP-SW programs, but still remains a possible avenue for future development to obviate the necessity for the "brute-force" technique that we finally adopted for the evaluation of the interstitial T-matrix.

Chap. 5 contains the main tests for the new programs and starts with the hydrogen molecular ion test of ENESHX. This showed considerable improvement in the eigenvalues compared with the MT case and showed moreover that the bulk of the improvement came from the extra-atomic regions (mainly the IR for the ground state and the EMR for the excited states). Thus the inclusion of non-spherical **atomic** potential components is not so important. In the more typical $Cr(CO)_6$ case the pattern was repeated, although a self-consistent potential was not available. (The inclusion of self-consistency in the treatment of the ground-state electron density (possibly via an external MO calculation) should be consdered a high priority step towards comparison with experiment.)

The lithium pseudo-cluster test for CNTSHX showed that non-MT effects reflect themselves strongly in the photoionization cross-sections and proved the validity of the method and program coding. Again the largest effects were seen to come from the inclusion of the proper modelling of the IR potential. In the case of

$Cr(CO)_6$ the inclusion of non-MT corrections showed an improvement with respect to the experiment (although this may be fortuitous). While the spacing of features in the XANES remained insensitive to the details of the potential (in particular how the core hole was modelled), the shape and magnitude of these features changed markedly even with the fairly minor modifications of the central-atom potential that were involved. This of course emphasizes the need for a better understanding of the core-hole problem (and the related one of self-consistency).

Irrespective of the choice of potential all calculations showed far greater variation in the magnitude of the cross-section than is seen in the experiment. This is undoubtedly due to inelastic scattering phenomena and is another high priority area for future research.

The use of full potentials for small open clusters must now be considered an indispensible part of any meaningful XANES calculations and further consideration of the physics of the photoionization process is necessary before comparison with experiment.

Appendix A. Mathematical Formulae.

A1: Spherical Bessel and Related Functions.

Define the spherical Bessel and Neumann functions, j_l and n_l respectively, for $l = 0, 1, 2, \ldots$, by

$$j_l(x) \equiv (-x)^l \left(\frac{1}{x}\frac{d}{dx}\right)^l \left(\frac{\sin x}{x}\right) \qquad n_l(x) \equiv -(-x)^l \left(\frac{1}{x}\frac{d}{dx}\right)^l \left(\frac{\cos x}{x}\right) \qquad \text{(A1)};$$

and then define the spherical Hankel functions of the first and second kinds, $h_l^{(1)}$ and $h_l^{(2)}$ respectively, from these by

$$h_l^{(1)}(x) \left(\equiv h_l^{+}(x)\right) \equiv j_l(x) + i n_l(x) \qquad h_l^{(2)}(x) \left(\equiv h_l^{-}(x)\right) \equiv j_l(x) - i n_l(x) \qquad \text{(A2)}.$$

Furthermore, define modified spherical Bessel, Neumann and Hankel functions by

$$i_l(x) \equiv i^{-l} j_l(ix) \qquad m_l(x) \equiv -i^{-l+1} n_l(ix) \qquad \text{(A3)}$$

and

$$k_l^{(1)}(x) \left(\equiv k_l^{+}(x)\right) \equiv -i^{-l} h_l^{(1)}(ix) \qquad k_l^{(2)}(x) \left(\equiv k_l^{-}(x)\right) \equiv -i^{-l} h_l^{(2)}(ix) \qquad \text{(A4)}.$$

Note that all of these functions are real except $h_l^{(1)}$ and $h_l^{(2)}$ which form a complex conjugate pair.

Let f_l be one of these eight functions, and let $S \equiv 1$ if f_l is one of the ordinary functions (j_l , n_l , $h_l^{(1)}$ or $h_l^{(2)}$) or $S \equiv -1$ if f_l is one of the modified functions (i_l , m_l , $k_l^{(1)}$ or $k_l^{(2)}$). Then f_l satisfies the second-order differential equation

$$f_l''(x) + \frac{2}{x} f_l'(x) - \left(\frac{l(l+1)}{x^2} - S\right) f_l(x) = 0 \qquad \text{(A5)}$$

(which is effectively the free-particle radial Schroedinger equation with $S = 1$ or -1 corresponding to positive or negative energies respectively). The f_l also satisfy a recurrence relation

$$f_{l+1}(x) = S\left(\frac{2l+1}{x} f_l(x) - f_{l-1}(x)\right) \qquad \text{(A6)};$$

and a differential-recurrence relation

$$f_l'(x) = S f_{l-1}(x) - \frac{l+1}{x} f_l(x) \qquad \text{(A7)}.$$

The behaviour of these functions for very small and very large values of the argument is given by

$$j_l(x) \xrightarrow[x \to 0]{} \frac{x^l}{(2l+1)!!} \qquad n_l(x) \xrightarrow[x \to 0]{} -\frac{(2l-1)!!}{x^{l+1}} \qquad \text{(A8)},$$

and

$$j_l(x) \xrightarrow[x\to\infty]{} \frac{1}{x}\cos\left(x-\frac{(l+1)}{2}\pi\right) \qquad n_l(x) \xrightarrow[x\to\infty]{} \frac{1}{x}\sin\left(x-\frac{(l+1)}{2}\pi\right) \tag{A9}$$

Finally we have the Wronskians

$$j_l(x)n_l'(x) - j_l'(x)n_l(x) = 1/x^2 \tag{A10}$$

$$j_l(x)h_l^{(1)\prime}(x) - j_l'(x)h_l^{(1)}(x) = i/x^2 \tag{A11}$$

and

$$i_l(x)k_l^{(1)\prime}(x) - i_l'(x)k_l^{(1)}(x) = -(-1)^l/x^2 \tag{A12}$$

A2: Spherical Harmonics.

Define the usual complex spherical harmonics $Y_{lm}(\hat{r})$, for integral l and m with $l \geq |m|$, by

$$Y_{lm}(\hat{r}) \equiv \sqrt{\frac{(2l+1)}{4\pi}\frac{(l-m)!}{(l+m)!}}\; P_l^m(\cos\theta)\, e^{im\phi} \tag{A13}$$

with the associated Legendre functions P_l^m defined by

$$P_l^m(x) \equiv (-1)^m (1-x^2)^{m/2} \frac{d^m}{dx^m} P_l(x) \quad (m \geq 0 \text{ only}) \tag{A14}$$

and

$$P_l^{-m}(x) \equiv (-1)^m \frac{(l-m)!}{(l+m)!} P_l^m(x) \tag{A15}$$

where P_l is the Legendre polynomial (with $P_l^0 = P_l$) defined by

$$P_l(x) \equiv \frac{1}{2^l l!} \frac{d^l}{dx^l}(x^2-1)^l \tag{A16}$$

The associated Legendre functions satisfy the differential equation

$$\left[(1-x^2)\frac{d^2}{dx^2} - 2x\frac{d}{dx} + l(l+1) - \frac{m^2}{1-x^2}\right]P_l^m(x) = 0 \tag{A17}$$

and the recurrence relation

$$(2l+1)x P_l^m(x) = (l+1-m)P_{l+1}^m(x) + (l+m)P_{l-1}^m(x) \quad (m \geq 0) \tag{A18}$$

The spherical harmonics satisfy the orthonormality relation

$$\int Y_{l'm'}(\hat{r})^* Y_{lm}(\hat{r})\, d\Omega(\hat{r}) = \delta_{ll'}\delta_{mm'} \tag{A19}$$

and have the parity and complex conjugation properties given by

$$Y_{lm}(-\hat{r}) = (-1)^l Y_{lm}(\hat{r}) \tag{A20}$$

and

$$Y_{l-m}(\hat{r}) = (-1)^m Y_{lm}(\hat{r})^* \tag{A21}$$

An important result is the Addition Theorem for spherical harmonics, which is

$$P_l(\hat{k}\cdot\hat{r}) = \frac{4\pi}{2l+1}\sum_{m=-l}^{l} Y_{lm}(\hat{k})^* Y_{lm}(\hat{r}) \qquad \text{(A22)}.$$

From the spherical harmonics we define the Gaunt coefficients

$$G(l_1 m_1 l_2 m_2 l_3 m_3) \equiv \int Y_{l_1 m_1}(\hat{r}) Y_{l_2 m_2}(\hat{r}) Y_{l_3 m_3}(\hat{r})^* d\Omega(\hat{r}) \qquad \text{(A23)}.$$

These may be expressed in terms of Clebsch-Gordan coefficients by

$$G(l_1 m_1 l_2 m_2 l_3 m_3) = \left\{\frac{(2l_1+1)(2l_2+1)}{4\pi(2l_3+1)}\right\}^{1/2} C(l_1 l_2 l_3 m_1 m_2 m_3) C(l_1 l_2 l_3 000) \qquad \text{(A24)}$$

which are themselves given by Wigner's closed formula

$$C(l_1 l_2 l_3 m_1 m_2 m_3) = \delta_{m_3 (m_1+m_2)}$$
$$\times \left[(2l_3+1)\frac{(l_3+l_1-l_2)!\,(l_3-l_1+l_2)!\,(l_1+l_2-l_3)!\,(l_3+m_3)!\,(l_3-m_3)!}{(l_1+l_2+l_3+1)!\,(l_1-m_1)!\,(l_1+m_1)!\,(l_2-m_2)!\,(l_2+m_2)!}\right]^{1/2}$$
$$\times \left[\sum_t \frac{(-1)^{t+l_2+m_2}(l_2+l_3+m_1-t)!\,(l_1-m_1+t)!}{t!\,(l_3-l_1+l_2-t)!\,(l_3+m_3-t)!\,(t+l_1-l_2-m_3)!}\right] \qquad \text{(A25)}$$

(t being such that the factorial arguments are non-negative).

Now $C(l_1 l_2 l_3 m_1 m_2 m_3)$ is non-zero only when $m_3 = m_1 + m_2$ and $l_1 + l_2 \geq l_3 \geq |l_1 - l_2|$ (the "triangle condition"), and has the symmetries

$$C(l_1 l_2 l_3 m_1 m_2 m_3) = (-1)^{l_1+l_2-l_3} C(l_1 l_2 l_3 -m_1 -m_2 -m_3)$$
$$= (-1)^{l_1+l_2-l_3} C(l_2 l_1 l_3 m_2 m_1 m_3) = (-1)^{l_1-m_1}\left(\frac{2l_3+1}{2l_2+1}\right)^{1/2} C(l_1 l_3 l_2 m_1 -m_3 -m_2) \qquad \text{(A26)}.$$

From the properties of the Clebsch-Gordan coefficients it follows that $G(l_1 m_1 l_2 m_2 l_3 m_3)$ is non-zero only if $m_3 = m_1 + m_2$, $l_1 + l_2 \geq l_3 \geq |l_1 - l_2|$ and $l_1 + l_2 + l_3$ is even; that it is real and that it has the following symmetries

$$G(l_1 m_1 l_2 m_2 l_3 m_3) = G(l_1 -m_1 l_2 -m_2 l_3 -m_3)$$
$$= G(l_2 m_2 l_1 m_1 l_3 m_3) = (-1)^{m_1} G(l_1 m_1 l_3 -m_3 l_2 -m_2) \qquad \text{(A27)}.$$

In the main body of the thesis we use only real spherical harmonics and quantities derived from them. These are defined by a unitary transformation as follows:

$$Y_{lm\alpha}(\hat{r}) \equiv \begin{cases} \frac{1}{\sqrt{2}}\left(Y_{lm}(\hat{r}) + Y_{lm}(\hat{r})^*\right) & (m>0,\ \alpha=1) \\ \frac{-i}{\sqrt{2}}\left(Y_{lm}(\hat{r}) - Y_{lm}(\hat{r})^*\right) & (m>0,\ \alpha=2) \\ Y_{l0}(\hat{r}) & (m=0) \end{cases} \qquad \text{(A28)}$$

where $\alpha = 1$ corresponds to cosine and $\alpha = 2$ corresponds to sine

real spherical harmonics; and $l \geq m \geq 0$. (Note that for $m=0$, α may be taken to be only 1.) For real spherical harmonics the addition theorem takes the form

$$P_l(\hat{k}\cdot\hat{r}) = \frac{4\pi}{2l+1} \sum_{m\alpha} Y_L(\hat{k}) Y_L(\hat{r}) \qquad \text{(A29)}$$

where $L \equiv (l, m, \alpha)$ and the sum over m and α goes through all allowed values for a fixed l. Furthermore the real spherical harmonics are orthonormal and have parity $(-1)^l$.

We define real spherical harmonic analogues of the Gaunt coefficients by

$$I(L\,L'\,L'') \equiv \int Y_L(\hat{r})\, Y_{L'}(\hat{r})\, Y_{L''}(\hat{r})\, d\Omega(\hat{r}) \qquad \text{(A30)}.$$

These may be directly related to those of (A23) by the compact expression

$$I(LL'L'') = \left\{ \begin{array}{ll} 1/\sqrt{2} & \text{if } m_1 m_2 m_3 \neq 0 \\ 1 & \text{if } m_1 m_2 m_3 = 0 \end{array} \right\} \times \left\{ \begin{array}{ll} (-1)^{\alpha/2} & \text{if } \alpha \text{ even} \\ 0 & \text{if } \alpha \text{ odd} \end{array} \right\}$$

$$\times \left\{ \begin{array}{ll} (-1)^{\alpha_k}\, G(l_i m_i\, l_j m_j\, l_k m_k) & \text{if } m_i + m_j = m_k \\ 0 & \text{otherwise} \end{array} \right\} \qquad \text{(A31)}$$

where $\alpha \equiv \alpha_1 + \alpha_2 + \alpha_3 - 1$. The $I(LL'L'')$ are much used in the FP-SW theory, but are quite complicated functions of their integer arguments. What is done in practice is to use (A31) and the ordinary Gaunt coefficients. However these last are too time-consuming to recalculate at need, so they are calculated once at the beginning of a program and stored away. We have developed a new algorithm for the storage and retrieval of these coefficients, which uses less space than previous methods (primarily because of our concern at the high l-truncations that are required for the potential model). The method uses the symmetry and restriction conditions of $G(l_1 m_1\, l_2 m_2\, l_3 m_3)$ quite heavily and the algebra is too long to reproduce here. For a high l-truncation the number of stored values goes roughly as $l(\max)^5/32$.

A3: Green Functions.

At a given energy E the free-particle Green function $G_o^+(\vec{r},\vec{s})$ satisfies

$$(\nabla_r^2 + E)\, G_o^+(\vec{r},\vec{s}) = \delta^3(\vec{r}-\vec{s}) \qquad \text{(A32)}.$$

The actual form of the Green function is determined by the boundary conditions. For negative energy, and defining $\kappa \equiv \sqrt{-E}$, we have

$$\begin{aligned} G_o^+(\vec{r},\vec{s}) &= -\exp(-\kappa|\vec{r}-\vec{s}|)/4\pi|\vec{r}-\vec{s}| \\ &= -\kappa \sum_L (-1)^l i_l(\kappa r)\, k_l^{(1)}(\kappa s)\, Y_L(\hat{r})\, Y_L(\hat{s}) \quad (\text{if } r<s) \end{aligned} \qquad \text{(A33)}.$$

For positive energy and $k \equiv \sqrt{E}$, we have either the standing-wave Green function

$$\begin{aligned} G_o^+(\vec{r},\vec{s}) &= -\cos(k|\vec{r}-\vec{s}|)/4\pi|\vec{r}-\vec{s}| \\ &= k \sum_L j_l(kr)\, n_l(ks)\, Y_L(\hat{r})\, Y_L(\hat{s}) \quad (\text{if } r<s) \end{aligned} \qquad \text{(A34)},$$

or

$$\begin{aligned} G_o^+(\vec{r},\vec{s}) &= -\exp(ik|\vec{r}-\vec{s}|)/4\pi|\vec{r}-\vec{s}| \\ &= -ik \sum_L j_l(kr)\, h_l^{(1)}\, Y_L(\hat{r})\, Y_L(\hat{s}) \quad (\text{if } r<s) \end{aligned} \qquad \text{(A35)}.$$

We also include the Green function for Poisson's equation, which satisfies

$$\nabla_r^2\, G_p(\vec{r},\vec{s}) = -4\pi\,\delta^3(\vec{r}-\vec{s}) \qquad \text{(A36)}.$$

This is well-known to be

$$\begin{aligned} G_p(\vec{r},\vec{s}) &= 1/|\vec{r}-\vec{s}| \\ &= \sum_l (r^l/s^{l+1})\, P_l(\hat{r}\cdot\hat{s}) \quad (\text{if } r<s) \end{aligned} \qquad \text{(A37)}.$$

A4: Re-expansion Theorems.

We give several important results concerning spherical harmonic expansions and re-expansions about different sites. Firstly,

$$\exp(i\vec{k}\cdot\vec{r}) = 4\pi \sum_L i^l j_l(kr)\, Y_L(\hat{k})\, Y_L(\hat{r}) \qquad \text{(A38)};$$

and so

$$\exp(-\vec{k}\cdot\vec{r}) = 4\pi \sum_L (-1)^l i_l(kr)\, Y_L(\hat{k})\, Y_L(\hat{r}) \qquad \text{(A39)}.$$

More importantly,

$$i_\ell(k|\vec{r}-\vec{s}|)Y_L(\widehat{\vec{r}-\vec{s}}) = 4\pi \sum_{L'} \sum_{L''} (-1)^{\ell+\ell'} I(LL'L'')\, i_{\ell'}(kr)\, i_{\ell''}(ks)\, Y_{L'}(\hat{r})\, Y_{L''}(\hat{s}) \quad \text{(A40)},$$

$$k_\ell^{(1)}(k|\vec{r}-\vec{s}|)Y_L(\widehat{\vec{r}-\vec{s}}) = 4\pi \sum_{L'} \sum_{L''} (-1)^{\ell+\ell'} I(LL'L'')\, i_{\ell'}(kr)\, k_{\ell''}^{(1)}(ks)\, Y_{L'}(\hat{r})\, Y_{L''}(\hat{s}) \quad \text{(A41)},$$

$$j_\ell(k|\vec{r}-\vec{s}|)Y_L(\widehat{\vec{r}-\vec{s}}) = 4\pi \sum_{L'} \sum_{L''} i^{\ell'-\ell-\ell''} I(LL'L'')\, j_{\ell'}(kr)\, j_{\ell''}(ks)\, Y_{L'}(\hat{r})\, Y_{L''}(\hat{s}) \quad \text{(A42)},$$

$$n_\ell(k|\vec{r}-\vec{s}|)Y_L(\widehat{\vec{r}-\vec{s}}) = 4\pi \sum_{L'} \sum_{L''} i^{\ell'-\ell-\ell''} I(LL'L'')\, j_{\ell'}(kr)\, n_{\ell''}(ks)\, Y_{L'}(\hat{r})\, Y_{L''}(\hat{s}) \quad \text{(A43)}$$

and

$$h_\ell^{(1)}(k|\vec{r}-\vec{s}|)Y_L(\widehat{\vec{r}-\vec{s}}) = 4\pi \sum_{L'} \sum_{L''} i^{\ell'-\ell-\ell''} I(LL'L'')\, j_{\ell'}(kr)\, h_{\ell''}^{(1)}(ks)\, Y_{L'}(\hat{r})\, Y_{L''}(\hat{s}) \quad \text{(A44)};$$

where (A41, A43 and A44) are valid only for $r < s$.

Appendix B. List of Programs.

The FP-SW programs were developed from the older MT-based programs. They are written in a dialect of FORTRAN IV; one that is used by the VAX series of computers, but which is transportable enough to be easily run on a wide range of other computers. We have retained some useful features (like dummy dimensioning of arrays to accomodate varying molecular sizes) and abandoned others (like COMMON block usage and implicit parameter passing). In general we have tried to make the new programs as modular as we could and format them clearly with plenty of comments. It was possible to use some of the old source code directly. (We estimate that this amounts to about 25% of the source code of the new programs. It consists mainly of subroutines for numerical integration, interpolation and approximation, special functions and matrix manipulation - some from the NAG and IMSL libraries. Not much of the rest was directly usable although it served as a general guide.)

We now list the important MT-based programs. The bound-state ones are essentially those of Smith and Johnson (1969), although they have been much altered by later programmers. The continuum program is that used in Natoli et al. (1980). After each program name we give the number of lines of source code, this being a good measure of its importance.

MOLPOT (527) - prepares initial MT potential from overlapped free atoms for use by ENERGY or CONTNM.

MOLSYM (857) - generates linear combinations of spherical harmonics at the atomic sites, that transform according to the irreps of the point group; used by ENERGY, SCF and CONTNM.

ENERGY (2214) - finds one-electron energy eigenvalues in a given

MT potential. It uses subroutines from AUXSUB.

SCF (3637) - iterates an input MT potential to self-consistency as the ground state or an excited state (with core hole). It uses subroutines from AUXSUB.

CONTNM (3023) - for given initial and final state MT potentials (from MOLPOT or SCF) it calculates core-level photoionization cross-sections. It uses subroutines from AUXSUB.

AUXSUB (1911) - is a collection of auxiliary subroutines used by the main MT-SW programs.

The FP-SW programs that we have developed are analogous to the MT ones. (However, no new version of SCF has yet been written.)

MLPSHX (1334) - generates spherical harmonic representation of the potential constructed from overlapped free atoms.

INPSHX (1119) - prepares potential from MLPSHX in a form usable by the main programs, performing optional smoothing of the asymptotic behaviour of the SHX radial functions. Uses some subroutines from the NAG library.

ENESHX (3869) - does the FP energy eigenvalue search for bound states.

CNTSHX (4211) - does the FP continuum photoionization cross-section calculations for given initial and final state potentials.

Two further programs are referred to in our discussion of the deficiencies of the MT approximation and their effects even in the EXAFS region. See Pettifer and Cox (1983) for details of the origins and development of these programs.

MTAHARA - calculates atomic scattering phase shifts in a MT potential. Uses Dirac-Hara energy-dependant exchange.

EXAFSFT - fits details of local structure around the absorbing site to match an experimental EXAFS spectrum using ab initio theory and phase shifts from MTAHARA.

VIII. REFERENCES.

1. S.L. Altmann, W. Barton and C.P. Mallett (1978) J. Phys. C11 1801.
2. O.K. Andersen (1975) Phys. Rev. B12 3060.
3. R. Arratia-Perez and C.Y. Yang (1985) J. Chem. Phys. 83 4005.
4. C.A. Ashley and S. Doniach (1975) Phys. Rev. B11 1279.
5. L.V. Azároff (1963) Rev. Mod. Phys. 35 1012.
6. E. Badralex (1987) Phys. Rev. B36 1378.
7. E. Badralex (1988) Phys. Rev. B37 1067.
8. W. Bardyszewski and L. Hedin (1987) J. Phys. (Paris) 48 C9 1101.
9. D.R. Bates, K. Ledsham and A.L. Stewart (1953) Phil. Trans. Roy. Soc. (London) A246 215.
10. F. Beleznay and M.J. Lawrence (1968) J. Phys. C1 1288.
11. H.A. Bethe and E.E. Salpeter (1957) "Quantum Mechanics of One- and Two-Electron Atoms" Springer-Verlag, Berlin.
12. R.G. Brown and M. Ciftan (1983) Phys. Rev. B27 4564.
13. R.G. Brown and M. Ciftan (1985) Phys. Rev. B32 1343.
14. R.G. Brown and M. Ciftan (1986) Phys. Rev. B33 7937.
15. D.A. Case and C.Y. Yang (1980) J. Chem. Phys. 72 3443.
16. E. Clementi and C. Roetti (1974) At. Data Nucl. Data Tables 14 177.
17. E.R. Cohen and B.R. Taylor (1987) Rev. Mod. Phys. 59 1121.
18. J.B. Danese (1974) J. Chem. Phys. 61 3071.
19. J.B. Danese (1977) Chem. Phys. Lett. 45 150.
20. J.B. Danese and J.W.D. Connolly (1974) J. Chem. Phys. 61
21. M. de Broglie (1913) C. R. Hebd. Seances Acad. Sci. 157 924.
22. J.P. Desclaux (1980) Physica Scripta 21 436.

23. J.B. Diamond (1973) Chem. Phys. Lett. 20 63.

24. D. Dill and J.L. Dehmer (1974) J. Chem. Phys. 61 692.

25. S. Doniach, M. Berding, T. Smith and K.O. Hodgson (1984) in "EXAFS and Near-Edge Structure III" (eds. K.O. Hodgson, B. Hedman and J.E. Penner-Hahn, Springer-Verlag, Berlin) 33.

26. P.J. Durham (1988) in "X-ray Absorption" (eds. D.C. Koningsberger and R. Prins, Wiley, New York) 53.

27. R. Evans and J. Keller (1971) J. Phys. C4 3155.

28. J.S. Faulkner (1979) Phys. Rev. B19 6186.

29. J.S. Faulkner (1985) Phys. Rev. B32 1339.

30. J.S. Faulkner (1986) Phys. Rev. B34 5931.

31. D.L. Foulis, R.F. Pettifer and C.R. Natoli (1986) J. Phys. (Paris) 47 C8 597.

32. H. Fricke (1920) Phys. Rev. 16 202.

33. G.V. Gadiyak, V.G. Malkin, Yu.N. Morokov and S.V. Chernov (1982) J. Struct. Chem. 23 274.

34. A. Gonis (1986) Phys. Rev. B33 5914.

35. J.E. Hahn, R.A. Scott, K.O. Hodgson, S. Doniach, S.R. Desjardins and E.I. Solomon (1982) Chem. Phys. Lett. 88 595.

36. T.M. Hayes and J.B. Boyce (1982) Sol. St. Phys. 37 173.

37. F. Herman and S. Skillman (1963) "Atomic Structure Calculations" Prentice-Hall, Englewood Cliffs, N.J.

38. F. Herman, A.R. Williams and K.H. Johnson (1974) J. Chem. Phys. 61 3508.

39. J.B. Johnson and W.G. Klemperer (1977) J. Am. Chem. Soc. 99 7132.

40. K.H. Johnson (1966) J. Chem. Phys. 45 3085.

41. K.H. Johnson (1973) Advan. Quantum Chem. 7 143.

42. K.H. Johnson (1975) Ann. Rev. Phys. Chem. 26 39.

43. K.H. Johnson and F.C. Smith Jr. (1972) Phys. Rev. B5 831.

44. B.D. Keister (1983) Annals of Physics 149 162.

45. J. Keller (1971) J. Phys. C4 L85.

46. W. Kohn and N. Rostoker (1954) Phys. Rev. 94 1111.

47. J. Korringa (1947) Physica 13 392.

48. R. de L. Kronig (1931) Z. Phys. 70 317.

49. R. de L. Kronig (1932) Z. Phys. 75 191.

50. R. de L. Kronig (1932) Z. Phys. 75 468.

51. F.W. Kutzler, C.R. Natoli, D.K. Misemer, S. Doniach and K.O. Hodgson (1980) J. Chem. Phys. 73 3274.

52. V.I. Lebedev (1977) Siberian Math. J. 18 99.

53. P.A. Lee and J.B. Pendry (1975) Phys. Rev. B11 2795.

54. P. Lloyd and P.V. Smith (1972) Advan. Phys. 21 69.

55. T.L. Loucks (1967) "Augmented Plane Wave Method" Benjamin, New York.

56. P.-O. Löwdin (1956) Advan. Phys. 5 1.

57. L.F. Mattheiss (1964) Phys. Rev. A133 1399.

58. A.D. McLaren (1963) Math. Comput. 17 361.

59. W.H. McMaster, N.K. Del Grande, J.H. Mallet and J.H. Hubbell (1969) National Bureau of Standards Report No. UCRL-50174, Sec. II, Rev. 1.

60. R. McWeeny and B.T. Sutcliffe (1984) Comput. Phys. Rep. 2 217.

61. J. Molenaar (1988) J. Phys. C21 1455.

62. J.E. Müller and J.W. Wilkins (1984) Phys. Rev. B29 4331.

63. R.S. Mulliken (1955) J. Chem. Phys. 23 1833, 1997, 2343.

64. C.R. Natoli, M. Benfatto and S. Doniach (1986) Phys. Rev. A34 4682.

65. C.R. Natoli, D.K. Misemer, S. Doniach and F.W. Kutzler (1980) Phys. Rev. A22 1104.

66. J.G. Norman Jr. (1976) Mol. Phys. 31 1191.

67. J.B. Pendry (1981) in "EXAFS for Inorganic Systems" (Daresbury Laboratory, DL/SCI/R17 (Experimental)) 5.

68. J.B. Pendry (1983) Comments Solid State Phys. 10 219.

69. R.F. Pettifer and A.D. Cox (1983) in "EXAFS and Near-Edge Structure" (eds. A. Bianconi, L. Incoccia and S. Stipcich, Springer-Verlag, Berlin) 66.

70. R.F. Pettifer, D.L. Foulis and C. Hermes (1986) J. Phys. (Paris) 47 C8 545.

71. D.G. Pettifor (1973) J. Chem. Phys. 59 4320.

72. N. Rösch, W.G. Klemperer and K.H. Johnson (1973) Chem. Phys. Lett. 23 149.

73. J.R. Rumble and D.G. Truhlar (1980) J. Chem. Phys. 72 3206.

74. U. Scherz (1972) J. Chem. Phys. 56 1315.

75. L.I. Schiff (1968) "Quantum Mechanics" 3rd edn. McGraw-Hill Kogakusha, Tokyo.

76. K. Schwarz (1972) Phys. Rev. B5 2466.

77. J. Siegel, D. Dill and J.L. Dehmer (1976) J. Chem. Phys. 64 3204.

78. J.C. Slater (1937) Phys. Rev. 51 846.

79. J.C. Slater (1972) Advan. Quantum Chem. 6 1.

80. J.C. Slater and K.H. Johnson (1972) Phys. Rev. B5 844.

81. F.C. Smith Jr. and K.H. Johnson (1969) Phys. Rev. Lett. 22 1168.

82. E.A. Stern and J.J. Rehr (1983) Phys. Rev. B27 3351.

83. A.H. Stroud (1971) "Approximate Calculations of Multiple Integrals" Prentice-Hall, Englewood Cliffs, N.J.

84. J.R. Taylor (1972) "Scattering Theory" John Wiley & Sons, New York.

85. M. Tinkham (1964) "Group Theory and Quantum Mechanics" McGraw-Hill, New York.

86. Univ. of Warwick, Dept. of Physics (1985) "Preparation of Ph.D. Theses" (PHYS/PG/2).

87. A.A. Volkov and L.V. Poluyanov (1980) J. Struct. Chem. 21 713.

88. A. Whitaker and J.W. Jeffery (1967) Acta Cryst. 23 977.

89. A.R. Williams and J. van W. Morgan (1974) J. Phys. C7 37.

90. C.Y. Yang (1978) J. Chem. Phys. 68 2626.

91. C.Y. Yang and S. Rabii (1975) Phys. Rev. A12 362.

92. R. Zeller (1987) J. Phys. C20 2347.

93. P. Ziesche (1974) J. Phys. C7 1085.

TITLE The Effects of the Use of Full Potentials in the Calculation of X-Ray Absorption Near-Edge Structure by the Multiple-Scattered-Wave X-alpha Method

AUTHOR David Laurence Foulis,